Universidad de Alcalá

COMISIÓN DE ESTUDIOS OFICIALES
DE POSGRADO Y DOCTORADO

ACTA DE EVALUACIÓN DE LA TESIS DOCTORAL
(FOR EVALUATION OF THE ACT DOCTORAL THESIS)

Año académico *(academic year)*: 2016/17

DOCTORANDO *(candidate PHD)*: **LIGUORI, GIOVANNI**
D.N.I./PASAPORTE *(Id.Passport)*: ******4349**
PROGRAMA DE DOCTORADO *(Academic Committee of the Programme)*: **D411-CIENCIAS**
DEPARTAMENTO DE *(Department)*: **FÍSICA Y MATEMÁTICAS**
TITULACIÓN DE DOCTOR EN *(Phd title)*: **DOCTOR/A POR LA UNIVERSIDAD DE ALCALÁ**

En el día de hoy 25/11/16, reunido el tribunal de evaluación, constituido por los miembros que suscriben el presente Acta, el aspirante defendió su Tesis Doctoral **con Mención Internacional** *(In today assessment met the court, consisting of the members who signed this Act, the candidate defended his doctoral thesis with mention as International Doctorate)*, elaborada bajo la dirección de *(prepared under the direction of)* WILLIAM DAVID CABOS NARVAEZ.

Sobre el siguiente tema *(Title of the doctoral thesis)*: *REGIONAL CLIMATE MODELING OF THE MEDITERRANEAN AND THE IBERIAN PENINSULA CLIMATE VARIABILITY*

Finalizada la defensa y discusión de la tesis, el tribunal acordó otorgar la CALIFICACIÓN GLOBAL[2] de (**no apto, aprobado, notable** y **sobresaliente**) *(After the defense and defense of the thesis, the court agreed to grant the GLOBAL RATING (fail, pass, good and excellent)*: SOBRESALIENTE (EXCELLENT)

Alcalá de Henares, a 25 de NOVIEMBRE de 2016

Fdo. *(Signed)*: D.A. gaertner

Fdo. *(Signed)*: FCO. ALVAREZ

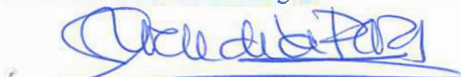Fdo. *(Signed)*: ENRIQUE SANCHEZ   Fdo. *(Signed)*: Dmitry Sein   Fdo. *(Signed)*: ALFREDO Izquierdo

FIRMA DEL ALUMNO (candidate's signature),

Con fecha 21 de diciembre de 2016 la Comisión Delegada de la Comisión de Estudios Oficiales de Posgrado, a la vista de los votos emitidos de manera anónima por el tribunal que ha juzgado la tesis, resuelve:
☒ Conceder la Mención de "Cum Laude"
☐ No conceder la Mención de "Cum Laude"

Fdo. *(Signed)*: Giovanni Liguori

GIOVANNI LIGUORI

La Secretaria de la Comisión Delegada

[2] La calificación podrá ser "no apto" "aprobado" "notable" y "sobresaliente". El tribunal podrá otorgar la mención de "cum laude" si la calificación global es de sobresaliente y se emite en tal sentido el voto secreto positivo por unanimidad. *(The grade may be "fail" "pass" "good" or "excellent". The panel may confer the distinction of "cum laude" if the overall grade is "Excellent" and has been awarded unanimously as such after secret voting.)*.

INCIDENCIAS / OBSERVACIONES:
(Incidents / Comments)

Universidad de Alcalá

COMISIÓN DE ESTUDIOS OFICIALES
DE POSGRADO Y DOCTORADO

En aplicación del art. 14.7 del RD. 99/2011 y el art. 14 del Reglamento de Elaboración, Autorización y Defensa de la Tesis Doctoral, la Comisión Delegada de la Comisión de Estudios Oficiales de Posgrado y Doctorado, en sesión pública de fecha 21 de diciembre, procedió al escrutinio de los votos emitidos por los miembros del tribunal de la tesis defendida por *LIGUORI, GIOVANNI*, el día 25 de noviembre de 2016, titulada *REGIONAL CLIMATE MODELING OF THE MEDITERRANEAN AND THE IBERIAN PENINSULA CLIMATE VARIABILITY*, para determinar, si a la misma, se le concede la mención "cum laude", arrojando como resultado el voto favorable de todos los miembros del tribunal.

Por lo tanto, la Comisión de Estudios Oficiales de Posgrado **resuelve otorgar** a dicha tesis la

MENCIÓN "CUM LAUDE"

Alcalá de Henares, 21 de diciembre de 2016
EL PRESIDENTE DE LA COMISIÓN DE ESTUDIOS
OFICIALES DE POSGRADO Y DOCTORADO

Juan Ramón Velasco Pérez

Copia por e-mail a:
Doctorando: LIGUORI, GIOVANNI
Secretario del Tribunal: FRANCISCO JOSÉ ÁLVAREZ GARCÍA.
Director de Tesis: WILLIAM DAVID CABOS NARVAEZ

UNIVERSIDAD DE ALCALÁ, PATRIMONIO DE LA HUMANIDAD

Giovanni
Liguori

Regional climate modeling of the Mediterranean and
the Iberian Peninsula climate variability

Universidad de Alcalá

Departamento de Física y Matemáticas

Regional climate modeling of the Mediterranean and the Iberian Peninsula climate variability

TESIS DOCTORAL
Programa de Doctorado en Matemáticas y Física

Giovanni Liguori

2016

2016

Regional climate modeling of the Mediterranean and the Iberian Peninsula climate variability

Universidad de Alcalá

Tesis dirigida por el doctor

William Cabos

Programa de Doctorado en

Matemáticas y Física

Giovanni Liguori

Departamento de Física y Matemáticas
Universidad de Alcalá

2016

Regional climate modeling of the Mediterranean and the Iberian Peninsula climate variability

TESIS DOCTORAL
para la obtención del grado de doctor

Dirigida por el doctor
William Cabos

Giovanni Liguori

Departamento de Física y Matemáticas
Universidad de Alcalá

2016

Ai miei genitori,
Angela e Gennaro

Contents

Resumen

La región Mediterránea se caracteriza por una fuerte interacción entre mar y atmósfera y por sistemas dominantes de alta y baja presión que resultan en un clima complejo y fuertemente estacional. Las proyecciones para el clima futuro obtenidas forzando el clima con concentraciones crecientes de gases a efecto invernadero muestran como esta región sea un "hotspot" del cambio climático proyectado por el siglo 21. La vulnerabilidad del clima Mediterráneo al cambio climático en curso, y el importante papel que la interacción océano-atmósfera juega en esta región, ha motivado la comunidad científica europea en coordinar un esfuerzo común finalizado a la realización de simulaciones regionales acopladas regionales. Este esfuerzo común se ha formalizado en el marco del proyecto Med-CORDEX que tiene como objetivos primarios tanto lo de mejorar el conocimiento de la variabilidad climática y de la tendencia en el clima del pasado, como de proporcionar proyecciones para el clima futuro con mayor precisión y exactitud. Parte de este trabajo de tesis ha sido desarrollado como contribución al proyecto Med-CORDEX.

En este trabajo de tesis se analiza un ensamble de modelos regionales climáticos (RCMs) para estudiar la variabilidad climática de la región mediterránea y de la Península Ibérica (IP). A pesar de que de la IP sea una región relativamente pequeña, su clima, que está influenciado tanto por el océano Atlántico como por el mar Mediterráneo, presenta una gran variedad climática. Puesto que la

variabilidad climática de la IP y de la región Mediterránea están conectadas, un estudio integrado de las dos regiones resulta ser un marco excelente para investigar los mecanismos físicos responsables de la variabilidad climática observada en estas regiones.

Aunque los proyectos de investigación que han producidos los ensembles de RCM usados en este trabajo han realizados simulaciones tanto para el clima actual como para el clima futuro, este manuscrito solo presenta los resultados obtenidos para las simulaciones del clima actual. Como primer paso nos hemos enfocado en la variabilidad climáticas de la cuenca mediterránea y en particular en la variabilidad asociada con el intercambio de calor entre el océano y la atmósfera. Este flujo de calor a la interfaz mar-aire afecta a muchos procesos que controlan el clima del Mediterráneo como, por ejemplo, la formación de aguas profunda, que es el principal motor de la circulación termohalina. Combinando modelos y observaciones, se ha podido asociar los primeros dos modos de variabilidad del flujo de calor a la interfaz mar-aire con algunos patrones de variabilidad atmosférica de gran escala. Además, calculando el balance calor entre mar y atmósfera, hemos identificado los mecanismos físicos que conectan la variabilidad de los flujos de calor con los patrones de variabilidad atmosférica.

Una vez valorada la variabilidad de los flujos de calor en la cuenca Mediterránea, se ha estudiado la variabilidad de la IP usando un ensemble de RCM formado por 4 modelos. En particular, se han investigado el estado medio de parámetros básicos atmosféricos y la variabilidad interanual de los extremos de temperatura y precipitación. También se ha valorado la distribución espacial de los eventos extremos y, comparando los cuatro RCMs, se han identificado las regiones con alta y baja variabilidad interna.

Abstract

The Mediterranean region is characterized by intense air-sea interaction and dominant high and low pressure systems that results in a complex and strongly seasonal climate system. Future climate projections performed with increasing concentrations of greenhouse gases, have revealed this region to be one of the climate change "hot spots" of the 21st century. The vulnerability of the Mediterranean climate system to the ongoing climate change, and the crucial role that air-sea interaction plays in this region, have motived the European scientific community at coordinating the climate modeling community towards the development of fully coupled regional climate models. This common effort has been formalized under the Med-CORDEX project, which primary goals are to improve understanding of past climate variability and trends, and to provide more accurate and reliable future projections. Part of this thesis is a contribution to the Med-CORDEX project.

In this thesis work we use multi-model ensembles of regional climate models (RCMs) to study the climate variability of the Mediterranean Sea and of the Iberian Peninsula(IP). Despite its relatively small extension, the IP, which is influenced by both Atlantic and Mediterranean basins, presents a large variety of climates. Since the IP climate variability is linked to the Mediterranean Climate, an integrated study of the two regions results in an excellent framework to investigate the physical mechanisms responsible for the observed climate in these regions.

The research projects that produced the RCM multi-model ensembles used in this thesis work, have produced both present- and future-time simulations. However, in this manuscript we present only the results of the present-time model outputs. First, we focused on the Mediterranean basin climate variability, and in particular on the variability of its air-sea heat fluxes, which affect several climate processes controlling the Mediterranean climate. These include the winter formation of deep waters, which is the primary driver of the Mediterranean Sea overturning circulation. Combing models and observations, we were able to connect the two leading modes of air-sea heat flux variability with large-scale atmospheric teleconnection patterns. Also, by performing a budget analysis, we were able to explain the physical mechanism linking these teleconnection patterns with the air-sea heat flux variability.

Once assessed the heat fluxes variability of the Mediterranean Sea, we connected this to the climate variability of the IP using a 4-model ensemble of RCM. In particular, we investigated mean fields of basic atmospheric parameters and the interannual variability of temperature and precipitation extremes. We assessed the spatial distribution of extreme events statistics and, comparing the four RCMs, we identified regions with high and low internal variability as well as with large bias among the models.

CHAPTER 1

Introduction

It seems that the influence of your teacher has been to give you a false idea of what are worthwhile problems. The worthwhile problems are the ones you can really solve or help solve, the ones you can really contribute something to. A problem is grand in science if it lies before us unsolved and we see some way for us to make some headway into it.

Richard P. Feynman - Letter to Koichi

In the last few decades, we have seen an increasing effort to understand the cause and consequences of the ongoing climate change. These efforts culminate with the intergovernmental panel on climate change (IPCC) reports which the international community produce every few years since the first assessment report that was completed in 1990. The last assessment report (AR5), completed in 2014, concluded that the warming of the climate system is unequivocal, and since the 1950s, many of the observed changes are unprecedented over decades to millennia. Moreover, the report attribute this ongoing global warming to human influence with an estimate probability between 95 to 100%. However, it is important to notice that global warming effects are spatially highly variable. In fact, although in most of the globe the Earth's surface temperature is projected to increase, there are certain regions where this parameter is projected to remain stable or even decrease. Indeed, our main concern isn't the warming but the climate change, which we may not be able to predict and thus mitigate its effect of human society.

Although the definition of global warming is associated with an increase in temperature, in some regions other physical parameters represent better the changes experienced by the local climate. For instance, major climate changes in the tropics and in the Mediterranean region are associated with precipitation rather than temperature. The Mediterranean region is one of the climate change hot-spots highlighted by the IPCC simulations (de Sherbinin 2014; Giorgi 2006). In particular, climate models are coherently projecting a pronounced decrease in precipitation, especially in the warm season, except for the northern Mediterranean areas (e.g. the Alps) in winter. The projected decrease in precipitation is especially pronounced in the Iberian Peninsula (IP), which will be likely suffering of more frequent and more extreme drought events. This particular vulnerability of the IP is consistent with previous paleoclimate studies revealing the strong climate sensitivity of this region to global-scale natural variability occurring from thousand-year to million-year timescales (e.g., Cacho et al., 2010).

This strong climate sensitivity that characterize the IP has attracted the interested of the climate modelling community resulting in several climate changes studies focusing in this region. For instance, Moberg et al. (2000) quantify an increased in the temperature of the IP of about 5% analyzing the period 1880-1998. However, this modest increase in temperature becomes much larger when the analysis is done using the second half of the 20th century (Klein Tank et al., 2002). These studies agree that the global warming observed in the IP is all but uniform, both in space and time. During the 20th century, depending of the region, we observed periods of hiatus as well as of strong warming (Staudt et. al., 2005). Moreover, these changes are characterized by distinct trends for minimum and maximum temperature that change according to the seasons.

This vulnerability of the Mediterranan and IP climate motivate us to focus this thesis work on the natural and forced climate variability of these regions. Most of the IP climate is a *subclimate* of the Mediterranean climate. Therefore, we focused first on the inter-annual variability of the Mediterranean Basin and then we moved our focus on the IP, which we study characterizing mean value and extreme events for temperature and precipitation in the present-time climate. In recent times we have assisted to important advances in the development of the climate models and their sub-components. This is not surprising since climate models are the best tool available to produce climate projection (e.g., Gutiérrez y Pons, 2006; Räisänen, 2007; Flato et al., 2013) and to test hypothesis on the physical mechanics responsible for the observed climate. In this thesis work, we used a combination of several regional climate models and observational dataset to improve our knowledge on the climate variability of both Mediterranean and IP regions.

1.1   Climate models

Climate modelling is the most common approach to investigate natural and forced climate variability on a wide range of time scales. A climate model is a computer

program aim to simulate physical and chemical processes occurring in the climate system and described by mathematical equations. These equations describe the temporal evolution of all the components of the climate system and are solved numerically using high performance computing systems. These models span a wide range of complexity that goes from the simplicity of zero-dimensional Earth's energy budget model to the complexity of the so called Earth system models(ESMs), which are commonly build by coupling an ocean general circulation model (GCM) to an atmospheric GCM. In a 3D model the equation are discretized on a finite 3D grid and in each grid point an approximate solution of the governing equation is obtained by solving the equation numerically. For instance, in the case of an atmospheric GCM, in each point of the grid we will have an approximation for the pressure, the temperature, the humidity, wind components, the precipitation and other variables.

The ESM simulate the entire globe, which translates in a spatial resolution currently used to perform the simulations between 0.25 to 3 degrees (these values are for atmospheric GCMs since oceanic counterparts are currently using spatial resolutions up to 0.1 degree). With the computing power currently available is impossible to simulate the whole Earth's climate at higher resolution. However, there are several important oceanic and atmospheric processes responsible for shaping the observed climate that require higher resolution to be accurately represented in the models. Perhaps the most important process strongly misrepresented in the GCMs is the orographic precipitation, which occurs when a moist flow is forced to raise topographic features such mountains and or hills. Misrepresenting the precipitation, impacts the hydrological cycle, the energy budget and in turn the atmospheric circulation. Moreover, this limitation in computer power prevent the realization of large ensembles of simulations that have been shown to be necessary disentailing the climate change signals from the natural climate variability, which is probably responsible for high internal variability characteristic of model simulations (Deser et al. ,2014; Thomson et al., 2015).

One way to overcome the shortcomings associated with the low spatial resolution of the ESM is to embed a regional climate models(RCMs), which domain cover only a limited part of the Earth's surface inside the GCM domain. Since the RCM domain is "small" it is possible to increase its grid spatial resolution keeping contained the computational cost. This approach, referred to as "nesting" allows for the regional climate model to produce results with spatial resolutions between 5 and 50 km. Information from the GCM is used to drive the RCM by establishing the initial condition and providing the boundary conditions for each time steps. RCMs provide dynamically downscaled climate information within the region of interest, allowing to tackle some of these challenges that face state of the art ESMs, as RCMs can account for climate phenomena and characteristics that are influenced by variable orography, land–sea and other surface contrasts, as well as various short-duration and spatially sharp extreme events, and small-scale weather features, providing information on these phenomena and characteristics for regional-to-local climate change assessment, climate change scenario analyses, and impact studies that currently are not provided by global models.

At this point, naturally raises the question of how much, if any, is the RCM output better than the driving global data (these possible improvements by the RCM are commonly termed "added value"). The superiority of the RCM output over the driving global data is not obvious: first, climate is by its very nature a large scale phenomenon, and current ESMs are able to reproduce adequately large scale patterns such as the intertropical convergence zone, or the monsoon circulation in the subtropics; and second, in most cases the spatial scale of these climate features are larger than the domain size of most regional models. Moreover, it has been argued that regional models are developed to reproduce an observed climatology rather than to predict the change of the climatology in response to a changing climate (Kerr, 2013) although, it seems that the global models also suffer at some extent of a similar problem. It has been argued that the inability of GCMs to simulate the global warming hiatus is at some extent due to the fact that global coupled models are tuned to simulate the climate characteristics of a given period, excluding the simulation of the hiatus. Also, it has been argued that

due to uncertainties related to lateral boundary conditions and model biases, regional climate models could essentially add meaningless spatial detail, limiting considerably their usefulness (Xie et al., 2015). However, a number of recent studies demonstrate added value of RCM. Feser et al. (2011) analyzed different regional atmospheric models for reanalysis hindcast simulations and simulations driven by climate model output. They argue that for atmospheric regional models there is a clear added value associated with the better representation of the orography, which improve the representation of those parameters that exhibit high spatial variability such as near surface temperature rather than sea level pressure.

Taking in mind advantages and shortcomings associated with the use of RCM and considering the limited extension of the study area of this research work, the Mediterranean and the IP, we choice to adopt a regional climate modelling framework to address our scientific questions, which are presented in details the next chapters.

1.2 Thesis structure

This research work, presented here in five chapters, has resulted in four scientific articles published in peer-reviewed scientific journals. Two articles have been published in *Climate Research*, one in *Bulletin of American Meteorological Society,* and one in *Climate Dynamics*.

This first chapter, named Introduction, presents the research subject, the scientific background, research motivations and goals, and the approach used to archive the goals. The second chapter presents the MED-CORDEX initiative, which is a unique framework where research community make use of both regional atmospheric, land surface, river and oceanic climate models and coupled regional climate system models for increasing the reliability of past and future regional climate information and understanding the processes that are responsible for the

Mediterranean climate variability and trends. In the third chapter, we use multiple observational datasets and a multi-model ensemble of 12 simulations to provide a more robust assessment of the statistical behavior of Mediterranean surface heat flux winter variability and to diagnose the mechanisms underlying links to the regional footprint of large-scale atmospheric teleconnection patterns. The fourth chapter focuses on the current climate of the IP and consists of two published works on present-time climate conditions with focus on mean fields and extreme events for temperature and precipitation. Last chapter, the fifth, remarks the main conclusion of this research study and present the lines of work that further research will follow.

CHAPTER 2

Med-CORDEX initiative for Mediterranean Climate studies

There were many, many fine reasons not to go, but attempting to climb Everest is an intrinsically irrational act— a triumph of desire over sensibility. Any person who would seriously consider it is almost by definition beyond the sway of reasoned argument.

Jon Kraukauer - Into Thin Air

It has been said that man is a rational animal. All my life I have been searching for evidence which could support this.

Bertrand Russell

This chapter presents the Med-CORDEX initiative, which is a European project aims at coordinating the Mediterranean climate modeling community towards the development of fully coupled regional climate simulations. The primary goals of Med-CORDEX are to improve understanding of past climate variability and trends, and to provide more accurate and reliable future projections. The chapter 3, which has been fully published in the peer-reviewd journal *Climate Dynamics* represent my personal contribution to the Med-CORDEX effort. The content of this chapter has been published in the following manuscripts:

Ruti P., Somot S., Dubois C., Calmanti S., Ahrens B., Aznar R., Bartholy J., Béranger K., Bastin S., Brauch J., Calvet J.C., Carillo A., Alias A., Decharme B., Dell'Aquila A., Djurdjevic V., Drobinski P., Elizalde Arellano A., Gaertner M., Galan P., Gallardo C., Giorgi F., Gualdi S., Bellucci A., Harzallah A., Herrmann M., Jacob D., Khodayar S., Krichak S., Lebeaupin C., Lheveder B., Li L., **Liguori G**., Lionello P., Baris O., Rajkovic B., Sevault F., Sannino G., 2015: MED-CORDEX Initiative for Mediterranean Climate Studies. *Bulletin of the American Meteorological Society*, doi:10.1175/BAMS-D-14-00176.1.

2.1   Abstract

The Mediterranean is expected to be one of the most prominent and vulnerable climate change "hot spots" of the 21st century, and the physical mechanisms underlying this finding are still not clear. Furthermore complex interactions and feedbacks involving ocean-atmosphere-land-biogeochemical processes play a prominent role in modulating the climate and environment of the Mediterranean region on a range of spatial and temporal scales. Therefore it is critical to provide robust climate change information for use in Vulnerability/Impact/Adaptation assessment studies considering the Mediterranean as a fully coupled environmental system. The Med-CORDEX initiative aims at coordinating the Mediterranean climate modeling community towards the development of fully coupled regional climate simulations, improving all relevant components of the system, from atmosphere and ocean dynamics to land surface, hydrology and biogeochemical processes. The primary goals of Med-CORDEX are to improve

understanding of past climate variability and trends, and to provide more accurate and reliable future projections, assessing in a quantitative and robust way the added value of using high resolution and coupled regional climate models. The coordination activities and the scientific outcomes of Med-CORDEX can produce an important framework to foster the development of regional earth system models in several key regions worldwide.

2.2 Introduction

The Mediterranean basin is characterized by complex coastlines and topographical features, such as the Alpine, Apennine, Pyrenees and Balkan mountain chains, the Italian and Hellenic peninsulas and large islands (Balearic, Sicily, Sardinia, Corsica, Crete and Cyprus). From the meteorological and climatic point of view this morphological complexity leads to fine scale spatial and temporal variability (Ruti et al. 2008, Chronis et al., 2010, Dobrinski et al. 2014), along with the formation of intense weather phenomena (Ducrocq et al. 2014, Tous et al. 2014). A typical example of such phenomena is the Mistral wind, which blows through the Rhone valley into the Gulf of Lions and across to Corsica and Sardinia through the Strait of Bonifacio (Chronis et al., 2010). Another example is the Bora wind, which blows in a north-easterly direction across a series of topographical channels into the North Adriatic Sea. Several coastal areas of the Central (e.g. the Gulf of Genoa) and Eastern (e.g. Cyprus island) Mediterranean are also centers of topographically-induced intense cyclogenesis (e.g. Buzzi and Tibaldi 1978; Alpert et al. 1995). Such events, in addition to having catastrophic consequences on different sectors of society, dramatically influence the Mediterranean ocean circulation (Herrmann and Somot 2008, Durrieu de Madron et al. 2013) through deep and bottom water formation.

The Mediterranean Sea is a semi-enclosed and evaporative basin in which a wide range of oceanic processes and interactions of regional interest occur. It is connected to the Atlantic Ocean by the shallow Strait of Gibraltar and is composed

of two basins of similar size, i.e. the Western and the Eastern Mediterranean Seas, separated by the shallow Strait of Sicily. It is also connected to the Black Sea to the northeast through the Bosphorus channel. In the Strait of Gibraltar, the comparatively fresher and warmer Atlantic water flows into the Mediterranean Sea at the surface to compensate for the negative mass balance inside the basin (where evaporation is greater than precipitation and river runoff) and to replace cooler and saltier Mediterranean water flowing out at depth into the Atlantic. Moreover, the Mediterranean water outflow strengthens and stabilizes the Atlantic Meridional Overturning Circulation through warm and saline water input (Artale et al., 2006; Ivaninovic et al., 2014).

Deep Mediterranean water is produced at different locations by intense air–sea interactions: in the Gulf of Lions (western Mediterranean), the Southern Adriatic, the northeast Levantine basin and the Aegean Sea in the eastern Mediterranean (see MEDOC group, 1970; Roether et al. 1996). The basin's circulation is 5 characterized by the presence of sub-basin gyres, intense mesoscale variability and a strong seasonal signal. Interannual variability is also observed, mostly related to the interannual variability of atmospheric forcings (Josey 2003; Mertens and Schott 1998; Vilibić and Orlić 2002; Herrmann et al., 2010; Josey et al., 2011; L'Heveder et al. 2013). Such physical processes have two critical characteristics: first, they derive from strong air–sea coupling and, second, they occur at fine spatial scales because the Rossby radius of deformation varies from 5 to 12 Km throughout the Mediterranean, setting the scales at which important energy redistribution processes occur. In order to explicitly resolve with high spatial resolution the two-way interactions at the atmosphere–ocean interface, fully-coupled high resolution atmosphere-ocean regional climate models (RCMs) are needed (Somot et al., 2008, The PROTHEUS group, 2010; Dell'Aquila et al., 2012; Gualdi et al. 2013).

Another important forcing of Mediterranean climate is due to aerosols of natural and anthropogenic sources (Lelieveld et al., 2002). Saharan dust outbreaks can carry large amounts of particulate material over the Mediterranean and Central

European regions (Moulin et al., 1998), modifying not only the radiative budget of the basin through their microphysical and optical properties (Bergamo et al., 2008), but also the basin bio- geochemical cycle (Guieu et al., 2010). Moreover, air pollution emissions by industries and large urban areas around the Mediterranean and in Central Europe can further affect regional air quality, surface energy and water budgets (Lelieveld et al., 2002). Biomass burning and forest fires constitute another important source of carbonaceous aerosols in summer (Sciare et al., 2008).

It is thus clear that complex interactions and feedbacks involving ocean, atmosphere, land and biogeochemical processes, along with the effects of complex morphological features, play a prominent role in modulating the climate of the Mediterranean region on a range of spatial and temporal scales. In addition, different generations of model projections have indicated that the Mediterranean is expected to be one of the most prominent and vulnerable climate change "hot spots" of the 21st century (Giorgi, 2006; Diffenbaugh and Giorgi 2012), and the physical mechanisms underlying this finding are still not clear. Indeed, several components of the Euro-Mediterranean climate have been already changing in the last decades. Over the Mediterranean, mean temperature has increased more than the global average, mean annual precipitation has decreased since the mid-20th century, and trends towards more frequent and longer heat waves and fewer extremely cold days and nights have been observed (IPCC 2013). Since the 1960s, the mean heat wave intensity, length and number across the Eastern Mediterranean region have increased by a factor of five or more (Kuglitsch et al., 2010; Ulbrich et al., 2012). In a study of European river flows by Stahl et al. (2010), a regionally coherent picture of annual stream-flow trends emerged, with negative trends in the 6 southern and eastern regions, suggesting that the observed drying trend is reflected in the state of rivers. This hydrologic trend should amplify in the future (Schneider et al., 2013).

These examples show that there is a growing and challenging need to better understand the processes that make the Mediterranean especially sensitive to

natural variability, global warming and local/regional forcings, particularly in view of the need to describe the interactions across all components of the regional hydrological cycle. Since the early' 90s, a number of research and intercomparison projects have focused on downscaling global climate simulations (reanalysis or Global Climate Models [GCMs]) over the Euro-Mediterranean region (RACCS, Machenauer et al., 1996a, Christensen et al., 1997; MERCURE, Machenauer et al., 1996b; STARDEX, Goodess, 2003; PRUDENCE, Christensen et al., 2007; ENSEMBLES, Van der Linden P and Mitchell JFB 2009; CIRCE, Gualdi et al., 2013). Building on these programs, and as part of the CORDEX (COordinated Regional Downscaling EXperiment) international effort (Giorgi et al., 2009), Med-CORDEX is a unique framework in which the research community makes use of coupled regional atmospheric, land surface, river, and ocean climate models, along with individual components of these systems run at very high resolution, to increase the reliability and process-based understanding of past and future fine scale climate information for the region. Med-CORDEX aims at addressing a number of key scientific challenges, including:

- To develop fully-coupled Regional Climate System Models (RCSM) for the Mediterranean basin (Figure 1), considering and improving all relevant components of the system, i.e. atmosphere, ocean, land surface, hydrology and biogeochemistry;
- To improve understanding of past climate variability and trends, and to provide more accurate and reliable future projections at high resolution, with emphasis on the role of coupled component interactions, fine scale processes and extreme events;
- To assess in a quantitative and robust way the Added Value of using high resolution and coupled RCMs;
- To coordinate the Mediterranean RCM community and promote the production of large model ensembles following internationally accepted protocols such as CMIP and CORDEX in order to optimally assess reliability and uncertainties in regional climate projections;

- To promote, gather and organize the use of ground-based and satellite-based observational data into tailored datasets for use in climate process evaluation;

- To strengthen the link with the Vulnerability/Impacts /Adaptation (VIA) research community through the provision of tailored climate information data-sets usable in VIA studies and in the development 7 of response policies.
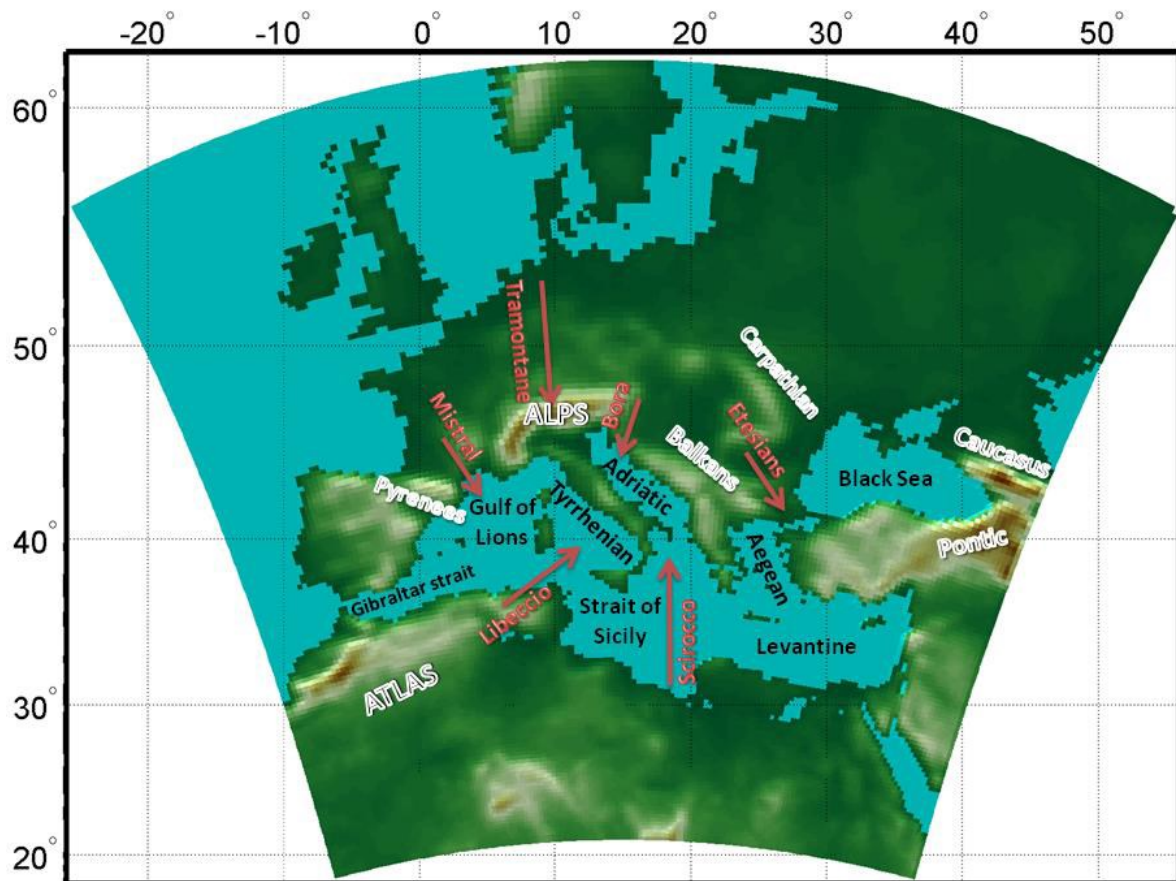

Figure1. Maximum model integration area for coupled systems.

Having defined these primary goals of the program, in the next sections we first provide an historical perspective of Med-CORDEX and present illustrative results from the first Med-CORDEX activities. We then discuss the Med-CORDEX plans and how they will contribute to address the scientific challenges outlined above.

Details on the model configurations and simulations can be found in www.medcordex.eu.

2.3 Background of the Med-CORDEX initiative and the production phase

The current CORDEX protocol envisions two simulation streams with RCMs run over continental scale domains covering essentially all land regions of the World at ~50 km grid spacing (Giorgi et al. 2009): in the first stream the RCMs are run in the so-called perfect boundary condition experiment mode, in which data from one of the most recent and high-resolution reanalysis (ERA-interim, Dee et al. 2011) provide the lateral meteorological boundary conditions for the RCMs. The ERA-Interim data are available for the period 1979-2013 and these simulations serve the purpose of assessing and optimizing the model performance against observations for the period (Giorgi and Mearns 1999). The second stream, which provides the climate change information for VIA use, consists of climate projections for the late 20th and full 21st century (1950-2100 or 1970-2100) with the RCMs driven at the lateral boundaries by fields from different GCMs from the Climate Model Intercomparison Project 5 (CMIP5, http://cmip-pcmdi.llnl.gov/cmip5/). More detail on the CORDEX experimental protocol can be found in http://wcrp-cordex.ipsl.jussieu.fr/.

In order to address the specific research challenges outlined in the previous section, the Med-CORDEX
phase 1 protocol adds to this base framework the following tiers:

- Production of ensembles of simulations with coupled Regional Climate System Models (RCSMs)

- including fully interactive Atmosphere-Land-River-Ocean components, covering the whole
- Mediterranean basin and its catchment basin at an intermediate grid spacing of ~20-50 km;
- Production of corresponding stand-alone simulations for all individual components in order to asses the importance of the coupled modeling approach;
- Use of the most recent validation data available, including datasets obtained from HyMeX (Ducrocq et al. 2014, Drobinski et al. 2014) field campaigns;
- Production of high-resolution simulations (~12 km grid spacing) to assess the added-value of high resolution in a number of relevant metrics, and in particular topography-forced spatial patterns, the simulation of mesoscale phenomena, precipitation intensity distributions, strong wind systems and extreme events;
- Advancement of regional reanalyses to serve as reference datasets and ocean initial conditions

The Med-CORDEX phase 1 gathers 22 different modelling groups from 9 countries (France, Italy, Spain,Serbia, Greece, Turkey, Tunisia, Germany, Hungary) in Europe, Middle-East and North-Africa and more than 75 active members of the modelling and evaluation teams that can follow the activities through a dedicated emailing list (medcordex@hymex.org) and web page (www.medcordex.eu). Since 2009, yearly side meetings at the HyMeX international workshops as well as four dedicated Med-CORDEX meetings (Toulouse in September 2009, Toulouse in March 2012, Palaiseau in May 2014, Mykonos in September 2015) have been organized thanks to the Mediterranean Integrated Studies at Regional And Local Scales (MISTRALS) meta-program which supports HyMeX.

Twelve coupled RCSMs covering the whole Mediterranean and its catchment basin have been developed, which include coupling of regional atmosphere and ocean components (see www.medcordex.eu for more details). Some models also include

coupling with river runoff, thereby closing the water cycle of the basin. Med-CORDEX is therefore the largest international coordinated multi-model initiative using fully-coupled RCSMs to provide long-term projections in a standardized and open way.

In addition to the 12 RCSMs, Med-CORDEX also includes the participation of 13 stand-alone atmosphere RCMs used at various resolutions (150 km, 50 km, 25 km, 12 km), as well as 10 stand-alone ocean models (resolution from 25 km to 3 km) and 4 stand-alone land surface models (50 km). Coordinated hindcast simulation ensembles for each of these components and for the coupled RCSMs have been completed and intercompared (http://www.medcordex.eu/simulations.php). All runs are documented through metadata forms. The ERA-Interim driven runs cover the 1989-2013 or the 1979-2013 periods (the latter having been available only late in the program), with 25 runs completed with atmosphere-only RCMs, 9 runs with coupled RCSMs, 4 runs with land-surface regional models (forced by ERA-Interim fields corrected following the WATCH protocol; Szczypta et al. 2012), and 11 runs with the ocean regional models (forced by ERA-Interim fields; Macias et al. 2013; or by dynamical downscaling of the reanalysis; Herrmann et al. 2010). In addition regional climate change simulations for the atmosphere (15 runs), ocean (1 run) and RCSMs (5 runs) have been performed using the RCP8.5 and RCP4.5 scenarios for the 1950-2100 period, with boundary fields from 6 different CMIP5 GCMs.

A centralized Med-CORDEX database was developed at ENEA in order to host the model outputs in the CORDEX standardized format and to provide information to the data producers and users (www.medcordex.eu). The Med-CORDEX data are freely available for non-commercial use. Ocean, land, river and atmosphere variables are available at various frequencies from monthly to 3-hourly. Currently, the database includes more than 3 Tb of data and 110.000 files. File format standardization, a powerfull search 10 tool and on-line computation service, allows an optimal download and use of the data (120.000 data files downloaded for a total of 5 Tb by the 130 registered users). Each simulation is described by

the data providers through metadata files completed on-line and hosted by the HyMeX database.

2.4 Illustrative examples of Med-CORDEX scientific achievements

In this section we provide a sample of results from the Phase I Med-CORDEX activities aimed at illustrating the types of analyses which are carried out in order to address the scientific issues highlighted in the previous sections. In particular, the examples below serve to illustrate the added value of the Med-CORDEX strategy based on the use of high resolution and coupled RCMs in better capturing climate statistics important for VIA applications and in improving the understanding of model errors. We also stress that many studies are still ongoing on the anlsysi of the Med-CORDEX experiments available to date.

2.4.1 The atmospheric component: Mediterranean cyclones and associated extremes

-- Cyclogenesis

Alpine lee cyclogenesis represents a paradigmatic example of a geophysical process which can integrate different spatial and temporal scales. It characterizes most of the winter rainfall variability over the Alpine region and produces orographic rainfall extremes. During the beginning stages of the event, a vortex develops on the cyclonic shear side of the Mistrals in a strong confluent frontogenesis area over the sea. In its mature phase, lee-cyclogenesis has a typical baroclinic evolution with spatial scales of the order of the Rossby radius of deformation (Buzzi and Tibaldi 1978). This type of cyclone draws moisture and energy from the adjacent western Mediterranean Sea and it leads to the

occurrence of extreme precipitation events over the surrounding coastal and mountain areas, often causing floods of exceptional severity (Rudari et al 2004; Pfahl and Wernli 2012, Ducrocq et al. 2014).
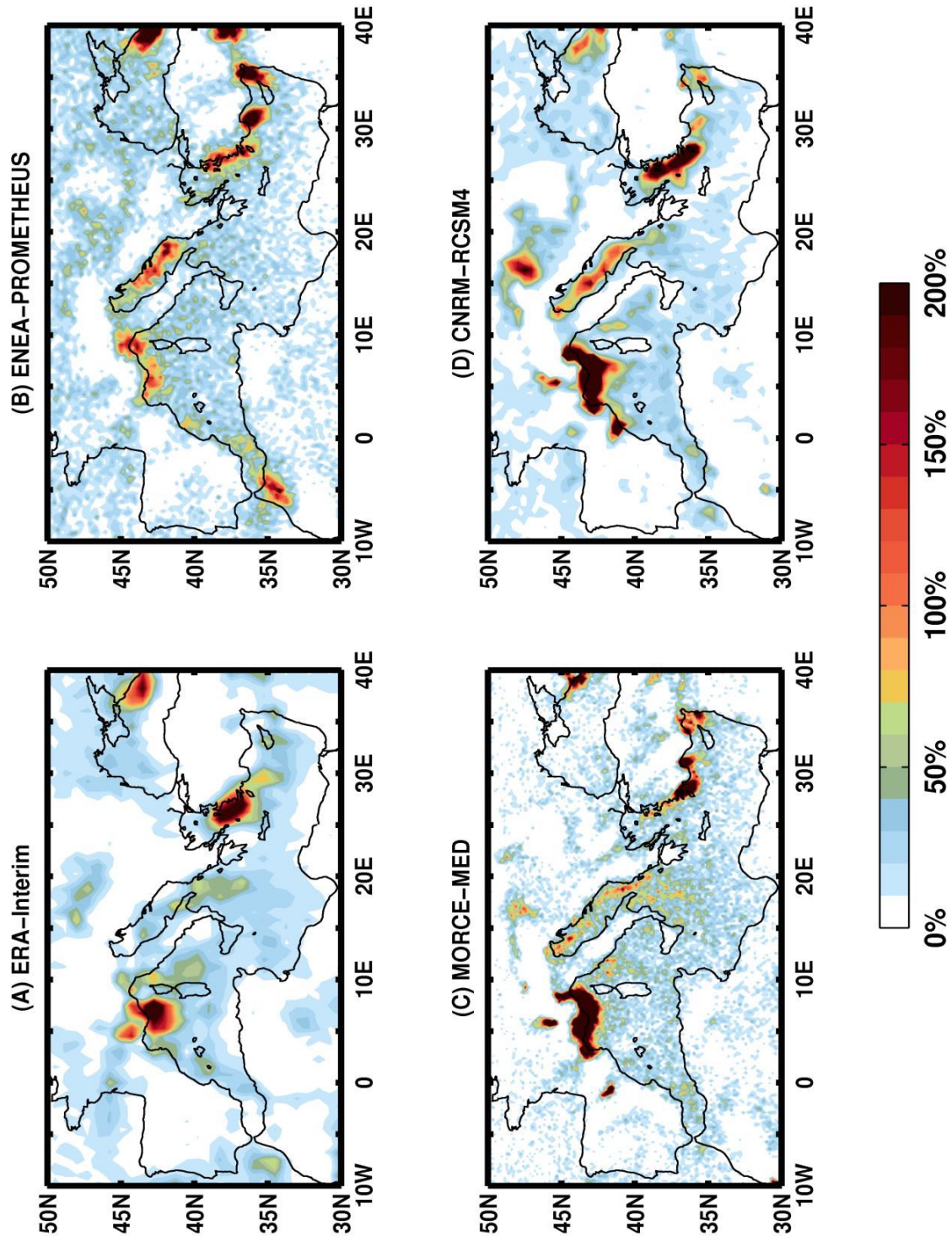
Figure 2. Frequency of cyclone occurrence per 1000km² per 25 days for autumns and winters of the period 1989-2008. For example, a 10% value suggests the occurrence of 10 cyclones in a 1000km² area in 25 days. Values exceeding 100% suggest the occurrence of more than one cyclone a) ERA-Interim; b) Protheus coupled run; c) Morce-Med coupled run; d) CNRM-RCSM4 coupled run.

Figure 2 shows the spatial patterns of cyclone center density (or cyclone frequency) for different ERA-Interim driven Med-CORDEX experiments, along with the driving ERA-interim data themselves, during the autumn and winter seasons for the years 1989-2008 (for methods see Flaounas et al. 2013). Here only two-way coupled RCSMs (~25-30 km grid spacing) are considered. Overall, a qualitative agreement between the ERA-Interim and model simulated spatial structures is found, as all models and reanalysis identify the major oceanic cyclone activity areas over the Western Mediterranean, along the Turkey coast line and over the Black sea. Many cyclones originate around the Alps and the Gulf of Lions and Genoa, over the Aegean sea, and over the Iberian Peninsula and Atlas chain (Campins et al., 2011 and references therein). Moreover, all models reproduce the oceanic cyclone activity over the Adriatic sea. Low pressure centers crossing this small basin surrounded by complex topography are well captured by the RCSMs at high-resolution, while the coarser resolution ERA-interim reanalysis does not simulate such small low centers. This result thus illustrates the added-value of the increase in resolution achievable with RCMs (Flaounas et al. 2013). The role of the ocean-atmosphere coupling in the representation of the Mediterranean cyclone life cycle (cyclogenesis, life time, intensity) has also been assessed by Sanna et al. (2013) and Akhtar et al. (2014), showing an improved representation of SST patterns and lower atmospheric stability compared to atmosphere-alone models.

 -- Intense precipitation events

Most of the severe rainfall events observed over the complex topography surrounding the Mediterranean basin occur in autumn, and model resolution is expected to be a key factor in simulating such events. Figure 3 shows the 99% quantile of autumn daily precipitation (mm/day) for the period 1989-2008 for ERA-interim (Panel 3a) and the COSMO-CLM and ALADIN regional simulations (driven by ERA-Interim fields) at 50 km (Panels 3c and 3e) and 12 km (Panels 3d

and 3f) grid spacing over the Med-CORDEX domain. In order to measure the model performance in reproducing the tail of the distribution with respect to an observation- based fine scale dataset, the same results are shown over france in Figure 4, where they are compared to a high-resolution mesoscale atmospheric analysis for rainfall (Système d'analyse fournissant des renseignements atmosphériques à la neige, SAFRAN, Quintana-Seguí et a., 2008). The results of Figure 3 and 4 clearly show that ALADIN and COSMO-CLM are able to simulate the tail of the probability distribution function of rainfall intensity with an increasing accuracy going from 50 to 12 km grid spacing. In particular, the 12 km versions are able to capture not only the topographic effect on extreme rainfall events but also the land-sea contrast along the Mediterranean coasts. By contrast, the ERA-Interim reanalysis and the coarse resolution ALADIN model strongly underestimate the magnitudes of these precipitation extremes (Figures 3a, b; 4a). The results shown in Figure 3 and 4 were also confirmed by the study of Harader et al. (2015) based on different quantitative metrics of model performance.
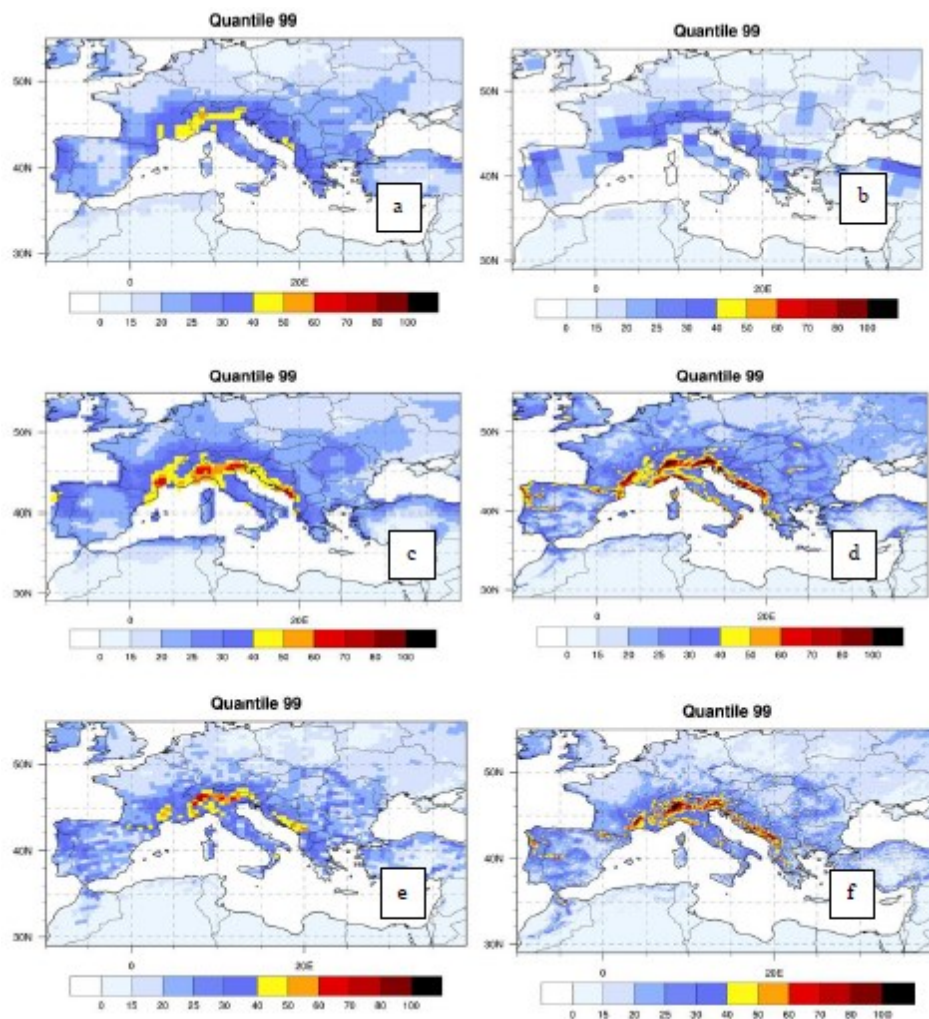
Figure 3. 99% quantile of daily precipitation (mm/day) in SON for the period 1989-2008 : a) ERA-interim reanalysis; b) ALADIN-Climat model 150 Kms ; c) COSMO-CLM model 50kms forced by ERA-interim reanalysis; d) COSMO-CLM model 12kms; e) ALADIN-Climat model 50 kms; f) idem for 12 kms.
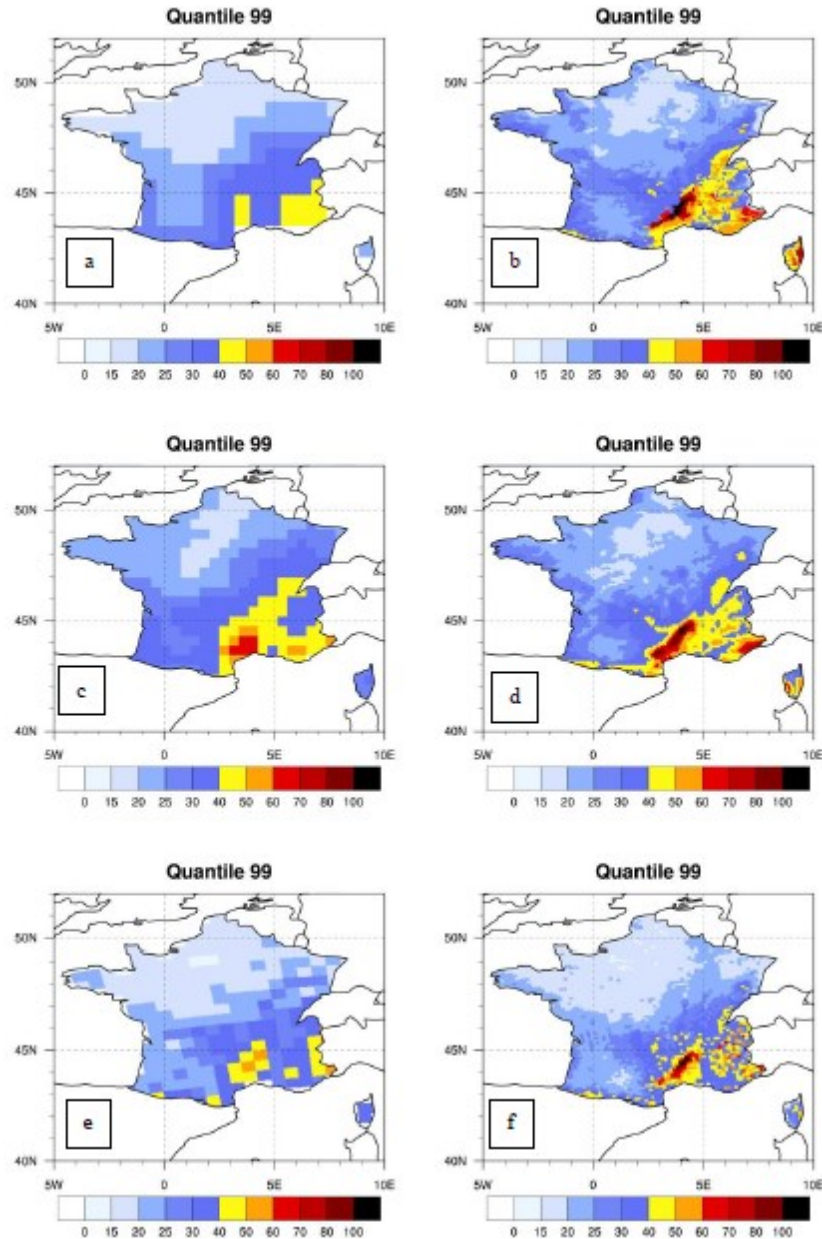
Figure 4. 99% quantile of daily precipitation (mm/day) in SON for the period 1989-2008 : a) ERA-interim renalysis ; b) SAFRAN renalysis 9 kms; c) COSMO-CLM model 50kms; d) COSMO-CLM model 12kms; e) ALADIN-Climat model 50 kms; f) idem for 12 kms.

The added-value highlighted over France in Figure 4 is found also when the regional models are forced by GCMs. For example, Torma et al. (2015) found a strong improvement in the simulation of precipitaiton spatial patterns, daily precipitaiton distributions and extremes over the Alpine region in high resolution RCMs compared to the driving GCMs (not shown). They also showed how the high

resolution representation of topography can substantially affect the precipitation change signal, for example during the summer when high elevation heating induces a positive precipitaiotn change over the high elevations of the Alpine chain. In addition, the influence of high-frequency ocean-atmosphere coupling on heavy precipitation case studies was investigated using twin experiments with a RCSM and the associated atmospheric RCM driven by observed SST and by the RCSM SST (Lebeaupin-Brossier et al. 2013; Berthou et al. 2014, 2015). These studies found that the coupling significantly influences the event intensity and position.

-- Intense wind events

Another extreme phenomenon often associated with Mediterranean cyclones is the occurrence of strong winds over the sea (Ruti et al, 2008; Herrmann et al. 2011) accompanied by intense air-sea exchanges (Herrmann and Somot 2008, Durrieu de Madron et al. 2013) which can lead to ocean deep convection in various sites of the Mediterranean Sea (Herrmann and Somot 2008, Herrmann et al. 2010, Beuvier et al. 2010). In such phenomena, the wind strength and direction are fundamental parameters which determine the vorticity and turbulent forcing for the ocean. Following two pioneering studies (Ruti et al 2008, Herrmann and Somot 2008) and new satellite-based datasets (Chronis et al. 2010), from an analysis of Med-CORDEX experiments with the regional model ALADIN at various resolutions (grid spacing of 125 km, 50 km and 12 km), Herrmann et al. (2011) confirmed the added-value of using high-resolution RCMs in simulating the wind field over the sea. They demonstrated that the 50-km resolution is a minimum to reproduce the sea wind field and that the 12-km resolution adds value close to the coastline. Note that the conclusions of this study were then used to design some of the Med-CORDEX RCSM experiments (Sevault et al. 2014, Nabat et al. 2014).

Figure 5 generalizes this result in a multi-model context. It shows plots of wind speed distribution over two main convective sites, the Gulf of Lion and the Ligurian

sea, for several models (coupled and uncoupled, 50 km and 12 km resolution) compared to Quikscat, ERA-interim and buoy (LION and AZUR) wind speed data. The models capture most of the observed variability at the LION buoy, while some discrepancies are seen at the AZUR site. The main wind regime into the Gulf of Lion is associated to the Tramontane and Mistral strong northwesterly winds which blow through the Garonne and Rhone valleys driven by large scale 13 pressure patterns. Over the Côte d'Azur site, two main regimes are present, i.e. from the northeast (associated to the Mistral) and from the southwest, due to atmospheric highs entering the gulf of Lion from the west or southwest and stationing over the Gulf of Genoa. The latter regime is not well reproduced by both the models and the reanalysis (Ruti et al., 2008). During the winter season, the wind forcing over the Gulf of Lion is reproduced reasonably well, suggesting a good skill in simulating related convective processes, however, the winter high wind speed tail is not well captured. Overall, Figure 5 shows that the 12km RCMs (COSMO-CLM, ALADIN-Climate) improve the representation of the wind probability density function at both locations with respect to the corresponding 50km versions and the coarse resolution ERA- Interim reanalysis. Conversely, the coupled model (PROTHEUS) does not show a clear improvement with respect to the uncoupled model for this specific variable and site (Herrmann et al. 2011).
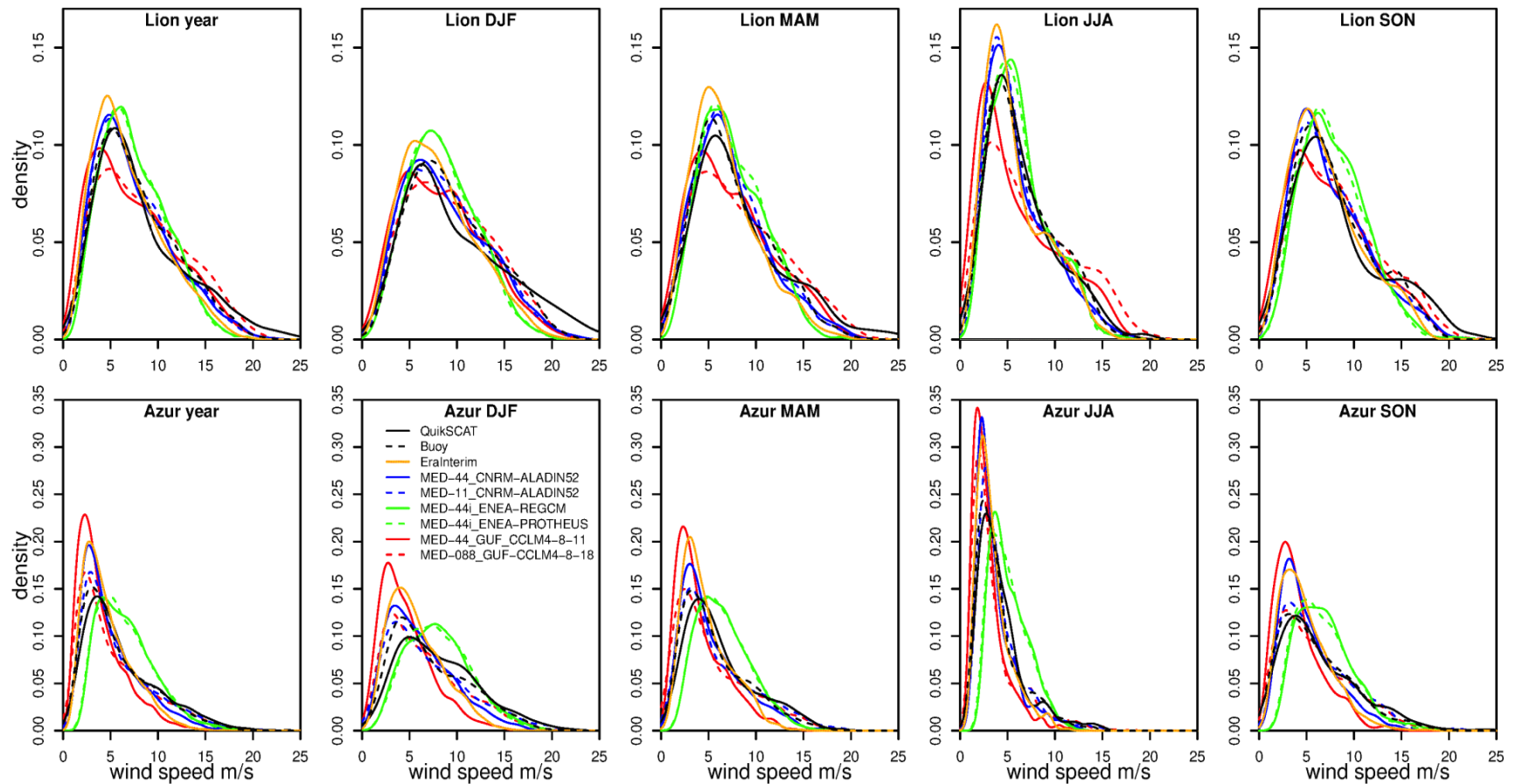
Figure 5. Plots of wind speed distribution at Lion and Azur buoy locations for several models in comparing to Quikscat, 1008 ERainterim and buoy wind speed. Whole time period (2000-2008) and the seasons.

2.4.2 Other components of the system: Mediterranean Sea, river discharge and aerosols

-- SST and water and heat budgets

The Mediterranean Sea is characterized by a negative water budget (excess evaporation compared to freshwater input) balanced by a two-layer exchange at the Strait of Gibraltar composed of a warm and fresh upper water inflow from the Atlantic superimposed to a cooler and saltier Mediterranean outflow. Light and fresh Atlantic water is transformed into denser water through interactions with the atmosphere that renew the Mediterranean waters at intermediate and deep levels and drive the Mediterranean thermohaline circulation.

The Mediterranean Sea water and heat budgets (MSWB and MSHB, respectively) can be seen as good integrators of climate variability at seasonal to interannual and decadal scales. A series of Med-CORDEX articles demonstrated how they are also main drivers for key Mediterranean phenomena, such as open-sea deep convection (Josey et al. 2011, Papadopoulos et al. 2012), Mediterranean thermohaline circulation (Adloff et al. 2015), strait transport (Soto-Navarro et al. 2014), river discharge (Sevault et al. 2014), energy and water sources for Mediterranean cyclones (Sanna et al. 2013, Akthar et al. 2014) and coastal heavy precipitation events (Berthou et al. 2014, 2015). In addition, the feedback of the Mediterranean Sea on the atmosphere through water and energy exchanges is of paramount importance to evaluate the impact of climate variability and change on human activities in the context of global warming. In this regard, of particular relevance is the effect of an increase of ocean heat content on the frequency and intensity of high- impact weather events and on sea level rise. 14 Two multi-model studies within the frame of the ENSEMBLES and CIRCE projects (Sanchez-Gomez et al. 2011 and Dubois et al. 2012) demonstrated that (i) the observed references for the MSWB and MSHB terms (evaporation, precipitation, river runoff, Black Sea freshwater inputs, shortwave radiation, longwave radiation, sensible

heat flux, latent heat flux) are far from being accurate and (ii) state-of-the-art RCMs still show large deficiencies in reproducing these terms at various scale (mean state, spatial pattern, interannual variability and trends). Due to the central role of the MSWB and MSHB in the Mediterranean climate, improving their representation in climate models and understanding their variability is one of the key challenge in Med-CORDEX. A large number of studies on this topic using Med-CORDEX simulations are still on-going but preliminary results are summarized here.

Dubois et al. (2012) demonstrated that the SST is one of the main factors driving the errors in the MSWB and MSHB terms. Figure 6 shows the interannual time series of SST averaged over the whole Mediterranean basin for ERA-Interim driven runs. Over the period 1980-2010, the interannual variability is well reproduced in all simulations, however a cold bias is found in most experiments. This error could be related to the model configurations, since in most Med-CORDEX models the first ocean level is about 5 meters deep, while the models with a reduced bias have a thinner first ocean level, about 1 m (yellow, light blue and green lines in the figure). It is also found that the SST trend is weaker in the models than in observations, perhaps as a result of the lack of representation of aerosol effects (see below).
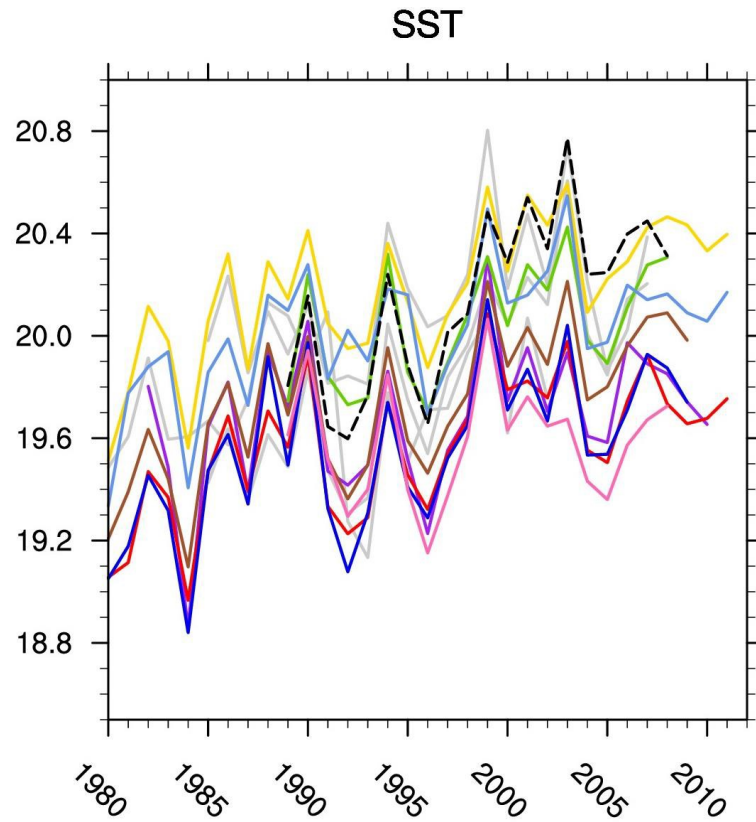
Figure 6. SST interannual variability time series for the values averaged over the Med Sea basin. In grey the observed references:(Satellite, Rixen, EN4), in Black dashed: ERA-Interim. All coupled simulations are in colors. In red: CNRM, in blue: LMDZ, in brown: INSTM, in yellow: GUF, in purple:ENEA-PROTHEUS, in pink:UniBel, in light blue:CMCC and in green: MORCE-MED.

Local evaluations of SST can be carried out using sea buoy data. Figure 7 shows a comparison between the LION buoy SST data (42.1°N, 4.7°E, North-West Mediterranean) and four Med-CORDEX coupled RCSMs at the daily temporal scale. The four coupled simulations agree in reproducing the seasonal cycle (Figure 7a) and the inter-annual variability of the observed SST (Figure 7b). The simulated SST distributions are then compared with observed SSTs in daily quantile-quantile plots for Winter (Figure 7c) and Summer (Figure 7d). In Winter, the central quantiles of the distribution are overestimated by all models, while the high end of the range is underestimated, a behavior which is probably due to the misrepresentation of ocean deep convective phenomena. In summer (Figure 7d), however, most of the models are able to reproduce the observed distribution (with two exceptions of underestimation).
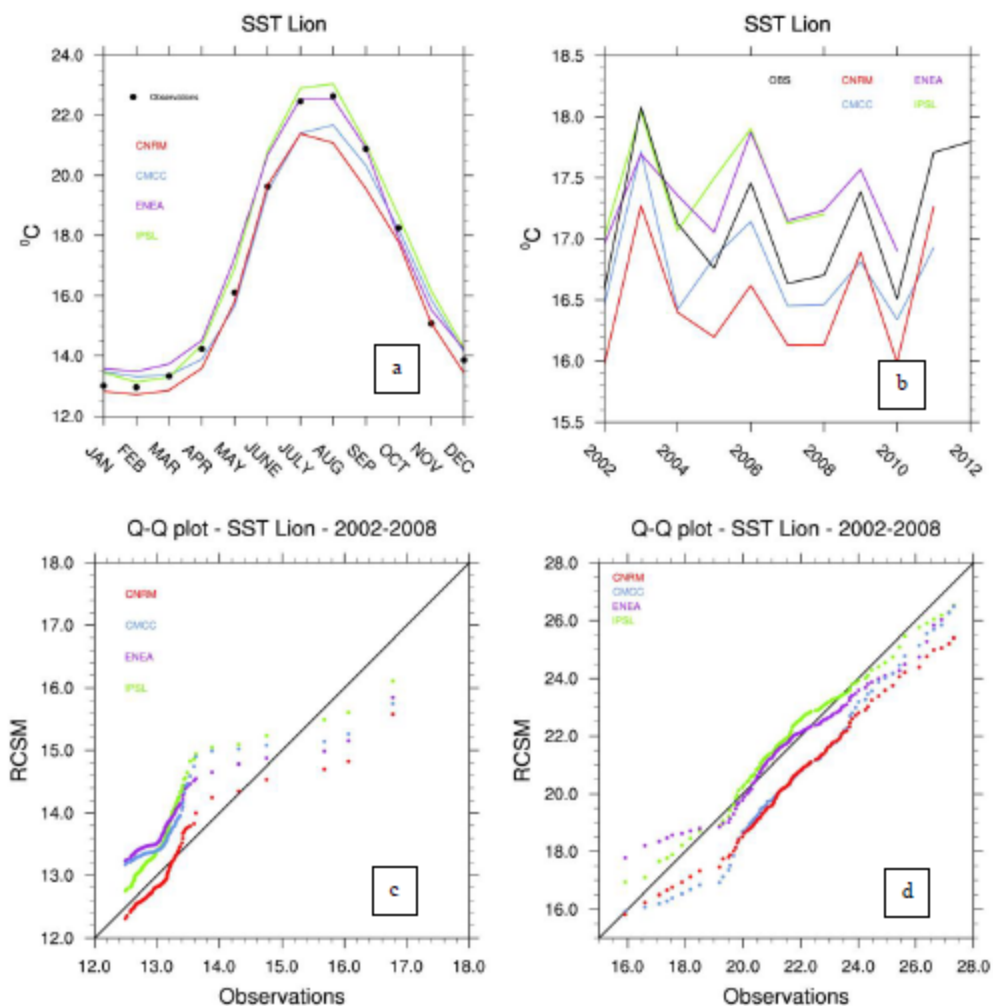
Figure 7. SST validation of the SST at the Lion buoy location (Lat: 42.10N, Lon: 4.70E) for different coupled models over the ERA-interim period: a) the time series; b) the annual cycle; c) DJF qq-plot; d) JJA qq-plot. CNRM coupled model, coupling the Limited Area Model ALADIN-Climate with the ocean model NEMOMED8 (red), CMCC, COSMO atmospheric model coupled with OPA ocean model (green), ENEA, RegCM4 regional atmospheric model coupled with MIT ocean model (blue), LATMOS, WRF atmospheric model coupled with NEMOMED8 ocean model (orange).

Finally, the evaluation of various terms of the surface MSWB and MSHB in some of the Med-CORDEX RCSMs and the corresponding RCMs is reported in L'Heveder et al. (2013), Sevault et al. (2014), 15 Lebeaupin-Brossier et al. (2015). Despite remaining biases in some the terms, these studies consistently demonstrate the added-value of the coupled vs. the uncoupled approach to reproduce the Mediterranean water and heat budgets.

-- Mediterranean ocean circulations, temperature and salinity

The ocean surface and thermohaline circulations are the engines of the heat and salt spatial redistribution and, in the vertical, determine the penetration of the climate change signal into the deep layers of the Mediterranean Sea. Within Med-CORDEX, various elements of the Mediterranean Sea circulation have been evaluated either in the RCSMs or in the stand-alone regional ocean models. For example, Soto-Navarro et al. (2014) evaluated the Strait of Gibraltar flow in an ensemble of NEMO-MED models using various horizontal and vertical resolutions and different forcings, while Pascual et al. (2014) and Meissignac et al. (2011) evaluated the eddy turbulent kinetic energy and sea level variability in a flux-driven ocean model.

The Mediterranean Sea thermohaline circulation is a complex and challenging phenomenon (MEDOC group 1970, Mertens and Schott 1998). It has been evaluated in many configurations of the Med-CORDEX models for the Eastern Mediterranean Basin in relation to the so-called Eastern Mediterranean Transient (Vervatis et al. 2013, Georgiou et al. 2014, Sevault et al. 2014) and for the Western Mediterranean Basin targeting the understanding of deep water formation (Beuvier et al. 2012, L'Heveder et al. 2013, Sevault et al. 2014). Note that RCSMs often show very good behaviours in simulating the interannual to decadal variability of the Mediterranean Sea thermohaline circulation (L'Heveder et al. 2013, Sevault et al. 2014) and sometimes are even better than the comparable flux-driven ocean runs (compare for example Sevault et al. 2014 and Beuvier et al. 2010).

Med-CORDEX offers a unique framework to intercompare various ocean models and better understand the way they reproduce the Mediterranean Sea circulation. We present here a first multi-model diagnostic study of stand-alone Med-CORDEX regional ocean models (figure 8) by analyzing the heat and salt content of the whole Mediterranean Sea (expressed as average temperature and salinity). The

ocean models are driven by different atmospheric forcings produced by dynamical downscaling of the ERA-40 or ERA-interim reanalyses. Two quality controlled subsurface ocean temperature and salinity observational data-sets are used for evaluation purposes (MedAtlas-II, Rixen et al 2005 and EN3, Ingleby and Huddleston 2007). The models represent quite well the inter-annual variability and long term trend of temperature, although 16 significant biases and differences can be found across the models. The choice of physical parameterizations (Sanchez-Gomez et al. 2011, Di Luca et al. 2012), and in particular the representation of clouds and turbulent fluxes, as well as the choice of system components (aerosols, ocean coupling, river coupling) are the dominant factors explaining the model biases and spread.
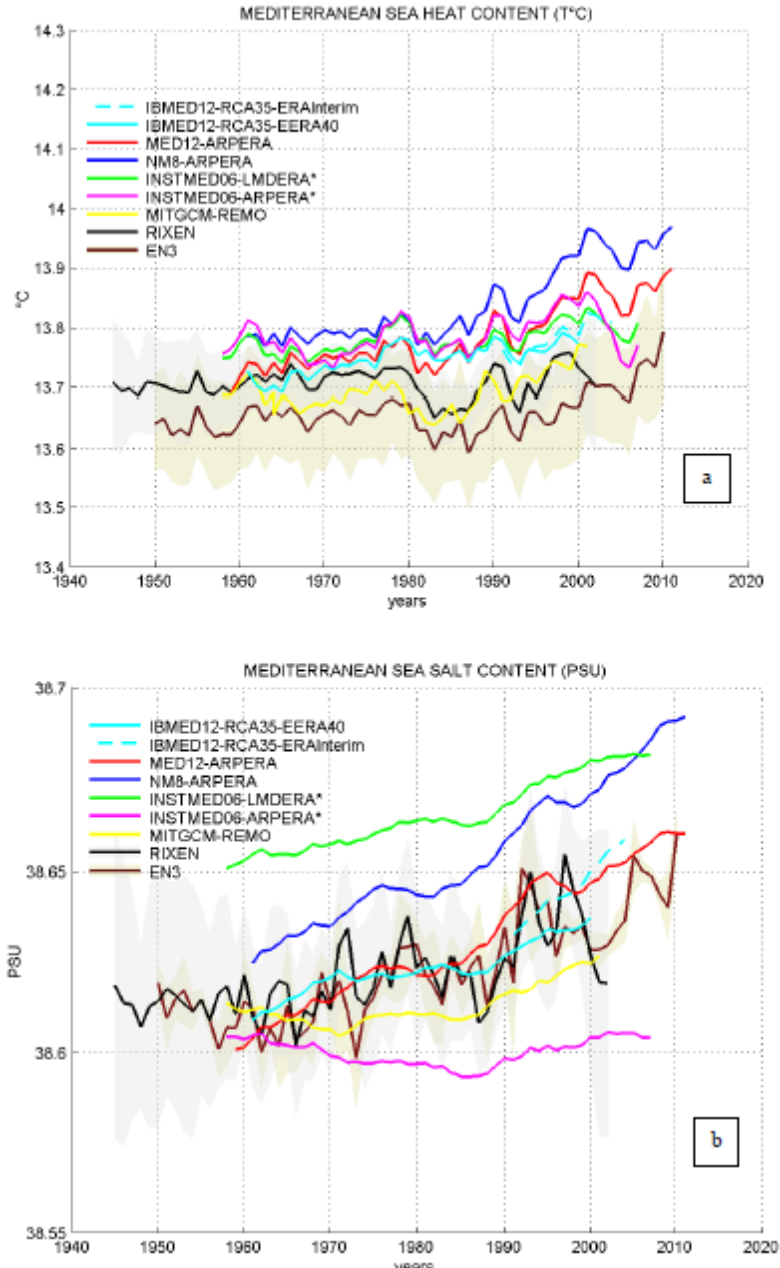
Figure 8. Time series of Mediterranean heat and salt content, defined as volume average of temperature (a) and salinity (b) for ocean stand-alone simulations using different atmospheric forcing produced by downscaling global reanalysis.

By comparison, the reproduction of salinity seems to be quite problematic both in terms of inter-annual variability and long term trends, also probably due to deficiencies in the observation sampling. In fact, the number, spatio-temporal coverage and quality of salinity in-situ observations is worse than for temperature,

leading to sampling errors when producing the gridded-products (Rixen et al. 2005, Jordà and Gomis 2013, Llasses et al. 2015).

-- River discharge

Med-CORDEX is also contributing to the integration of all components of the hydrological cycle throughout the coupling of land and ocean via river discharge. As an example of this contribution, Figure 9 shows the seasonal cycle of runoff for the most important Mediterranean rivers in observations and as computed by the river routing models embedded in two of the Med-CORDEX RCSMs. It can be seen that, although the amplitude of the seasonal cycle of discharge is mostly overestimated, the phase of this cycle, and in particular the peak discharge months, are well captured for all catchments. River discharge is an integrator of different processes, such as precipitation, soil infiltration, snowmelt and river routing, so that such type of analysis can provide valuable information on the ability of the coupled RCSMs to simulate the full hydrologic cycle of the basin. Other evaluations of river discharge can be found in Szczypta et al. (2012) for stand-alone land-hydrology models and in Sevault et al. (2014) for the CNRM coupled model RCSM4
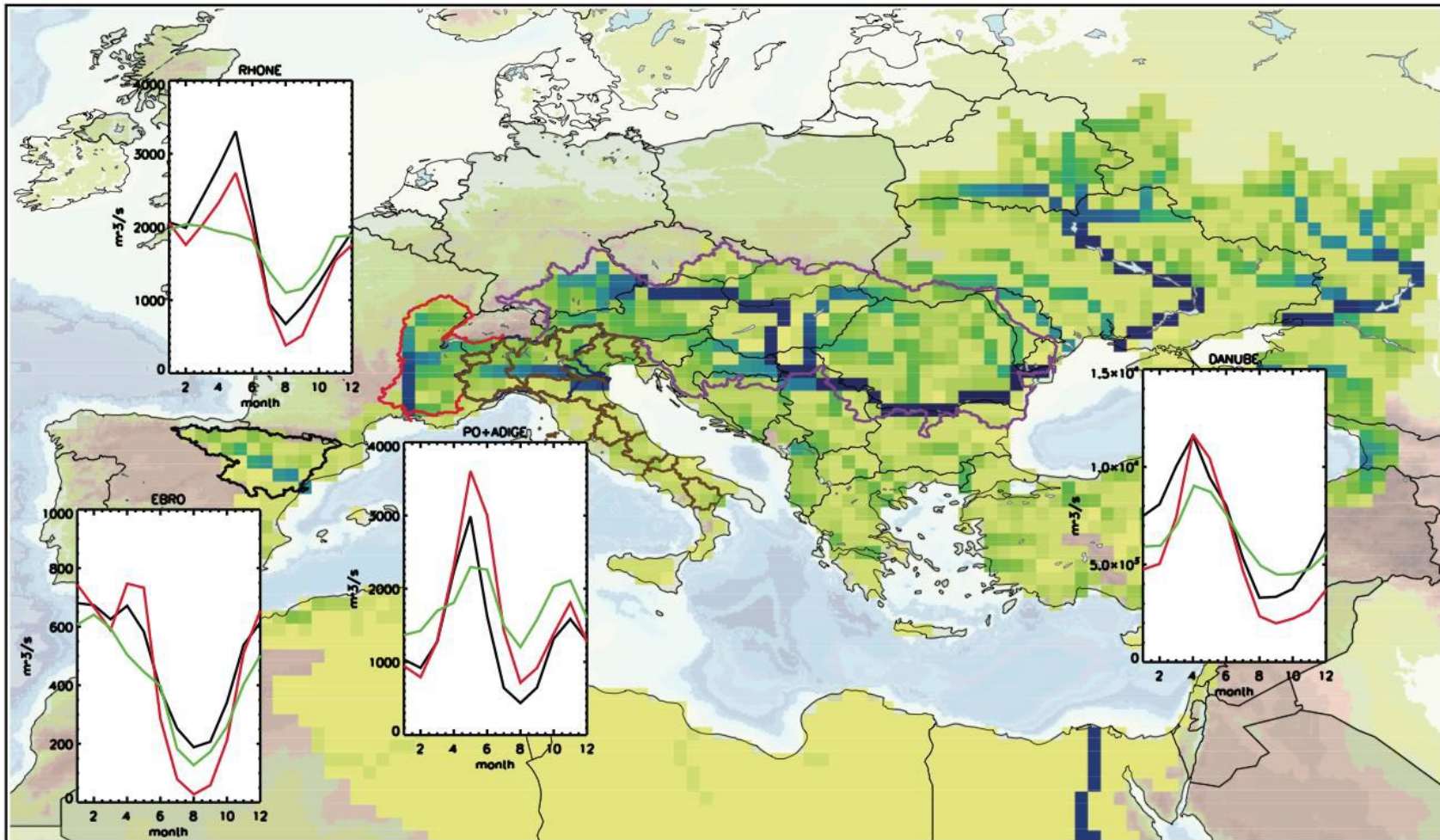
Figure 9. Seasonal cycle of runoff for the most important Mediterranean rivers. Black, ENEA coupled system; red, 1033 CNRM; green, observations. Average for the reference period 1970-2000. The four catchments are: the Ebro in Spain, 1034 the Rhone in France and Switzerland, the Po plus Adige in Northern Italy, the Danube.

-- Aerosols

Aerosols of natural and anthropogenic sources are an important component of the Mediterranean climate system. Within the Med-CORDEX context, the influence of the aerosol direct effect on biases, interannual variability and long-term trends of temperature and shortwave and longwave radiation have been investigated by Nabat et al. (2014, 2015a,b). In particular, Nabat et al. (2014) showed that the underestimation of the SST trend by the Med-CORDEX models noted in previous sections is at least partly due to the lack of the representation in the models of the decrease in European anthropogenic aerosol emissions starting from the 1980s, which resulted from stricter air pollution legislations and the economic crisis in Eastern Europe. This aerosol decreasing trend induces a positive surface shortwave trend and a detectable SST warming trend. Nabat et al. (2015a,b) then demonstrate the clear added-value in using coupled RCSMs with respect to SST-driven RCMs for the simulation of regional aerosol effects. These effects are indeed amplified when the Mediterranean SST is able to cool or warm in response to the aerosol radiative forcing over the sea. Aerosol-ocean-atmosphere regional feedbacks were highlighted by Nabat et al. (2015a,b) as important factors for the low-level humidity advection from the Eastern Mediterranean Sea towards the Sahara with a potential effect on the African monsoon.

2.4.3   Strengthening the link with the VIA research community

An important connection has been established between Med-CORDEX climate modeling groups and key impact sectors (ocean acidification, forest ecosystem, marine ecosystem, sea level). Through the use of Med-CORDEX simulations, several studies have been conducted to evaluate the climate variability and change impact on the Mediterranean region, here we provide key examples to marine ecosystems. Although marine ecosystems are influenced by many factors

such as eutrophication and overfishing, rising atmospheric CO2 and climate change are associated with shifts in temperature, circulation, stratification, and ocean acidification, with potentially wide-ranging biological impacts. A certain effort has been devoted to better link climate models with ecosystem models. It has been demonstrated that the use of modeled weather data can yield predictions similar to those generated from measured data, but only when data are provided at relatively high frequency. Montalto et al. (2014) modeled the effects of environmental change on the physiological response of an ecologically and commercially important species of mussel in the Mediterranean. Their results suggest that ecosystem model skill can be significantly influenced by the temporal resolution of environmental data. In addition, a better use of Mediterranean climate model information into community ecology models limits the uncertainty of future ranges of marine species (Hattab et al., 2014). Auger et al. (2014) analyzed the role of the winter mixing on the inter-annual variability of Mediterranean plankton dynamics using a high-resolution coupled hydrodynamic-biogeochemical model. They demonstrated how winter mixing induced inter-annual variability of winter nutrient contents controls spring primary production. Going from sub-regional to local impacts, Andrello et al. (2015) analyzed how the climate change will influence connectivity of marine protected areas over the period 1970-2099.

2.5 Med-CORDEX future plans

While considerable work is still ongoing on the analysis of the Med-CORDEX experiments completed to date, the discussion has started on the identification of key future challenges to be addressed by Med-CORDEX within the context of the next cycle of climate change research activities (e.g. the phase 6 of CMIP). Here we highlight three main foci for future Med-CORDEX activities:

A. **Understand the past variability of the Mediterranean regional climate system and characterize its possible future evolution, with emphasis on an integrated multi-component approach and on the**

study and attribution of the relative role of different regional/local climate drivers (natural and anthropogenic aerosols, high-resolution SST, land-use) with respect to the large-scale forcings (climate natural variability, greenhouse gas induced global climate change).

Motivations : Over the Mediterranean area, recent studies have shown that natural and anthropogenic aerosols can improve the representation of the regional climate mean state (Nabat et al. 2015a), shortwave and temperature daily variability (Nabat et al. 2015b) and long-term trends (Nabat et al. 2014). In addition, Anav et al. (2010) show that human-induced land-use and land-cover changes can influence the Mediterranean climate, while Stéfanon et al. (2014) illustrate how an interactive representation of vegetation can contribute to develop positive feedbacks during extreme climate events such as droughts and heat waves. Auger et al. (2014) and Palmieri et al. (2015) suggest that long-term Mediterranean Sea biogeochemistry is reaching a mature state allowing the coupling with the other climate system components, and ocean waves not yet commonly represented in RCMs could also play a key role at the atmosphere-ocean interface (Kudryavtsev et al. 2014) and in influencing the regional aerosol load (Ovadnevaite et al. 2014). Finally, the key role of complex topography and coastlines in modulating regional climates and extreme events has been amply illustrated above. It is thus clear that an increased understanding of the role of regional/local vs. global drivers of climate change within the context of a fully interactive regional climate system is central for a better understanding of the impacts of global warming in the Mediterranean.

Examples of scientific questions to be addressed within this challenge: What are the main drivers of the observed trends in Mediterranean SST ? Can we characterize, reproduce and explain the interannual variability of the Mediterranean salinity ? Can we quantify the role of the massive decrease in anthropogenic 19 aerosols in Europe on the Mediterranean climate trends since

1980 ? Can we reproduce and attribute the trends in latent heat loss and water mass observed over the Mediterranean Sea ? Can we reproduce and understand the regional/local sea level variability and change of the Mediterranean ? What are the main drivers of the Mediterranean river runoff long-term variability ? What are the main global and regional drivers of the climate variability of the Mediterranean aerosol load ? Can we characterize, reproduce and explain the interannual variability of the Mediterranean marine ecosystems ? Can we characterize, reproduce and explain the interannual variability and long-term trends of the Mediterranean climate extremes ? How will the Mediterranean regional climate and its various regional components evolve? How does the complex physiography of the Mediterranean region affect current and future climate trends over the region?

Modelling framework: Exploring the relative role of the large-scale drivers versus regional forcings on the regional climate variability and change requires the development, evaluation and use of a new generation of Mediterranean Regional Earth System Models (RESMs) in which the various components of the climate system are fully coupled (as in RCSMs) and the human component if adequately considered. This new generation RESMs will allow the Med-CORDEX community to explore the complex interactions and regional feedbacks which modulate the climate of the region and will need to have sufficient horizontal resolution to adequtely capture the Mediterranean topography and coasline features. Specifically, an innovative aspect of 26 this coupling exercise will be the better representation in the models of the influence of human activities on regional climate drivers, such as aerosols land-use and land-cover, urbanization, dams, reservoirs and irrigation, air quality.

Model evaluation: Evaluating RCSMs (or RESMs) is a new open challenge for the climate modelling community. Indeed high-resolution and multi-component observations are often missing at the regional scale. The future Med-CORDEX evaluation strategy will have to rely on a hierarchy of approaches : model evaluation on detailed case studies taken, for example, from the HyMeX, MerMex

or Charmex programmes, model evaluation against long-term multi-component in-situ super sites, evaluation using multi-component gridded products coming from satellite products or model-data regional reanalyses.

B. Investigate, understand and improve the description of regional climate phenomena critical for determining past climate variability and future evolution of Mediterranean climate, with emphasis on phenomena of importance for VIA applications.

Motivations : The Mediterranean is characterized by a plethora of phenomena of relevance not only for the climate of the region, but also for impacts on ecosystem and society: among others, heavy precipitation events, flash floods, Mediterranean cyclones and associated strong winds, strong air-sea exchanges and associated open-sea deep water formation, aerosol-radiation-cloud interactions, Mediterranean surface circulations, Mediterranean dense water formation and associated Mediterranean thermohaline circulation, droughts, heat waves, medicanes, strait transports, Mediterranean Sea oligotrophy and dynamic of the deep chlorophyll maximum. Med-CORDEX has evidenced a number of limitations of the present generation of models in simulating such events, tied to the coarse model resolution, drawbacks in model physics and dynamics representations, lack of descriptions of key feedbacks and interactions. Targeted activities will thus need to be designed in order to improve knowledge and modeling of these processes.

Examples of scientific questions to be addressed: What are the main processes underlying the triggering and evolution of the Mediterranean heavy precipitation events (e.g. > 100 mm/d) ? Can we improve the representation and characterization of the Mediterranean cyclogenesis ? Are "Medicanes" going to be more frequent in the future? Can we improve the understanding and representation of the interactions and feedbacks that can enhance Mediterranean drought events ? Can we improve the understanding and representation of Mediterranean dense water formation phenomena in climate models ? Can we

improve the representation of the occurrence and characteristics of intense wind events (e.g. Mistral, Bora)? Can we improve the characterization of changes in storm surges as affected by regional sea level rise and the occurrence of intense storms?

Modelling framework: RCMs allow us to test in a well-constrained framework many modeling options targeting the understanding and representation of key climate phenomena and their variability for a given region. Case studies, long-term hindcast and historical-scenario configurations can be used towards this goal. Model improvements can be achieved by increasing the spatial resolution up to convection-resolving Atmosphere-RCMs or eddy-resolving Ocean-RCMs, by adding new components in the RCSMs (e.g. towards the development of RESMs including the human component) or by developing new targeted physical parameterizations.

Model evaluation: This task will require the development of high quality, fine scale datasets suitable for the process-based assessments of the models. Improving the representation of regional phenomena in the Mediterranean RCMs will also strengthen collaborations with the observation and process-based analysis 21 communities (e.g. HyMeX), the numerical weather prediction communities and the global circulation model development community, as weather forecast models, RCMs and GCMs often share common deficiencies in reproducing some of the key regional climate phenomena. A further goal of this challenge is to provide a robust and quantitative assessment of the added value obtained in using RCSMs to simulate important regional phenomena over the region.

C. **Improve the characterization of the impacts of the Mediterranean climate variability and climate change on human activities and natural ecosystems, towards the development of actionable Mediterranean climate services.**

Motivations: The increasing need to assess the impacts of climate variability and change over the Mediterranean requires a better characterization, in particular, of the uncertainties associated with regional climate projections. This in turn requires the completion of large ensembles of coordinated model experiments, both for the historical past and future climate conditions, with multiple models, scenarios, realizations and model configurations. Providing consistent and comprehensive scenarios for the various regional components of the Mediterranean climate system is also a key challenge.

Climate services to be addressed: Covering the whole range of potential climate services is not feasible, thus the Med-CORDEX efforts will be directed towards providing climate information, and evaluation of related uncertainties, for areas that are specific to the Mediterranean, e.g.: maritime activities (ocean biodiversity and marine protected areas, maritime transport, ocean pollution, fish and fisheries, aquaculture), coastal activities such as tourism (coastal, islands, sea-related tourism), sustainable energy (solar energy, wave energy, wind farm, ...), water resources and agriculture (combining human and climate influence), regional/local geoengineering, biodiversity conservation planning.

Modelling framework: Targeted experiments will be designed to explore the importance of specific forcings (e.g. aerosols, land use, wave) in shaping the future of the Mediterranean climate. This will complement the completion of a large coordinated multi-model ensemble of regional climate change scenarios using RESMs and very high resolution atmospheric RCMs in coordination with the CMIP6 and CORDEX frameworks. This will require the development of strategies for the selection of CMIP6 GCMs to be used to drive the regional simulations. Climate change information concerning all the components of the regional climate will be provided in user-friendly format and with associated metadata. Post-processing techniques will be needed to 22 distill the most robust and accurate information for use in VIA studies (e.g. model weighting, bias correction, local scale downscaling, specific sectorial indicators) and techniques will need to be developed for a quantitative estimation of uncertainties within a risk-based

probabilistic approach (e.g. Bayesian approaches). This activity will allow a strong interaction with the Med-CLIVAR community and will promote the Med-CORDEX results within the context of the next Intergovernmental Panel on Climate Change (IPCC) report or of a possible forthcoming Regional Assessment of Climate Change in the Mediterranean (RACCM).

Future Med-CORDEX activities will gather momentum in the next decades for a number of reasons. The Mediterranean has been recognized as a hotspot for climate change, vulnerability, adaptation issues and biodiversity loss; the Mediterranean has been selected as a GEWEX region (HyMeX) and a CLIVAR focus area (Med-CLIVAR); the contacts between the RCM community and the observation and process community are already very strong, in particular due to long term initiatives such as HyMeX and Med-CLIVAR. In addition, most of the new Grand Challenges identified by the WCRP are particularly relevant within the Mediterranean context: (1) Clouds, Circulation and Climate Sensitivity can be explored at regional scale for an area that is particularly sensitive to global climate change, (2) Changes in the cryosphere can profoundly affect Alpine glaciers, (3) Climate Extremes are one of the key challenges for impacts in the Mediterranean, (5) Regional Sea-level Rise is highly relevant for Mediterranean coastal activities and ecosystems, and (6) Water Availability is a central issue in many water stressed areas of the Mediterranean.

Med-CORDEX will provide an optimal framework for coordinating the modeling activities in the region towards addressing these challenges with common simulation protocols. We also envision an enhanced coordination with other CORDEX regional programs for which the Med-CORDEX specificities (coupled regional modeling, high resolution modeling, aerosol and land-use modeling) are especially relevant:, for example CORDEX Africa on the key topics of the dust aerosols and on the effect of the Mediterranean Sea on the African monsoon; Euro-CORDEX on the development of convection-resolving RCMs and the study of land use effects; Middle Eastern North Africa (MENA) domain concerning the water resources issue; and Arctic and Baltic communities for common developments of

coupled RESMs. The discussion on specific future experiment strategies and protocols for Med-CORDEX are currently under way and they will be finalized during the next Pan-CORDEX conference to take place in Stockholm in May 2016.

2.6   References

Adloff F., Somot S., Sevault F., Déqué M., Herrmann M., Dubois C., Aznar R. Padorno E., Alvarez-Fanjuls E., Jordà G., Gomis D. (2015). Mediterranean Sea response to climate change in an ensemble of twenty first century scenarios. Clim. Dyn. 10.1007/s00382-015-2507-3

Akhtar, N., Brauch, J., Dobler, A., Béranger, K., & Ahrens, B. (2014). Medicanes in an ocean–atmosphere 641 coupled regional climate model. Natural Hazards and Earth System Sciences Discussions, 2(3), 2117-2149.

Alpert, P, Stein U, Tsidulko M (1995) Role of sea fluxes and topography in eastern Mediterranean cyclogenesis. In: The global atmosphere and ocean system, vol 3, pp 55–79 645

Anav, A., Ruti, P. M., Artale, V., Valentini, R. (2010). Modelling the effects of land-cover changes on surface 647 climate in the Mediterranean region. Climate research, 41(2), 91.

Andrello M., Mouillot D., Somot S., Thuiller W., Manel S. (2015). Additive effects of climate change on connectivity among marine protected areas and larval supply to fished areas. Diversity and Distributions, 21, 139-150.

Artale V, S Calmanti, PM Rizzoli, G Pisacane, V Rupolo, M Tsimplis (2006). The Atlantic and Mediterranean Sea as connected systems. Developments in Earth and Environmental Sciences, Volume 4, 2006, Pages 283-323

Auger P.A., Ulses C., Estournel C., Stemman L., Somot S., Diaz F. (2014). Interannual control of plankton ecosystem in a deep convection area as inferred from a 30-year 3D modeling study: winter mixing and prey/predator interactions

in the NW Mediterranean. Progress in Oceanography: 12-27, DOI: 10.1016/j.pocean.2014.04.004

Bergamo, A., Tafuro, A. M., Kinne, S., De Tomasi, F., and Perrone, M. R. (2008). Monthly-averaged anthropogenic aerosol direct radiative forcing over the Mediterranean based on AERONET aerosol properties, Atmos. Chem. Phys., 8, 6995–7014, doi:10.5194/acp-8-6995-2008.

Berthou S, Mailler S, Drobinski P, Arsouze T, Bastin S, Béranger K, Lebeaupin-Brossier C. (2014). Prior history of mistral and tramontane winds modulates heavy precipitation events in southern france. Tellus A 66(0), doi:10.3402/tellusa.v66.24064.

Berthou S, Mailler S, Drobinski P, Arsouze T, Bastin S, Beranger K, Lebeaupin-Brossier C. (2015). Sensitivity of an intense rain event between atmosphere-only and atmosphere-ocean regional coupled models: 19 september 1996. Q. J. R. Meteorol. Soc. 141:258–271, doi:10.1002/qj.2355.

Beuvier J., Béranger K., Lebeaupin-Brossier C., Somot S., Sevault F., Drillet Y., Bourdallé-Badie R., Ferry N., Lyard F. (2012) Spreading of the Western Mediterranean Deep Water after winter 2005: time scales and deep cyclone transport. J. Geophys. Res.-Oceans. doi:10.1029/2011JC007679

Buzzi A, Tibaldi S (1978) Cyclogenesis in the lee of the Alps: a case study. Quart J Roy Meteor Soc 104:271

Campins, J., Genovés, A., Picornell, M. A. and Jansà, A. (2011), Climatology of Mediterranean cyclones using the ERA-40 dataset. Int. J. Climatol., 31: 1596–1614. doi: 10.1002/joc.2183

Christensen, J.H., B. Machenhauer, R.G. Jones, C. Schar, P.M. Ruti, M. Castro and G. Visconti (1997). "Validation of present-day regional climate simulations over Europe: LAM simulations with observed boundary conditions''. Climate Dynamics, 13, pp 489-506, 10.1007/s003820050178.

Christensen, J.H., Carter, T.R., Rummukainen, M. and Amanatidis, G. (2007). Evaluating the performance and utility of regional climate models: the PRUDENCE project, Climatic Change, vol. 81, 1–6.

Chronis, T., Papadopoulos, V., and Nikolopoulos, E. (2010). QuickSCAT observations of extreme wind events over the Mediterranean and Black Seas during 2000–2008, Int. J. Clim., doi:10.1002/joc.2213.

Dee, D. P., S. M. Uppala, A. J. Simmons, P. Berrisford, P. Poli, S. Kobayashi, U. Andrae, M. A. Balmaseda, 60 G. Balsamo, P. Bauer, P. Bechtold, A. C. M. Beljaars, L. van de Berg, J. Bidlot, N. Bormann, C. Delsol, R. Dragani, M. Fuentes, A. J. Geer, L. Haimbergere, S. B. Healy, H. Hersbach, E. V. Holm, L. Isaksen, P. Kallberg, M. Khler, M. Matricardi, A. P. McNally, B. M. Monge-Sanzf, J.-J. Morcrette, B.-K. Park, C. Peubey, P. de Rosnaya, C. Tavolato, J.-N. Thepaut, and F. Vitart (2011), The era-interim reanalysis: conguration and performance of the data assimilation system, Quarterly Journal of the Royal Meteorological Society, 137, doi:10.1002/qj.828.

Dell'Aquila A, S Calmanti, PM Ruti, MV Struglia, G Pisacane, C Adriana, G Sannino, (2012) Impacts of seasonal cycle fluctuations over the Euro-Mediterranean area using a Regional Earth System model. Climate Research, 2, 135.

Diffenbaugh, N.S., and F. Giorgi (2012). Climate change hot-spots in the CMIP5 global climate model ensemble. Climate Change Letters, 114, 813-822.

Di Luca, A., Flaounas, E., Drobinski, P., & Brossier, C. L. (2014). The atmospheric component of the Mediterranean Sea water budget in a WRF multi-physics ensemble and observations. Climate Dynamics, 43(9-10), 2349-2375.

Drobinski, P, V Ducrocq, P Alpert, P Alpert, E Anagnostou, K Beranger, M Borga, I Braud, S Davolio, G 699 Delrieu, C Estournel, N Filali Boubrahmi, J Font, V Grubisic, S Gualdi, V Homar, B Ivancna-Picek, C Kottmeier, V Kotroni, K Lagouvardos, P Lionello, MC Liasat, W Ludwig, C Lutoff, A Mariotti, E Richard, R

Romero, R Rotumno, O Roussot, I Ruin, S Somot, I taupier-Letage, J Tintore, R Ujlenhoet, and H Wernill, (2014). Humex a 10-year multidisciplinary program on the Mediterranean water cycle. BAMS, 95, 1063-1082, doi: 10.1175/BAMS-D-12-00242.1.

Dubois C., S. Somot, S. Calmanti, A. Carillo, M. Déqué, A. Dell'Aquilla, A. Elizalde-Arellano, S. Gualdi, D. Jacob, B. Lheveder, L.Li, P. Oddo, G. Sannino, E. Scoccimarro, F. Sevault (2012) Future projections of the surface heat and water budgets of the Mediterranean sea in an ensemble of coupled atmosphere-ocean regional climate models, Clim. Dyn. 39 (7-8):1859-1884. DOI 10.1007/s00382-011-1261-4.

Ducrocq, V., Braud, I., Davolio, S., Ferretti, R., Flamant, C., Jansà, A., Kalthoff, N., Richard, E., Taupier- Letage, I., Ayral, P.-A., Belamari, S., Berne, A., Borga, M., Boudevillain, B., Bock, O., Boichard, J.-L., Bouin, M.-N., Bousquet, O., Bouvier, C., Chiggiato, J., Cimini, D., Corsmeier, U., Coppola, L., Cocquerez, P., Defer, E., Delanoë, J., Di Girolamo, P., Doerenbecher, A., Drobinski, P., Dufournet, Y., Fourrié, N., Gourley, J. J., Labatut, L., Lambert, D., Le Coz, J., Marzano, F. S., Molinié, G., Montani, A., Nord, G., Nuret, M., Ramage, K., Rison, B., Roussot, O., Said, F., Schwarzenboeck, A., Testor, P., Van-Baelen, J., Vincendon, B., Aran, M. and Tamayo, J. (2014). HyMeX-SOP1, the field campaign dedicated to heavy precipitation and flash flooding in the northwestern Mediterranean Bulletin of the American Meteorological Society, 95, 1083-1100.

Durrieu de Madron X., Houpert L., Sanchez-Vidal A., Puig P., Testor P., Estournel C., Somot S., Bourrin F., Canals M., Palanques A., Mortier L., Bouin M.N., Heussner S., Calafat A., Martin J., Font J., Kunesch S., Raimbault P. (2013) Interaction of deep dense shelf water cascading and open-sea convection in the Northwestern Mediterranean in winter 2012 , Geophysical Research Letters, 40, 1–7, doi:10.1002/grl.50331

Flaounas E., Drobinski P., Bastin S. (2013). Dynamical downscaling of IPSL-CM5 CMIP5 historical simulations over the Mediterranean: Benefits on the

representation of regional wind and cyclogenesis Clim Dyn, 40 (9-10) 40:2497-2513. DOI 10.1007/s00382-012-1606-7

Georgiou, S., Mantziafou A., Sofianos S., Gertman I., Özsoy E., Somot S., Vervatis V. (2014) Climate variability and deep water mass characteristics in the Aegean Sea, Atmospheric Research (in press), http://dx.doi.org/10.1016/j.atmosres.2014.07.023

Giorgi, F., (2006). Climate change hot-spots. Geophys. Res. Lett., 33:L08707, doi:10.1029/2006GL025734 Giorgi, F. and Mearns, L.O. (1999). Introduction to special section: Regional Climate Modeling Revisited. Journal of Geophysical Research 104: doi: 10.1029/98JD02072. issn: 0148-0227.

Giorgi F, C Jones, GR Asrar , (2009). Addressing climate information needs at the regional level: the CORDEX framework. WMO Bulletin 58 (3) – July 2009.

Goodess, (2003) The EGGS, Issue No. 6, 10 December 2003. Gualdi S., S. Somot, L. Li, V. Artale, M. Adani, A. Bellucci, A. Braun, S. Calmanti, A. Carillo, A. Dell'Aquilla, M. Déqué, C. Dubois, A. Elizalde, A. Harzallah, B. Lheveder, W. May, P. Oddo, P. Ruti, A. Sanna, G. Sannino, E. Scoccimarro, F. Sevault and A. Navarra (2013a) The CIRCE simulations: a new set of regional climate change projections performed with a realistic representation of the Mediterranean Sea. Bull. Amer. Meteor. Soc., 94, 65-81, DOI 10.1175/BAMS-D-11-00136.1

Guieu, C., Dulac, F., Desboeufs, K., Wagener, T., Pulido-Villena, E., Grisoni, J.-M., Louis, F., Ridame, C., Blain, S., Brunet, C., Bon Nguyen, E., Tran, S., Labiadh, M., and Dominici, J.-M. (2010). Large clean mesocosms and simulated dust deposition: a new methodology to investigate responses of marine oligotrophic ecosystems to atmospheric inputs, Biogeosciences, 7, 2765– 2784, doi:10.5194/bg-7-2765- 2010.

Hattab T., Albouy C., Lasram F.B.R., Somot S., Leloc'h F., Leprieur F. (2014). Towards a better understanding of potential climate change impacts on marine species distribution. Global Ecology and Biogeography, 23, Issue 12, 1417-1429.

Harader E., Ricci S., Borrell-Estupina V., Boé J., Terray L., Somot S. (2015). The added value of regional climate model resolution for the reproduction of precipitation extremes over France, Clim Dyn (in revision) Herrmann, M. and Somot, S. (2008). Relevance of ERA40 dynamical downscaling for modeling deep convection in the Mediterranean Sea, Geophys. Res. Lett., 35, L04607, doi:10.1029/2007GL032442.

Herrmann M., Sevault F., Beuvier J., Somot S. (2010) What induced the exceptional 2005 convection event in the Northwestern Mediterranean basin? Answers from a modeling study. JGR-O (in press), doi:10.1029/2010JC006162

Herrmann M., Somot S., Calmanti S., Dubois C., Sevault F. (2011) "Representation of daily wind speed spatial and temporal variability and intense wind events over the Mediterranean Sea using dynamical downscaling: impact of the regional climate model configuration", Nat. Hazards Earth Syst. Sci., 11, 1983-2001, doi:10.5194/nhess-11-1983-2011

Ingleby, B., and M. Huddleston (2007). Quality control of ocean temperature and salinity profiles - historical and real-time data. Journal of Marine Systems, 65, 158-175 10.1016/j.jmarsys.2005.11.019

Ivanovic RI, PJ. Valdes, L Gregoire, R Flecker, M Gutjahr, (2014). Sensitivity of modern climate to the presence, strength and salinity of Mediterranean-Atlantic exchange in a global general circulation model. Climate Dynamics, Volume 42, Issue 3-4, pp 859-877.

Jordà , G. and Gomis, D. (2013). On the interpretation of the steric and mass components of sea level variability: the case of the Mediterranean basin. J. Geophys. Res. Oceans. 118(2), 953 963.

Josey S (2003) Changes in the heat and freshwater forcing of the eastern Mediterranean and their influence on deep water formation. J Geophys Research 108 (C7)

Josey, S. A., S. Somot, and M. Tsimplis (2011), Impacts of atmospheric modes of variability on Mediterranean Sea surface heat exchange, J. Geophys. Res., 116, C02032, doi:10.1029/2010JC006685.

Kudryavtsev, V., Chapron, B., & Makin, V. (2014). Impact of wind waves on the air-sea fluxes: A coupled model. Journal of Geophysical Research-Oceans, 119(2), 1217–1236. doi:10.1002/2013JC009412

Kuglitsch, F. G., A. Toreti, E. Xoplaki, P. M. Della-Marta, C. S. Zerefos, M. Türkeş, and J. Luterbacher (2010), 783 Heat wave changes in the eastern Mediterranean since 1960, Geophys. Res. Lett., 37, L04802, doi:10.1029/2009GL041841.

L'Heveder B., Li L., Sevault F., Somot S. (2013). Interannual variability of deep convection in the Northwestern Mediterranean simulated with a coupled AORCM. Climate Dyn., 41:937-960. doi : 10.1007/s00382-012-1527-5.

Lebeaupin-Brossier C., Drobinski P., Beranger K., Bastin S., Orain F. (2013). Ocean memory effect on the dynamics of coastal heavy precipitation preceded by a mistral event in the North-Western mediterranean. QJRMS, 139 (675), 1583-1597, 2013

Lebeaupin Brossier, C., S. Bastin, K. Béranger, and P. Drobinski, (2015). Regional mesoscale air-sea coupling impacts and extreme meteorological events role on the Mediterranean Sea water budget. Clim. Dyn., 44 (3), 1029-1051, doi:10.1007/s00382-014-2252-z.

Lelieveld, J., Berresheim, H., Borrmann, S., Crutzen, P. J., Dentener, F. J., Fischer, H., Feichter, J., Flatau, P. J., Heland, J., Holzinger, R., Korrmann, R., Lawrence, M. G., Levin, Z., Markowicz, K. M., Mihalopoulos, N., Minikin, A., Ramanathan, V., de Reus, M., Roelofs, G. J., Scheeren, H. A., Sciare, J., Schlager, H., Schultz, M., Siegmund, P., Steil, B., Stephanou, E. G., Stier, P., Traub, M.,Warneke, C.,Williams, J., and Ziereis, H. (2002). Global Air Pollution

Crossroads over the Mediterranean, Science, 298, 794–799, doi:10.1126/science.1075457, 2002.

Llasses, J., Jordà , G. and Gomis, D. (2014). Skills of different hydrographic networks to capture changes in the Mediterranean Sea at climate scales. Clim. Res. (in press)

Machenhauer B, Wildelband M, Botzet M, Jones RG, Déqué M. (1996). Validation of present-day regional climate simulations over Europe: Nested LAM and variable resolution global model simulations with observed or mixed-layer ocean boundary conditions. Max-Planck Institute Report 191. Max-Planck-Institut fur Meteorologie: Hamburg, Germany.

Machenhauer B, Windelband M, Botzet M, Christensen JH, Déqué M, Jones J, Ruti PM, Visconti G (1998) Validation and analysis of regional present-day climate and climate change simulations over Europe. MPI Report No 275, MPI, Hamburg, Germany, 87 pp

Macias, D., Garcia-Gorriz, E., Stips, A. (2013). Understanding the causes of recent warming of Mediterranean waters. How much could be attributed to climate change? PloS one, 8(11), e81591.

MEDOC Group (1970) Observations of formation of deep-water in the Mediterranean Sea. Nature 227:1037-1040

Mertens C and Schott F (1998) Interannual variability of deep-water formation in the Northwestern Mediterranean. J Phys Oceanogr 28:1410-1424

Meyssignac B., Calafat F., Somot S., Rupolo V., Stocchi P., Llovel W., Cazenave A. (2011) Two-dimensional reconstruction of the Mediterranean sea level over 1970-2006 from tide gauge data and regional ocean circulation model outputs. Global and Planetary Change, doi:10.1016/j.gloplacha.2011.03.002

Montalto, V, G Sara, PM Ruti, A Dell'Aquila, B Helmuth (2014). Testing the effects of temporal data resolution on predictions of the effects of climate change

on bivalves. Ecological Modelling (Impact Factor: 2.07). 04/2014; 278:1–8. DOI: 10.1016/j.ecolmodel.2014.01.019

Moulin, C., Lambert, C. E., Dayan, U., Masson, V., Ramonet, M., Bousquet, P., Legrand, M., Balkanski, Y. J., 835 Guelle, W., Marticorena, B., Bergametti, G., and Dulac, F.: Satellite climatology of African dust transport in the Mediterranean atmosphere, J. Geophys. Res., 103, 13137–13144, doi:10.1029/98JD00171, 1998.

Nabat P., Somot S., Mallet M., Sanchez-Lorenzo A., Wild M. (2014) Contribution of anthropogenic sulfate aerosols to the changing Euro-Mediterranean climate since 1980. Geophys. Res. Lett., Volume 41, Issue 15, pages 5605–5611, doi:10.1002/2014GL060798

Nabat P., Somot S., Mallet M., Sevault F., Chiacchio M., Wild M. (2015a). Direct and semi-direct aerosol radiative effect on the Mediterranean climate variability using a coupled Regional Climate System Model. Clim. Dyn. 44, 1127-1155, DOI:10.1007/s00382-014-2205-6,

Nabat P., S. Somot, M. Mallet, M. Michou, F. Sevault, F. Driouech, D. Meloni, A. Di Sarra, C. Di Biagio, P. Formenti, M. Sicard, J.-F. Léon, and M.-N. Bouin (2015b). Dust aerosol radiative effects during summer 2012 simulated with a coupled regional aerosol-atmosphere-ocean model over the Mediterranean. ACPD/AMTD (in revision).

MS No.: acp-2014-527, Special Issue: CHemistry and AeRosols Mediterranean EXperiments (ChArMEx) http://dx.doi.org/10.1175/BAMS-D-11-00154.1

Ovadnevaite, J., Manders, A., de Leeuw, G., Ceburnis, D., Monahan, C., Partanen, A. I., et al. (2014). A sea spray aerosol flux parameterization encapsulating wave state. Atmospheric Chemistry and Physics, 14(4), 1837–1852. doi:10.5194/acp-14-1837-2014

Palmiéri J., Orr J.C., Dutay J.C., Béranger K., Schneider A., Beuvier J., Somot S. (2015) Simulated anthropogenic CO2 storage and acidification of the Mediterranean Sea Biogeosciences, 12, 781-802, 2015, doi:10.5194/bg-12-781-2015

Papadopoulos V.P., S. Josey; A. Bartzokas; S. Somot; S. Ruiz; P. Drakopoulou (2012) Large scale atmospheric circulation favoring deep and intermediate water formation in the Mediterranean Sea. J. Climate, 25 (18): 6079–6091, doi: 10.1175/JCLI-D-11-00657.1

Pascual A., Vidal-Vijande E., Ruiz S., Somot S., Papadopoulos V. (2014) Spatio-temporal variability of the surface circulation in the Western Mediterranean: a comparative study using altimetry and modeling. In The Mediterranean Sea: Temporal Variability and Spatial Patterns, Geophysical Monograph 202". Eds.

Borzelli G.L.E., M. Gacic, P. Lionello, P. Malanotte-Rizzoli, American Geophysical Union (First Edition). ISBN-10: 1118847342 862 863 Pfahl, Stephan, Heini Wernli (2012). Quantifying the Relevance of Cyclones for Precipitation Extremes. J. 864 Climate, 25, 6770–6780. doi: http://dx.doi.org/10.1175/JCLI-D-11-00705.1

The PROTHEUS group (2010). An Atmosphere-Ocean Regional Climate Model for the Mediterranean area: Assessment of a Present Climate Simulation. Climate Dynamics DOI 10.1007/s00382-009-0691-8

Quintana-Seguí, P., and Coauthors (2008). Analysis of Near-Surface Atmospheric Variables: Validation of the SAFRAN Analysis over France. J. Appl. Meteor. Climatol., 47, 92–107.

Rixen, M., et al. (2005), The Western Mediterranean Deep Water: A proxy for climate change, Geophys. Res. Lett., 32, L12608, doi:10.1029/2005GL022702.

Roether W, Manca B, Klein B, Bregant D, Georgopoulos D, Beitzel W, Kovacevic V, Luchetta A (1996). Recent changes in Eastern Mediterranean Deep Waters. Science 271:333-334

Rudari, Roberto, Dara Entekhabi, Giorgio Roth (2004). Terrain and Multiple-Scale Interactions as Factors in Generating Extreme Precipitation Events.J. Hydrometeor, 5, 390–404.doi: http://dx.doi.org/10.1175/1525-7541(2004)0052.0.CO;2

Ruti P.M., S. Marullo, F. D'Ortensio and M Tremant, (2008). Comparison of analyzed and measured wind speeds in the perspective of oceanic simulations over the Mediterranean basin: analyses, QuikSCAT and buoy data. Journal of Marine System, 70, 33-48, DOI 10.1016/j.jmarsys.2007.02.026.

Sanchez-Gomez E., Somot S., Josey S.A., Dubois C., Elguindi N., Déqué M. (2011). Evaluation of the Mediterranean Sea Water and Heat budgets as simulated by an ensemble of high resolution Regional Climate Models. Clim. Dyn., 37:2067-2086, doi:10.1007/s00382-011-1012-6

Sanna, A., Lionello, P., & Gualdi, S. (2013). Coupled atmosphere ocean climate model simulations in the Mediterranean region: effect of a high-resolution marine model on cyclones and precipitation. Natural Hazards and Earth System Science, 13(6), 1567-1577.

Schneider, C.; Laize, C.L.R.; Acreman, M.C.; Florke, M. (2013). How will climate change modify river flow regimes in Europe? Hydrology and Earth System Sciences, 17 (1). 325-339. 10.5194/hess-17-325-2013

Sciare, J., Oikonomou, K., Favez, O., Liakakou, E., Markaki, Z., Cachier, H., and Mihalopoulos, N.: Long-term measurements of carbonaceous aerosols in the Eastern Mediterranean: evidence of long-range transport of biomass burning, Atmos. Chem. Phys., 8, 5551–5563, doi:10.5194/acp-8-5551-2008, 2008.

Sevault F., Somot S., Alias A., Dubois C., Lebeaupin-Brossier C., Nabat P., Adloff F., Déqué M. and Decharme B. (2014). A fully coupled Mediterranean

regional climate system model: design and evaluation of the ocean component for the 1980-2012 period. Tellus A, 66, 23967

Somot S. , Sevault F., Déqué M., Crépon M. (2008). 21st century climate change scenario for the Mediterranean using a coupled Atmosphere-Ocean Regional Climate Model. Global and Planetary Change, 63(2-3), pp. 112-126, doi:10.1016/j.gloplacha.2007.10.003

Soto-Navarro J., Somot S., Sevault F., Beuvier J., Béranger K., Criado-Aldeanueva F., García-Lafuente J. (2014). Evaluation of regional ocean circulation models for the Mediterranean Sea at the strait of Gibraltar: volume transport and thermohaline properties of the outflow. Clim.Dyn. Climate Dynamics, 1-16. doi: 914 10.1007/s00382-014-2179-4

Stahl, K., Hisdal, H., Hannaford, J., Tallaksen, L. M., van Lanen, H. A. J., Sauquet, E., Demuth, S., Fendekova, M. and Jódar, J., Hydrology and Earth System Sciences 14(12), 2367–2382. doi:10.5194/hess- 918 14-2367-2010

Stéfanon, M., Schindler, S., Drobinski, P., de Noblet-Ducoudré, N., & D'Andrea, F. (2014). Simulating the 33 effect of anthropogenic vegetation land cover on heatwave temperatures over central France. Climate research, 60(2), 133-146.

Szczypta C., Decharme B., Carrer D., Calvet J.-C., Lafont S., Somot S., Faroux S., and Martin E. (2012) .Impact of precipitation and land biophysical variables on the simulated discharge of European and Mediterranean rivers. Hydrol. Earth Syst. Sci., 16, 3351-3370, doi:10.5194/hess-16-3351-2012

Torma Cs, Giorgi F and Coppola E (2015). Added value of regional climate modeling over areas characterized by complex terrain - Precipitation over the Alps. (Submitted to Journal of Geophysical Research: Atmospheres.)

Tous, M., Romero, R., & Ramis, C. (2013). Surface heat fluxes influence on medicane trajectories and intensification. Atmospheric Research, 123, 400-411.

Uwe, Ulbrich, et al. (2012). Climate of the Mediterranean: Synoptic patterns, temperature, precipitation, winds and their extremes, pp. 301—334. Chapter 5 of The Climate of the Mediterranean Region from the past to the future Ed P Lionello, 2012. Elsevier, Amsterdam, ISBN: 978-0-12-416042-2

Van der Linden P, Mitchell JFB (eds). (2009). ENSEMBLES: Climate change and its impacts: Summary of research and results fromthe ENSEMBLES project. Met Office Hadley Centre, Exter.

Vervatis, V. D., S. S. Sofianos, N. Skliris, S. Somot, A. Lascaratos, and M. Rixen (2013), Mechanisms controlling the thermohaline circulation pattern variability in the Aegean-Levantine region. A hindcast simulation (1960-2000) with an eddy resolving model, Deep-Sea Research Part I, 74:82-97, 942 doi:10.1016/j.dsr.2012.12.011   943 (http://www.sciencedirect.com/science/article/pii/S0967063713000198)

Vilibić, I., & Orlić, M. (2002). Adriatic water masses, their rates of formation and transport through the Otranto Strait. Deep Sea Research Part I: Oceanographic Research Papers, 49(8), 1321-1340.

CHAPTER 3

A multi-model ensemble view of winter heat flux dynamics and the dipole mode in the Mediterranean Sea

The scientist does not study nature because it is useful to do so. He studies it because he takes pleasure in it, and he takes pleasure in it because it is beautiful. If nature were not beautiful it would not be worth knowing, and life would not be worth living.

Henri Poincaré - Science and Method

This chapter, which is my personal contribution to the Med-COREDX project, investigates the Mediterranean Sea heat flux climate variability during winter in a set of 12 regional climate models as well as observations. The content of this chapter has been published in the following manuscripts:

3.1 Abstract

Changes in surface heat fluxes affect several climate processes controlling the Mediterranean climate. These include the winter formation of deep waters, which is the primary driver of the Mediterranean Sea overturning circulation. Previous studies that characterize the spatial and temporal variability of surface heat flux anomalies over the basin reveal the existence of two statistically dominant patterns of variability: a monopole of uniform sign and an east-west dipole of opposite signs. In this work, we use the 12 regional climate model ensemble from the EU-FP6 ENSEMBLES project to diagnose the large-scale atmospheric processes that control the variability of heat fluxes over the Mediterranean Sea from interannual to decadal timescales (here defined as timescales > 6 year). Our findings suggest that while the monopole structure captures variability in the winter- to-winter domain-average net heat flux, the dipole pattern tracks changes in the Mediterranean climate that are connected to the East Atlantic/Western Russia (EA/WR) atmospheric teleconnection pattern. Furthermore, while the monopole exhibits significant differences in the spatial structure across the multi-model ensemble, the dipole pattern is very robust and more clearly identifiable in the anomaly maps of individual years. A heat budget analysis of the dipole pattern reveals that changes in winds associated with the EA/WR pattern exert dominant control through both a direct effect on the latent heat flux (i.e., wind speed) and an indirect effect through specific humidity (e.g., wind advection). A simple reconstruction of the heat flux variability over the deep-water formation regions of the Gulf of Lion and the Aegean Sea reveals that the combination of the

monopole and dipole time series explains over 90% of the heat flux variance in these regions. Given the important role that surface heat flux anomalies play in deep-water formation and the regional climate, improving our knowledge on the dynamics controlling the leading modes of heat flux variability may enhance our predictability of the climate of the Mediterranean area.

3.2   Introduction

The Mediterranean Sea is a morphologically complex basin where intense local air-sea interactions together with the inflow of Atlantic water drive Mediterranean overturning circulation. Among the air-sea interactions, anomalies in the surface net heat flux (NHF) play a crucial role in the climate of the region (Haines and Wu 1995; Madec et al. 1991; Roether et al. 1996; Theocharis et al. 1999), particularly in the formation of intermediate and deep-water masses, a process of fundamental importance for regional- and global-scale meridional overturning circulation (Artale et al. 2006; Calmanti et al. 2006; Josey 2003; Rahmstorf 1996; Rahmstorf 1998).   Therefore, to enhance our understanding of climate in this area, we must also improve our understanding of the air-sea exchange variability of NHF.

The influence of large-scale atmospheric circulation on the air-sea NHF variability over the Mediterranean region is well represented by several relevant teleconnection patterns in this region (Josey et al. 2011; OrtizBevia et al. 2012). The patterns with the greatest impact (see Fig. 3) are the North Atlantic Oscillation (NAO) (Hurrell 1995), the Eastern Atlantic (EA) pattern (Wallace and Gutzler 1981), the East Atlantic-Western Russia (EA/WR) pattern (Krichak et al. 2002), and the Scandinavian pattern (Bueh and Nakamura 2007).   The NAO pattern is characterized by two opposite centers of action with anomalously high and low pressure over Azores and Iceland islands, respectively. This mode controls the strength and direction of westerly winds and storm tracks across the North Atlantic. The EA pattern is characterized by a broad low-pressure system centered to the west of the British Isles, which is approximately midway between the two

centers of action of the NAO system. Negative phases of EA are associated with high pressure over the northern Atlantic and a relatively strong pressure gradient over the western Mediterranean. This pressure gradient produces a cold northerly airflow that enhances ocean heat loss over this region. The EA/WR pattern is characterized by three alternate-in-sign centers of action located in the northern Atlantic, central Europe, and western Russia. Positive values of EA/WR are associated with northerly/southerly winds in the eastern/western Mediterranean. Finally, the SCAN pattern presents, in its positive phase, a dipole structure with a low pressure over the Iberian Peninsula and a high pressure over northwestern Russia. In its positive phase, this mode promotes weak low pressure and southerlies over the entire Mediterranean Sea.

Josey et al. (2011) examined the impact of these modes on Mediterranean Sea surface heat flux during extreme seasons (i.e., summer and winter) and concluded that the NAO—the dominant mode of atmospheric variability in this region—has a minor impact on NHF variability compared to the EA and EA/WR patterns, which explain the largest fraction of NHF variability. Zveryaev and Hannachi (2011) found a direct link between the EA pattern and the leading mode of evaporation variability but no significant correlation with the EA/WR pattern. Papadopoulos et al. (2012b) identified two main responses of the NHF to the regional atmospheric teleconnection patterns: a uniform basin-wide response and an out-of-phase response in the western and eastern sub-basins, which we will refer to as the dipole pattern. While they found that the uniform response was attributed to the EA, the dipole pattern appeared to be a response to a combination of the first four modes of the Euro-Atlantic region (i.e., EA. EA/WR, NAO, and SCAN).

These previous analyses provide an understanding of the statistical and in some cases, mechanistic, relationships between NHF variability in the Mediterranean Basin and large-scale atmospheric modes. For instance, Josey et al. (2011) recognized that the EA mode has a coherent-basin-wide impact resulting from its associated northeasterly flow of cold dry air, which increases the air-sea humidity and temperature gradients and thus heat loss. The same work also connected the

EA/WR mode with the heat flux anomalies of opposite signs in the eastern and western Mediterranean Basins. They hypothesized that this pattern occurs because the mode (EA/WR) drives a northerly flow of cold dry air over the eastern basin, enhancing heat loss, and a southerly flow of relatively warm moist air over the western basin, weakening heat loss. However, these studies focus on individual modeling or observational datasets to examine the spatial and temporal variability of surface heat fluxes. In this study, we use multiple observational datasets and 12 simulations of a multi-model ensemble to provide a more robust assessment of the statistical behavior of Mediterranean surface heat flux winter variability and to diagnose the mechanisms underlying links to the regional footprint of large-scale atmospheric teleconnection patterns. Moreover, this work is the first to assess the spatial and temporal variability of the Mediterranean air-sea heat fluxes in a multi-model ensemble of high-resolution regional climate models. Such model outputs, which are commonly used to investigate the climate over a specific region, may also be used as surface boundary conditions for hind-cast ocean simulations. In this regard, Herrmann and Somot (2008) have shown that a correct representation of air-sea heat fluxes is crucial to accurately modeling the key aspects of the Mediterranean Sea circulation such as the deep convection of the northwestern Mediterranean Sea.

Like many of the above-cited cited papers on the Mediterranean Sea heat flux variability, this paper focuses on the winter season. Studying the cold season has many advantages. For one, the formation of intermediate and deep water masses, which play a crucial role for the Mediterranean Sea circulation, is linked to air-sea heat flux exchanges occurring during the winter (Lascaratos et al. 1999). Additionally, winter anomalies dominate the annual mean heat budget (Josey et al., 2011), and extreme heat loss during this season has been linked to profound deep-water changes known as the Eastern Mediterranean Transient (Josey et al., 2003). Furthermore, the influence of large-scale atmospheric modes on the Mediterranean climate is generally much stronger during the extreme seasons (i.e., winter and summer) than during the transition seasons (i.e., spring and fall). To examine the high- and low-frequency dynamics of heat flux variability

in the Mediterranean Sea during the winter season, we combine two independent observational datasets with an ensemble of 12 high-resolution regional climate models. This work primarily focuses on the relationship between the two leading modes of winter NHF variability, which closely track the latent heat flux (LHF), and the climate of the Euro-Mediterranean region. Section 2 presents the dataset and methodology for the computation of the leading modes of LHF variability and Section 3 a multi-model ensemble view of the spatial and temporal statistics of the modes. Section 4 analyzes the relationships between the modes and large-scale atmospheric forcing and Section 5 summarizes and discusses the results.

3.3   Dataset and Methodology

3.3.1   The observational datasets

Before presenting the observational and modeling data used in this work, we would like to examine the relationship between NHF and LHF. NHF consists of a balance of four components of heat flux: LHF, sensible heat flux (SHF), longwave radiation (LWR), and shortwave radiation (SWR). The first two are turbulent while the last two are radiative. The estimation of these two kinds of heat fluxes involves measurements of different physical parameters, which are typically not available in observational datasets at the same spatial resolutions and temporal coverages. Table 1 shows the most commonly used observational datasets for both turbulent and radiative fluxes.

Table 1 Observational datasets for the air-sea heat flux components. In bold, the datasets used in this work.

Variable	Dataset	Period	Resolution
Radiative fluxes (SWR and LWR)	ISCCP2, **NOC**	1984-2008,**1980-2004**	2.5deg. , **1deg.**
Turbulent fluxes (SHF and LHF)	**OAFlux**, HOAPS, **NOC**	**1958-2008**,1988-2005,**1980-2004**	**1deg.,** 0.5deg., **1deg.**
Net heat flux (NHF)	**OAFlux**, **NOC**	**1958-2008**, **1980-2004**	**1deg., 1deg.**

In this work, estimations of radiative fluxes come from a modified Mediterranean Sea version of the National Oceanography Centre 1.1 (NOC1.1 – hereafter referred to as NOC) dataset (Josey et al. 1999). Estimations of turbulent fluxes come from two sources: the NOC dataset and the Objectively Analyzed air-sea Fluxes (OAFlux). While the OAFlux dataset provides estimations for NHF, the NOC dataset does not, so we compute the NHF from its four heat-flux components. The NOC dataset is based on ship observations provided by the International Comprehensive Ocean–Atmosphere Data Set (ICOADS, Woodruff et al., 1998) and presented on a 1deg. x 1deg. spatial grid for the period 1979 to 2004. The NOC dataset analyzed in our study is a modified version of the standard datasets computed using another formulation of the radiative flux components and analyzed by Josey et al. (2011). Specifically, the longwave flux is estimated by an improved formula calibrated with in-situ measurements from the Mediterranean Sea (see Bignami et al. 1995). In addition, the shortwave flux has been corrected for aerosol loading following the method of Gilman and Garrett (1994). OAFlux is a 50-year global dataset on a 1deg. x 1deg. grid for the period 1958 to 2008. This product is a result of merging satellite observations with surface moorings, ship reports, and atmospheric model reanalysis data.

With the exception of the NOC dataset, which provides estimations at a 1deg. x 1deg. resolution and covers the same period for all four components of the surface heat flux, radiative fluxes are available for shorter periods and lower spatial

resolution with respect to turbulent fluxes. For instance, the widely used International Satellite Cloud Climatology Project (ISCCP 2) dataset (Zhang et al. 2004) provides gridded estimations on a 2.5deg. x 2.5deg. horizontal resolution that cover the period 1984 to 2009. However, for the Mediterranean Sea, where important processes take place on a small scale, data with a spatial resolution of 2.5deg. x 2.5deg. are mainly useful for basin-integrated budget purposes (e.g., Sanchez-Gomez et al. 2011). Moreover, no estimations are available for radiative fluxes before 1980, and the longest period covered consists of 25 years (i.e., 1984-2009 for ISCCP 2), which limits possible inferences on low-frequency variability. Therefore, the ISCCP 2 dataset is not used in this study. In contrast, datasets of turbulent flux estimates often cover a longer period with a higher spatial resolution such as the 0.5deg. x 0.5deg. for the Hamburg Ocean Atmosphere Parameters and Fluxes from the Satellite (HOAPS) dataset (Andersson et al. 2007) and 1deg. x 1deg. for the NOC and OAflux datasets. However, the HOAPS dataset has several limitations. In addition to its relatively short coverage, HOAPS does not cover the Adriatic Sea, the Aegean Sea, or some coastal regions. This lack of spatial coverage strongly affects our ability to study air-sea heat exchange, as explained in the introduction and further confirmed by the strong variance shown by the multi-model ensemble (see next section). For these reason, we select the NOC and OAflux for comparing the multi-model ensemble outputs to observational datasets.

Our analyses mainly focuses on air-sea heat fluxes; however, in Section 3, we also use sea- level pressure (SLP) from the ERA40 reanalysis (Uppala et al. 2005), and in Section 4.2, we also use 2m air specific humidity and the SST from the OAflux database, and 10m winds from the NCEP reanalysis (Kalnay et al. 1996). To examine the influence of large-scale atmospheric circulation on the variability of air-sea heat fluxes over the Mediterranean region, we employ the NOAA Climate Prediction Centre (CPC) monthly mean values of the four prominent atmospheric modes of the Euro-Atlantic region (i.e., EA, EA/WR, NAO, and SCAN) for the period 1958 to 2010.

3.3.2   Regional climate model experiments

In addition to the above-presented observations, we use the multi-model dataset from the regional climate model experiments performed within the EU-FP6 ENSEMBLES project framework. In this work, we use 12 RCMs driven by the ERA40 reanalysis data and operating at a 25 km horizontal resolution. The models, which must cover a common minimum domain that includes the entire Mediterranean Sea, simulated the period 1961 to 2000. The RCMs differ for the model setup and the grid specifications such as the rotation grid, and the number of vertical levels. Table 2 lists more details about the experiments and the ENSEMBLES project website (http://ensemblesrt3.dmi.dk) provides more information regarding each model.

Table 2 Summary of the main features of the RCM used in the EU-FP6 ENSEMBLES project. [Table adapted from Sanchez-Gomez et al. (2011)]

Institution	RCM	Vertical levels	Reference
CNRM	ALADIN	31	Radu et al. (2008)
C4I	RCA	31	Kjellstrom et al. (2005)
DMI	HIRHAM	31	Christensen et al. (1996)
ETHZ	CLM	21	Bhom et al. (2006)
ICTP	RegCM	34	Georgi and Mearns (1999)
KNMI	RACMO	40	Lenderink et al. (2003)
METNO	HIRHAM	31	Haugen and Haakensatd(2006)
METOHC	HadRM	19	Collins et al. (2001)
MPI	REMO	27	Jacob (2001)
SMHI	RCA	24	Kjellstrom et al. (2005)

UCLM	PROMES	28	Sanchez et al. (2004)
OURANOS	CRCM	28	Plummer et al. (2006)

3.3.3   LHF as a proxy for NHF variability

In the open ocean, turbulent latent heat flux generally controls the variability of the NHF (Alexander et al. 2002). This finding also applies to the Mediterranean Sea (Garrett et al. 1993; Josey 2003; Josey et al. 2011; Papadopoulos et al. 2012a), especially during the boreal winter (December–January–February–March, hereafter DJFM) when the short-wave component becomes less important than it is during the summer (June–July–August–September, hereafter JJAS). Fig. 1 shows maps of the winter mean and normalized standard deviation of NHF and LHF fields (A sign convention used is that fluxes out of the ocean are positive) for the multi-model ensemble and both observations, NOC and OAflux. These maps reveal different means but very similar normalized standard deviations in both observations and the multi-model ensemble mean (ENSm). We normalized the standard deviation by its maximum value in order to use the same color scale and highlight the strong similarity of the spatial structure of LHF and NHF variances.

This simple but fundamental analysis suggests that the winter NHF mean results from a combination of turbulent and radiative fluxes while its spatial variance, represented here by the standard deviation, is controlled by the LHF alone. Although both the mean and the standard deviation present significant differences, this result is valid for all of the analyzed datasets. ENSm and OAflux often present similar patterns while NOC shows somewhat different features. To identify regions with large inter-model uncertainties, we compute the spread among models as an inter-model standard deviation. This parameter, shown in Fig. 1, reveals a larger spread associated with the coastal region and the Aegean Sea for both NHF and LHF. This result was already noted by Sanchez-Gomez et al. (2011), which uses the same multi-model ensemble to analyze heat and fresh water budgets in the Mediterranean Sea. In this work, the authors suggested that

the large spread in coastal regions and the land-enclosed basin (i.e., the Aegean Sea) are likely due to the difficulty in accurately representing processes related to the local wind fields, orography, and, in the case of the Aegean Sea, the locally increased internal variability of the RCMs.

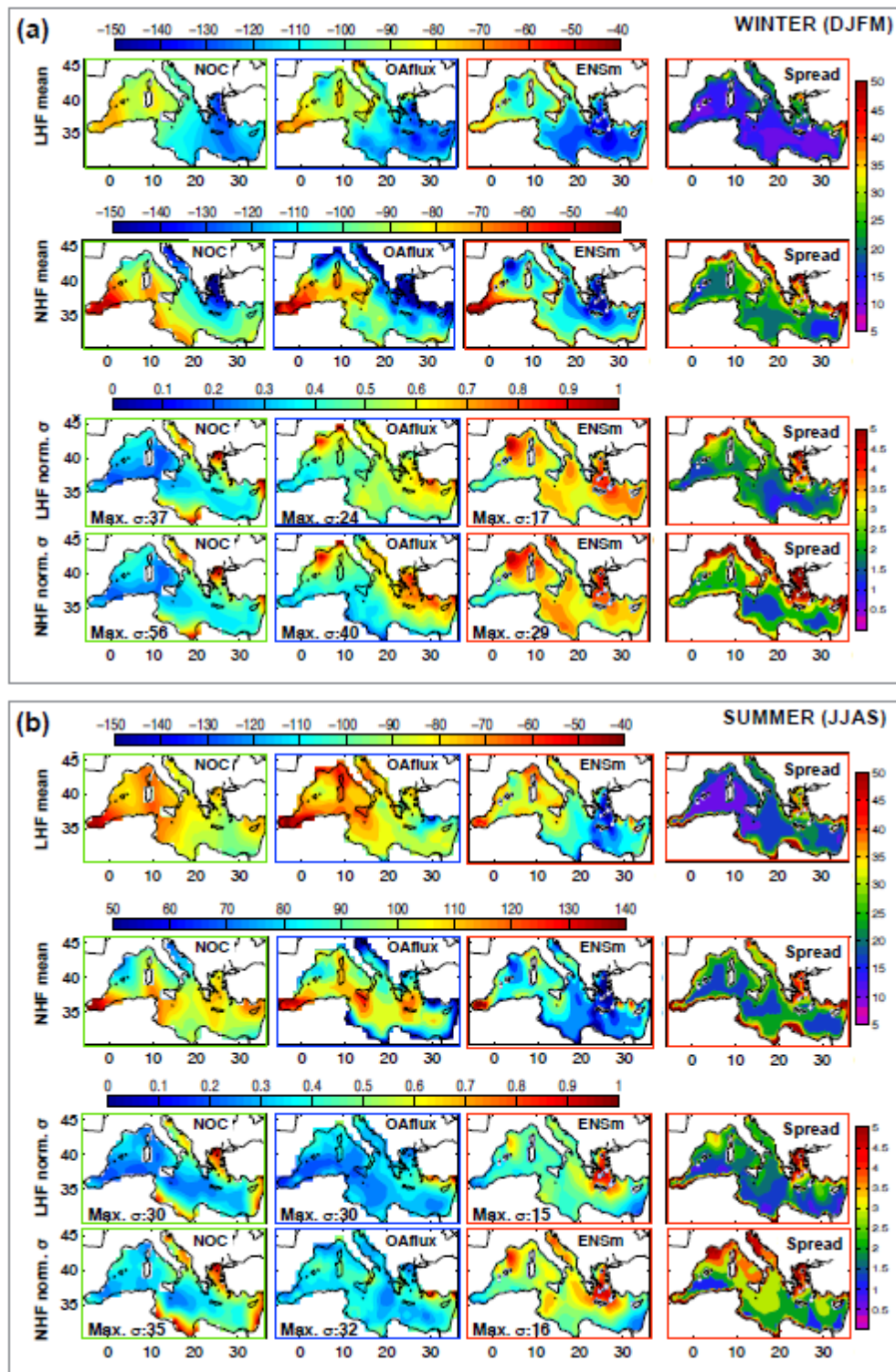**Fig. 1** Spatial distribution of the temporal mean and normalized standard deviation of latent heat flux (LHF) and net heat flux (NHF) for the OAflux dataset, the NOC dataset, and the multi-model ensemble mean. The Period analyzed is 1961–2000 for RCM simulations and ENSm, 1980-2004 for NOC dataset, and 1958-2010 for OAflux dataset. A sign convention used is that fluxes into the ocean are positive. The Inter-model spread

has been calculated as the standard deviation of the individual model climatological winter mean. Units are in [W/m2] for the mean and the spread. The standard deviation has non-dimensional units as it has been normalized by its maximum value, which is indicated in each subfigure as "Max. σ" .

Although Fig. 1a reveals that the spatial structures of winter LHF and NHF variances are similar, this does not assure similar variability of the two fields. However, a decomposition of the winter anomalies using empirical orthogonal functions (EOFs) and principal components (PCs) analysis reveals a close relationship between the spatial and temporal variability of NHF and LHF. The EOF/PC analysis decomposes the variance of the NHF and LHF into a dominant pattern of spatial variability (e.g., EOFs) and their associated temporal modulation (e.g., PCs). Fig. 2a shows the correlation coefficient (the methodology used to assess its statistical significance is explained in the caption of Fig. 2) between the first four PCs of NHF and LHF anomalies (i.e., NHFa and LHFa) during DJFM for the observational datasets, the simulations, and the ENSm (green, blue, and red rectangles, respectively). On average, the two leading modes explain about 77% of the total variance. The correlations for the first two modes are generally very high and often close to one. For higher modes, the correlations slightly decrease, but they are considerably large even for the fourth mode. The uniquely low correlation value (i.e., PC4 of NOC) occurs when the order of the modes between LHF and NHF is inter-changed. In fact, when this occurs, the correlation is close to zero because of the orthogonality condition of the PCs. For instance, the correlation coefficient of LHF-PC4 and NHF-PC5 of NOC was about 0.90, confirming the expected change in the order of the PCs. The results shown in Fig. 2a demonstrate that at least during the winter and for the first few modes, LHF variability strongly captures variations in the NHF. As discussed in Section 2.1, LHF estimates cover longer periods with a higher spatial resolution with respect to NHF estimates. Therefore, for the remainder of the analyses, we focus on winter LHF to diagnose the dynamics controlling the variability of the winter NHF. Last, we would like to conclude this section by pointing out that at least for the first two

modes and especially for the RCMs, this close relationship between the LHF and NHF also holds, to some extent, during the summer season (Fig. 2b).
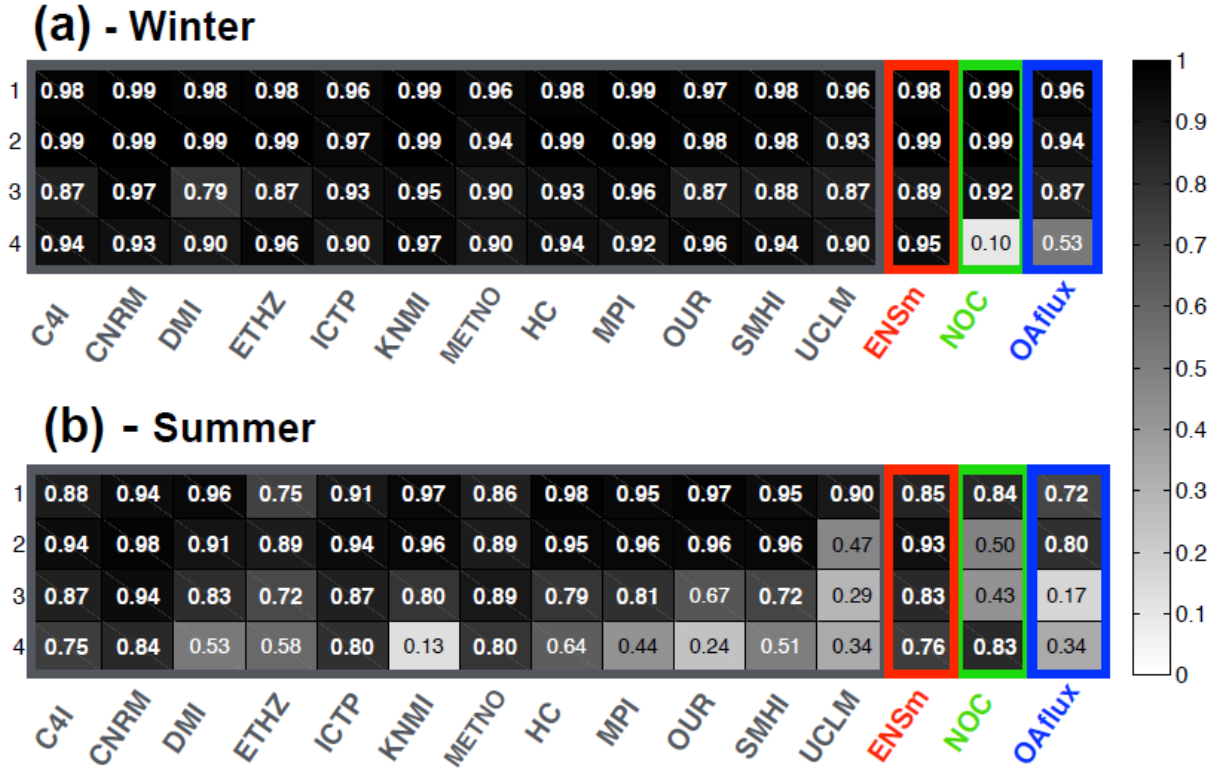

Fig. 2 Panel (a) shows the correlation coefficients for first 4 PCs between winter (DJFM) anomalies of NHF and LHF for the simulations, the multi-model ensemble mean (ENSm), the NOC and the OAflux datasets (grey, red, green, and blue rectangles, respectively). The grey shading indicates the absolute value of the correlation coefficient and boldface indicates a significant correlation at a 99% level. The significance of the correlation coefficients throughout this paper are estimated by computing empirical probability distribution functions (EPDFs) for the correlation coefficient of two red-noise time series with the same autoregression coefficients of those estimated in the original signals. The EPDF is used to assess significance levels of 95% and 99%. In (b) the same analysis is performed using summer (JJAS) anomalies.

3.4   Statistical Analysis of the Leading Modes of LHF

To investigate the spatial and temporal structure of the interannual variability of Mediterranean LHFa during the boreal winter (DJFM), we perform an EOF analysis of the winter mean latent heat flux for both models and observations. In this paper before analyzing any dataset, we remove a linear trend for each grid point and for each time series (i.e., CPC indices). We restrict our statistical analysis to the

first two leading modes, as they explain most of the observed variability (in average 77% of the total variance). The steps of the analysis include (a) a description of the EOF structures, (b) a comparison between the models and observations, and (c) a correlation analysis of the PC1 and PC2 with known large-scale atmospheric teleconnection patterns (i.e., NAO, EA, EA/WR, and SCAN).

To characterize the temporal scales at which these teleconnections are more active, we also analyze the correlations for the low- and high-pass filtered PCs (below and above a period of 6 years). Finally, by comparing the results of the models and observations, we assess the capability of RCMs to represent the atmospheric teleconnections dynamics that affect LHF variability. To present the employed climatic indices and their relationship with the atmospheric circulation, we compute the correlation maps (Fig. 3) between the indices and the SLP of the multi-model ensemble mean and the ERA40 reanalysis. We choose the ERA40 observational dataset since it has been used to drive the multi-model ensemble simulations, and thus it is important that the consistency between the large-scale features of the dynamical downscaling and of the forcing fields be checked. In addition to the correlation maps, we compute the inter-model spread to identify regions with large uncertainties among the models. Fig. 3 shows the correlation maps between the indices and the SLP of the ERA40 reanalysis and of the multi-model ensemble mean along with the spread, as defined in Fig. 1.

Fig. 3 reveals strong consistency between the multi-model ensemble mean and the ERA40 reanalysis. For all the analyzed climatic indices, the correlation map for ENSm is similar to that obtained for ERA40. One minor but noteworthy difference is the slightly smaller correlation for the center of action of the EA/WR mode in the multi-model ensemble mean. As the center of action of this mode is located far from the prescribed lateral boundary conditions, it is weakly influenced by the driving field and therefore more prone to revealing differences in the model dynamics. The inter-model spread (last column) shows generally low values over the centers of action, again confirming that most of the models closely represent these atmospheric modes. Regions of high inter-model spread are mostly located

in the eastern part of the domain since the prevalent westerly flow, which characterizes the circulation of the region, exerts control from the western lateral boundary that decreases as it moves eastward. Moreover, except for NAO, which also shows a high spread over the northern Africa and eastern Mediterranean regions, high-spread areas are mostly over regions of low correlation, which can be partially explained by the weak atmospheric mode in regions where the internal variability of the models dominates the signal.
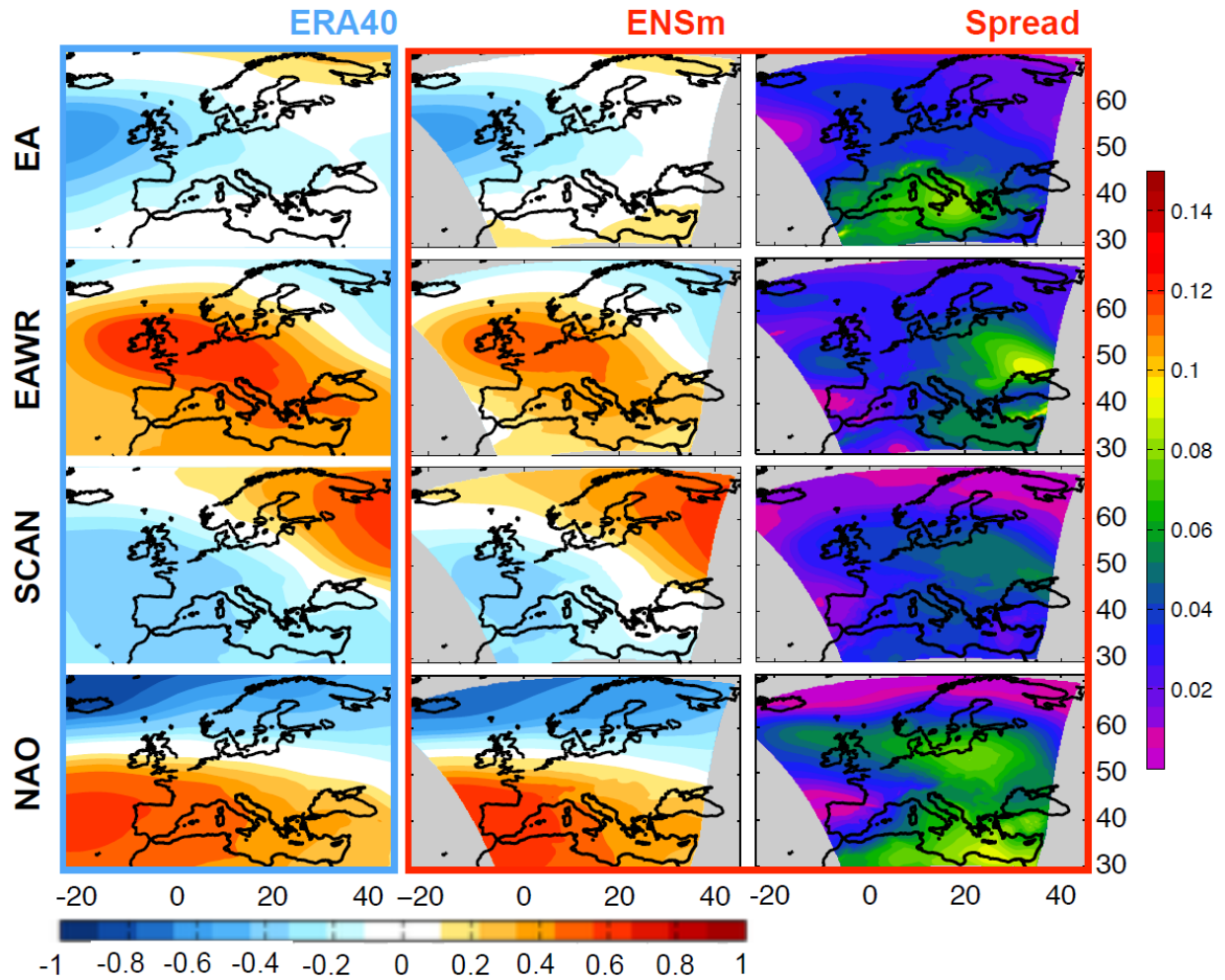

Fig. 3 Correlation maps between indices of atmospheric variability and SLP during winter season (DJFM) for ERA40 (left column) and multi-model ensemble mean (ENSm; middle column). The figure shows also the inter-model spread (right column) calculated as in Fig. 1.

3.4.1   First mode

Fig. 4 shows the first mode of the LHFa for both models and observations. The first four rows show the RCM fields while the fifth row presents the two independent observational datasets, NOC and OAflux, and the multi-model ensemble mean (ENSm). In addition to the spatial pattern, each subfigure also shows the amount of explained variance and the temporal/spatial correlation between the associated PC1/EOF1 and OAflux PC1/EOF1. Before examining the spatial structure of the patterns, we report the explained variance for both models and observations. For RCMs, the explained variance associated with the first mode ranges from a minimum of 47% for UCLM to a maximum of 59% for OURANOS. The average value is 52%, and the associated standard deviation is 6%. For the observations, the explained variance is 42% for the NOC and 58% for the OAflux, which reveals a range similar to the one find in the models even though we analyzed only two datasets. Thus, the amount of explained variance for each RCM is consistent with the uncertainty of the observations.
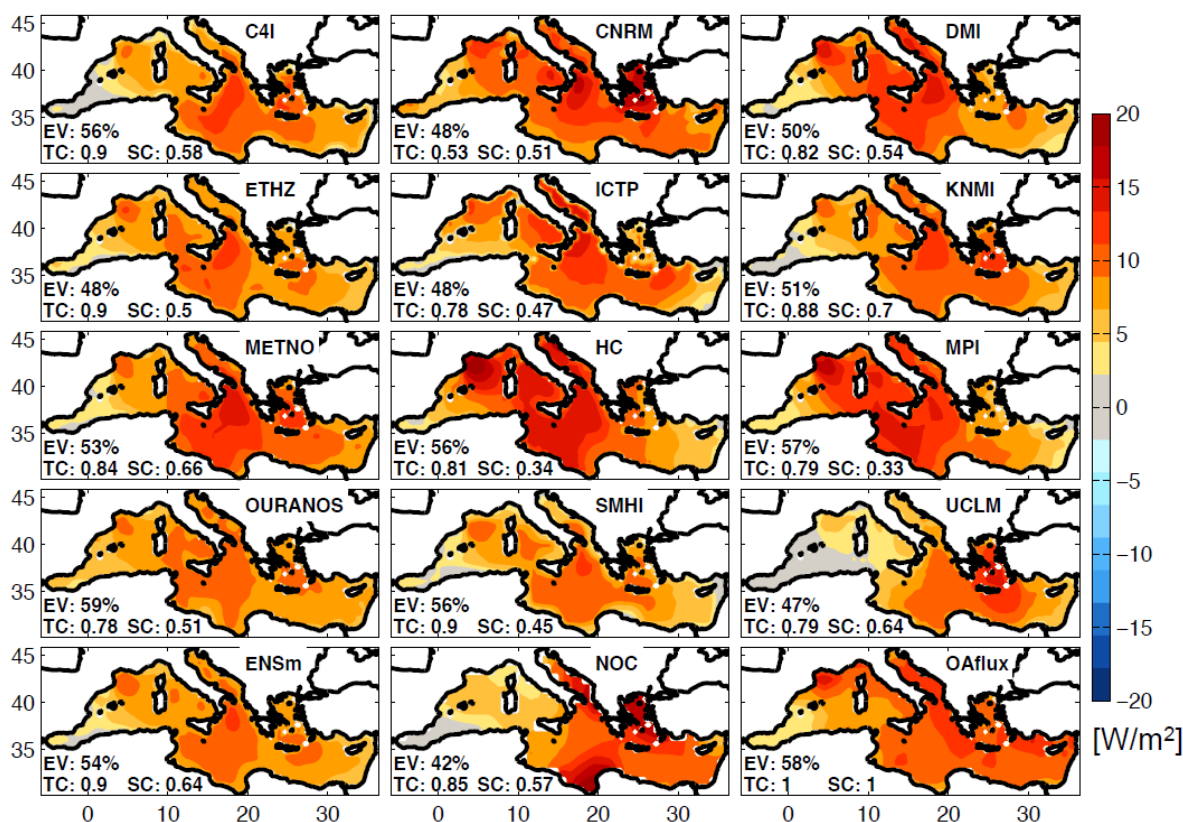
Fig. 4 Spatial patterns of the first mode (EOF1) of the winter mean LHFa for the observational datasets, the simulations, and the multi-model ensemble. Each subfigure also indicates the amount of explained variance (EV), and the values of the spatial and temporal correlation (SC and TC, respectively) between the simulated mode and the OAflux mode. The SC (TC) is obtained computing the spatial (temporal) correlation between the simulated and observed EOF1 (PC1). Units are [W/m2].

The spatial pattern of EOF1 for both models and observations (Fig. 4) reflects coherent same-sign variations of LHF over the entire Mediterranean Basin. Despite some differences in the spatial representation of the EOF 1 that are also evident in the two observational datasets, the models and observations share important features such as large values of the loadings in the Gulf of Lion and the Ionian Sea and small loading values in the western-most region of the basin in the Alboran Sea. Both the Gulf of Lion and the Ionian Sea are locations of deep-water formation (Roether et al. 2007; Schroeder et al. 2008), and their appearance in

the first mode is not surprising because they are characterized by intense LHF variations at inter-seasonal and annual timescales.

To evaluate the multi-model ensemble skills in reproducing the observed variability associated with the first mode, we have computed the correlations between PC1 of each RCM and OAflux. These correlations (Fig. 4) are generally very high with a mean value of 0.81 and a maximum of 0.90 for the ENSm. Physically, the PC1 time series represents the variability of the basin-averaged winter LHFa. For both observations and simulations, represented here by the multi-model ensemble mean along with the inter-model spread, Fig. 5 shows the PC1 time series against the area-averaged basin winter LHFa time series. This figure reveals how PC1 nearly parallels the basin-averaged mean value with correlation coefficients as high as 0.99 for both observations and simulations. Therefore, we conclude that the multi-model ensemble is able to capture the temporal variability of the first mode despite some differences in the spatial patterns of the individual models that likely reflect uncertainty associated with regional expressions of the large-scale dynamics of basin-wide warming and cooling

3.4.1.1   Interannual to decadal links to the regional climate

The EOF analyses of spatial modes (Fig. 4) show relatively inconsistent patterns among the models, which are able to track a high correlation with observations in time. Now, we examine the links between the leading mode of variability of the Mediterranean latent heat flux and the patterns of regional atmospheric circulation. We compute the correlations between the leading PCs and the four climate indices (i.e., NAO, EA, EA/WR and the SCAN) with larger impact on the Mediterranean region. Moreover, to characterize the temporal scales at which these teleconnections are active, we analyze high- and low-pass filtered time series. The filtering method that we use is a simple Fourier filter. After performing an FFT analysis, we reconstruct the time series using only selected Fourier components. In particular, for the high- and low-frequency analyses, we retain

Fourier components that are shorter and longer than a six-year period, respectively. With the aim of separate interannual (1-6yr) and decadal (8-12yr) timescales, we decided, after performing some sensitivity tests, to choose six years as the threshold at which we separate these scales. Fig. 6 shows the correlations for the non-filtered (NF) time series as well as for the high-passed (HP) and low-passed (LP) time series. The boldfaced numbers in Fig. 6 indicate a significant correlation at a 99% level.

In agreement with previous studies of Josey et al. (2011), Zveryaev, and Hannachi (2011), the first mode is highly correlated with the EA mode (see also Fig. 5, bottom time series). The NF correlations reveal that, except for two RCMs (i.e., CNRS and DMI), all models show noteworthy correlations above 0.44 with a value of 0.52 for the ENSm, which is very close to the correlation found for the OAflux dataset. The connection between the EA mode and the heat fluxes over the Mediterranean Sea can be summarized as follows: the negative phases of EA are associated with anticyclonic circulation centered over the northern Atlantic and a relatively strong pressure gradient over the western Mediterranean that produces a cold northerly airflow, which, in turn, enhances ocean heat loss over this region. However, the correlation maps in Papadopoulos et al. (2011) show that the LHFa in the westernmost part of the basin is mostly independent from the EA mode, which is consistent with the low value of the first mode loading over this region. Although we remove a linear trend for each grid point from the dataset before performing the EOF analysis, the PC1 shows strong multi-decadal variability that result in a negative trend after 1990, which is not present in the EA time series (Fig. 5). Previous studies have already reported such a trend in the Mediterranean Sea LHF, which has been attributed to SST-driven changes in the surface humidity gradient linked to global warming (Mariotti 2010; Skliris et al. 2011). The EA represents a large-scale atmospheric mode of variability, but it does not capture these basin-scale signals (e.g., the LHF trend).
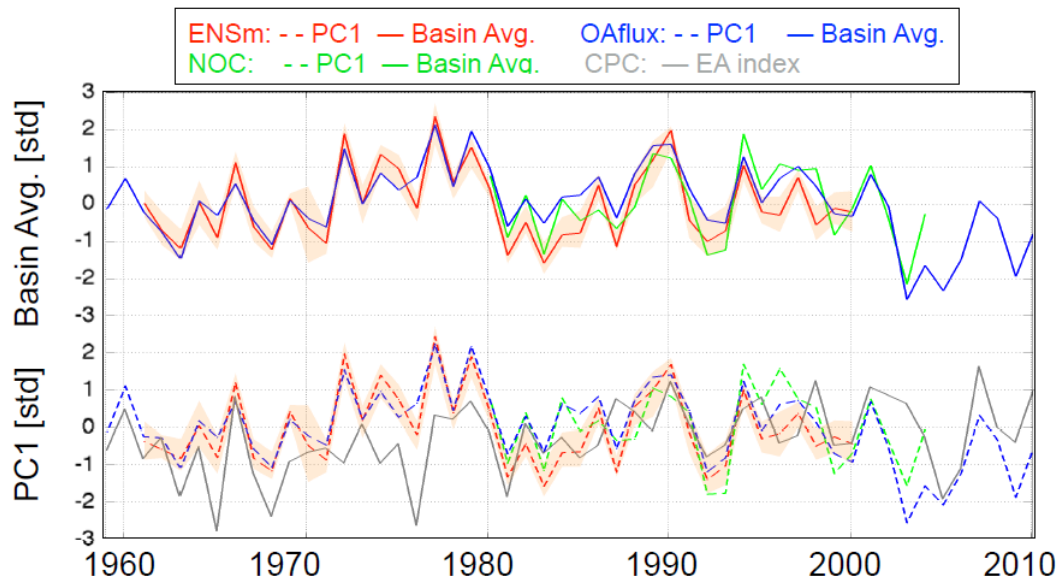
Fig. 5 Time series of normalized PC1 (Solid line) and normalized basin-averaged winter LHF anomalies (Dashed line) for ENSm (in red), NOC, (in green), and OAflux (in blue). In the lower part the PC1s are compared with the EA index(grey line). The red shading, representing the inter-model spread, has been calculated as the standard deviation of the individual model value of the PC1 and of the basin-averaged winter LHF anomaly. All timeseries are normalized by their standard deviations therefore units are in standard deviations (std).

An examination of filtered time series correlations reveals a noteworthy feature of the PC1-EA relationship: except for NOC, the correlation is slightly enhanced by the low-pass filter. Although not present in the OAflux dataset, Fig. 6 reveals an interesting high-frequency correlation between the PC1 and the EA/WR mode in most of the models, the ENSm, and the NOC dataset. Regarding the other regional climate indices, that is, the NAO and SCAN indices, Fig. 6 reveals low correlations, mostly below the significance level. While the NAO index presents a significant correlation only for the LP time series of OAflux and CNRM, the SCAN presents significant correlation only for few RCMs. These analyses confirmed the PC1-EA relationship and revealed a slight increase in this teleconnection at periods longer than six years. Although rather speculative, these analyses also suggest a high frequency (i.e., periods shorter than six years) relationship between the PC1 and the EA/WR mode.
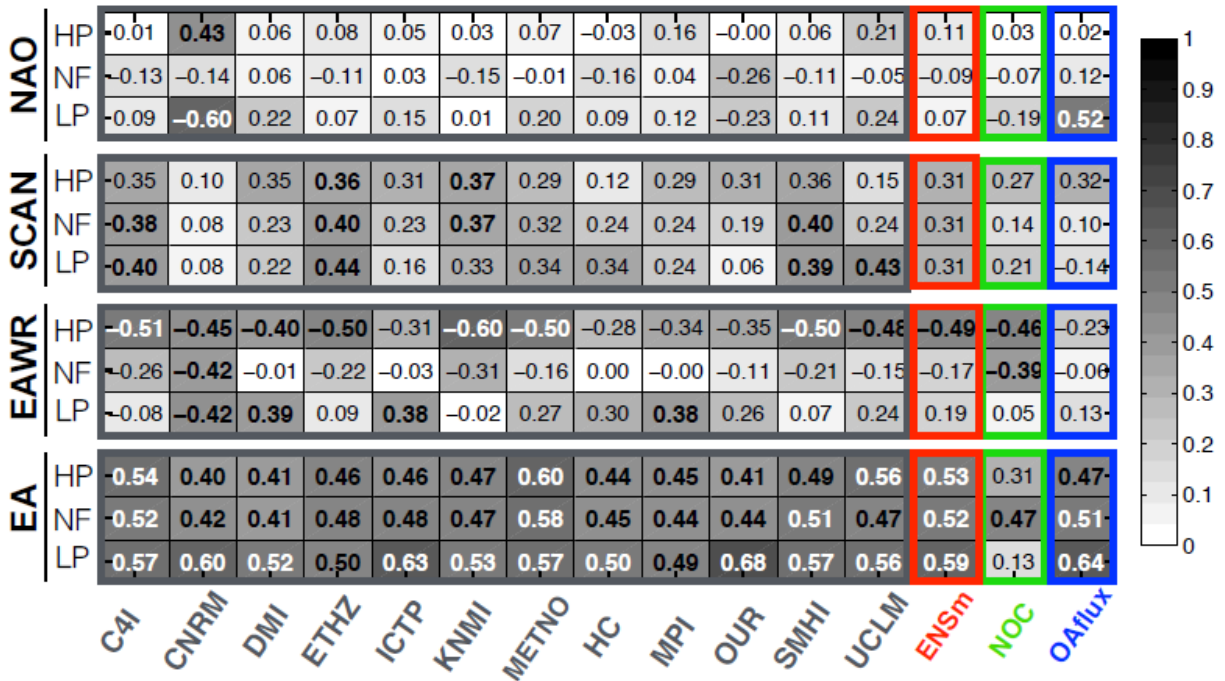
Fig.6 Values of the correlation coefficient between the winter (DJFM) LHFa-PC1 time series and the corresponding winter indices of the four main atmospheric modes. The Period analyzed is 1961–2000 for RCM simulations and ENSm (respectively grey and red rectangles), 1980-2004 for NOC dataset (green rectangle), and 1958-2010 for OAflux dataset (blue rectangle). The grey shading indicates the absolute value of the correlation coefficient and boldface indicates a significant correlation at a 99% level. In addition to the non-filtered (NF) time series we also analyzed high-pass (HP) and low-pass (LP) filtered time series. For the high- and low-frequency analysis, we retained Fourier components shorter and longer than a 6-year period, respectively.

3.4.2   Second mode

Unlike the first mode, the spatial pattern of the second mode shows strong consistency among the models and the observations (Fig. 7). For instance, the spatial correlation between the RCMs and the OAflux is generally strong, ranging from a minimum of 0.92 for ICTP to a maximum of 0.97 for MPI.   This mode is characterized by a well-defined dipole structure that represents opposite variations of LHF in the eastern and western parts of the Mediterranean Sea. While the positive pole of the dipole structure is almost always located in the GOL region, the negative pole is not always located in the same region. The negative

pole is often located in the Aegean Sea, but in many cases, it appears to be spread between two locations, the Aegean Sea and the area south of Cyprus (Fig. 7). Moreover, the slightly diverse character of NOC, which does not show any clear pole in the Eastern basin, is worth mentioning. Compared to the first mode, the explained variance of the second mode shows a remarkable difference between RCMs and observations. While the explained variance for the RCMs is always above 24%, with most of the models around 26%, the explained variance for the observations is smaller, 20% for OAflux and only 16% for NOC. The PC2 time series for the observational datasets are always significantly correlated with those of the models (Fig. 8). Excluding CNRS, the correlation is always above 0.63 with an average value of 0.75 and a maximum value of 0.83 (C4I).
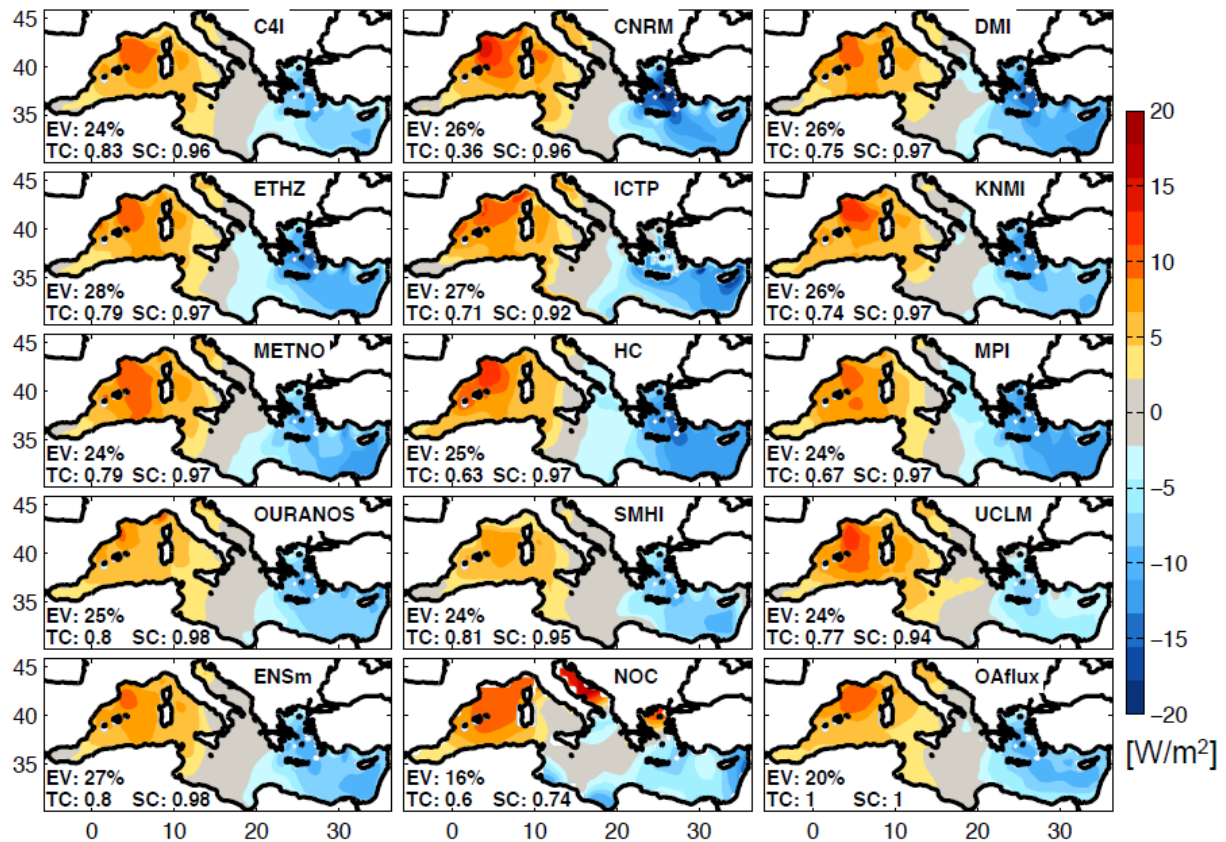

Fig. 7 The same as Fig. 4, but for the second mode.

3.4.2.1   Interannual to decadal links to the regional climate

We examine the links between PC2 and the four atmospheric climate modes, shown in Fig. 9. Except for several RCMs and the NOC dataset, the NF time series reveal significant correlations between the PC2 and the EA/WR index, ranging from 0.38 to 0.53 (the time series of the PC2 and the EA/WR index are shown in Fig. 8).
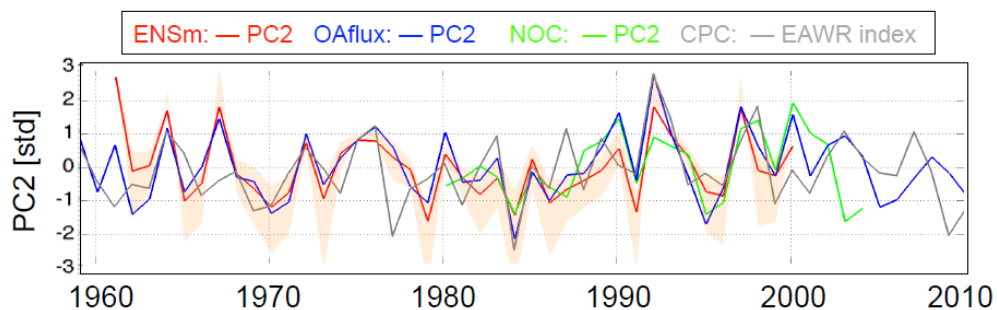
Fig. 8 Time series of normalized PC2 for ENSm (in red), NOC, (in green), and OAflux (in blue). The grey line is the EA/WR index. The red shading, representing the inter-model spread, has been calculated as the standard deviation of the individual model value of the PC1 and of the basin-averaged winter LHF anomaly. All timeseries are normalized by their standard deviations therefore units are in standard deviations (std).

Moreover, the analyses of the low- and high- frequency-filtered time series (Fig. 9) reveal that this correlation is significantly enhanced by the low-pass filter with average correlation coefficients of about 0.68. Josey et al. (2011) were the first to recognize the influence of the EA/WR in the analysis of a NCEP/NCAR and ARPERA datasets. They showed that the EA/WR mode is associated with an east-west dipole structure in the heat exchange, which is characterized by an approximately equal opposite signal of about 15 Wm-2. However, as noted by others (Papadopoulos et al. 2012b), the time series of the PC2 is also connected to other teleconnection patterns in this region. To better understand the large-scale dynamics underlying the expression of this dipole mode (DM), we conduct a diagnostic and budget analysis of the LHF dipole during the period when this mode is most active.

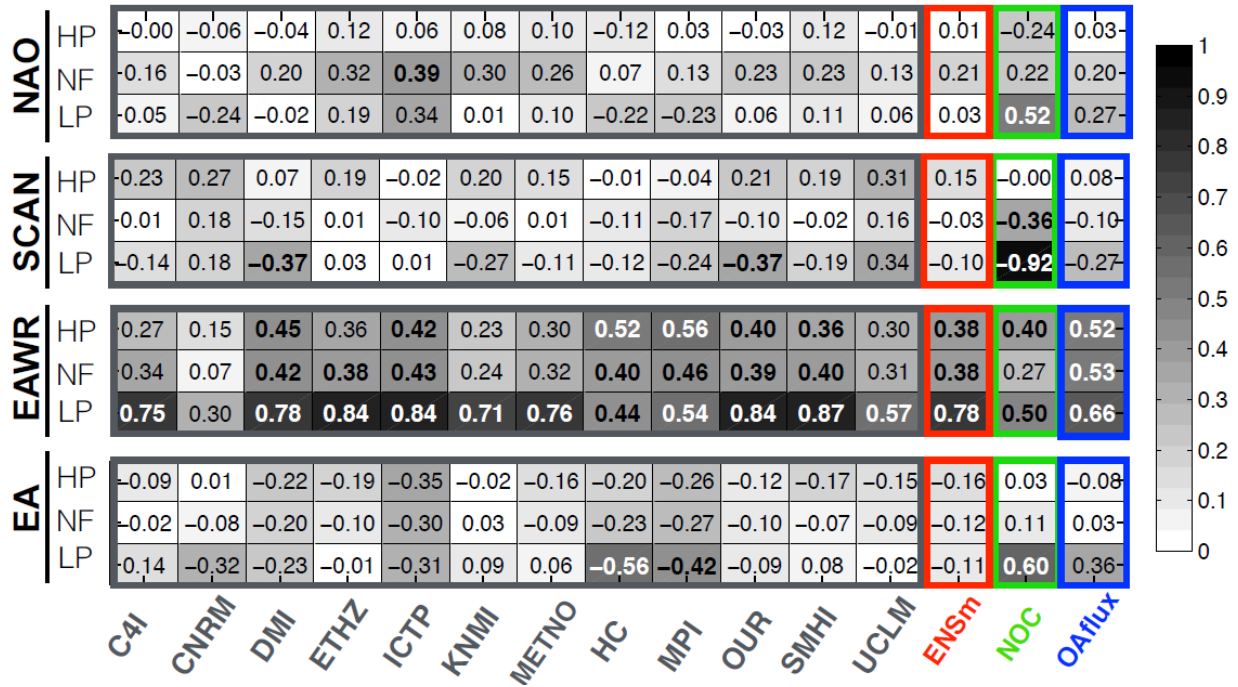|		C4I	CNRM	DMI	ETHZ	ICTP	KNMI	METNO	HC	MPI	OUR	SMHI	UCLM	ENSm	NOC	OAflux
NAO	HP	-0.00	-0.06	-0.04	0.12	0.06	0.08	0.10	-0.12	0.03	-0.03	0.12	-0.01	0.01	-0.24	0.03
	NF	-0.16	-0.03	0.20	0.32	**0.39**	0.30	0.26	0.07	0.13	0.23	0.23	0.13	0.21	0.22	0.20
	LP	-0.05	-0.24	-0.02	0.19	0.34	0.01	0.10	-0.22	-0.23	0.06	0.11	0.06	0.03	**0.52**	0.27
SCAN	HP	0.23	0.27	0.07	0.19	-0.02	0.20	0.15	-0.01	-0.04	0.21	0.19	0.31	0.15	-0.00	0.08
	NF	0.01	0.18	-0.15	0.01	-0.10	-0.06	0.01	-0.11	-0.17	-0.10	-0.02	0.16	-0.03	**-0.36**	-0.10
	LP	-0.14	0.18	**-0.37**	0.03	0.01	-0.27	-0.11	-0.12	-0.24	**-0.37**	-0.19	0.34	-0.10	**-0.92**	-0.27
EAWR	HP	0.27	0.15	**0.45**	0.36	**0.42**	0.23	0.30	**0.52**	**0.56**	**0.40**	**0.36**	0.30	**0.38**	**0.40**	**0.52**
	NF	0.34	0.07	**0.42**	**0.38**	**0.43**	0.24	0.32	**0.40**	**0.46**	**0.39**	**0.40**	0.31	**0.38**	0.27	**0.53**
	LP	**0.75**	0.30	**0.78**	**0.84**	**0.84**	**0.71**	**0.76**	**0.44**	**0.54**	**0.84**	**0.87**	**0.57**	**0.78**	**0.50**	**0.66**
EA	HP	-0.09	0.01	-0.22	-0.19	-0.35	-0.02	-0.16	-0.20	-0.26	-0.12	-0.17	-0.15	-0.16	0.03	-0.08
	NF	-0.02	-0.08	-0.20	-0.10	-0.30	0.03	-0.09	-0.23	-0.27	-0.10	-0.07	-0.09	-0.12	0.11	0.03
	LP	0.14	-0.32	-0.23	-0.01	-0.31	0.09	0.06	**-0.56**	**-0.42**	-0.09	0.08	-0.02	-0.11	**0.60**	0.36

Fig. 9 The same as Fig. 6, but for PC2.

3.5 Decomposing the Temporal and Spatial Dynamics of the Dipole Mode

As statistically derived modes are constrained to be orthogonal while physical modes may show some inter-dependence, they do not always reflect real physical modes (Simmons et al. 1983). Thus, the physical interpretation of the statistically derived modes (e.g., DM) can be controversial (Dommenget and Latif 2003). Furthermore, a close explained variance of higher order EOFs might indicate that two or more EOFs capture oscillations or propagation dynamics in the physical field. To determine if the variance associated with the DM (EOF2) is statistically distinct from the variance associated with higher modes, we compute the uncertainties of each eigenvalue using North's rule (North et al. 1982). This analysis reveals that PC1 and PC2 (i.e., DM) have well-separated eigenvalues at the 95% significance level in OAflux and ENSm, but not in NOC, which has

overlapping second and third eigenvalues. This last result may partially explain why the EOF2 of NOC shows a relatively distinct pattern among all of the analyzed datasets (see Fig. 7). The statistical significance of the DM (EOF2) does not guarantee the existence of a real physical mode. Moreover, the explained variance of the DM is about one-third of the variance explained by the first mode, and therefore, even if it is a real structure, the dipole may not be physically relevant. Therefore, we dedicate this section to assess the relevance, the physical meaning, and the dynamics of the DM.

3.5.1 Is the dipole structure a relevant feature in the Mediterranean?

The first issue we wish to address is whether the DM represents a real feature of the Mediterranean climate. To answer this question, we examine how often the first and second mode (i.e., the monopole and the dipole) structures occur in the winter anomalies of the raw data. To this end, we compute the spatial correlation between each mode and the winter anomalies of LHF for both models and observations (Fig. 10). We find that while EOF1 explains most of the variance in the LHF, it is EOF2 (the DM) that occurs more frequently in the anomaly structure in both observations and models (e.g., the ENSm). While EOF1 captures strong interannual events and tracks the large-scale mean, EOF2 captures the recurring spatial pattern, which often emerges as a dipole structure. Although this spatially predominant role of the DM occurs in all the analyzed datasets, we should note several important differences. First, OAflux and ENSm show similar correlations, which is consistent with the strong correlations between their first two modes (see Section 3). In contrast, NOC shows no clear dominance of EOF2 in the spatial structure and misses the peaks of correlations above 0.80, which characterizes the EOF2 of OAFlux and ENSm.
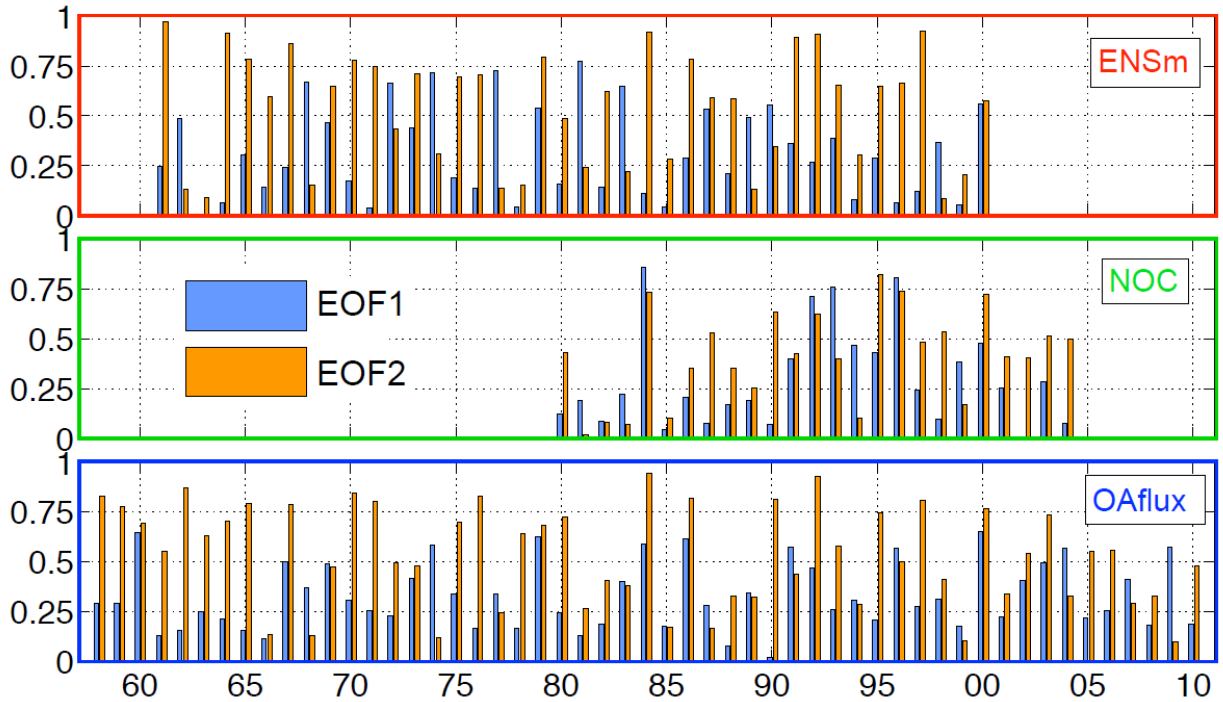
Fig. 10 Values of the spatial correlation coefficient between the winter mean LHFa pattern and the corresponding two leading EOFs for ENSm (1961-2000), NOC (1980-2004), and OAflux (1958-2010).

Another feature in Fig. 10 worth noting is related to the OAflux correlations series in the period 2000 to 2010. Starting from the year 1998, the first mode becomes dominant, and the dipole correlation does not exceed 0.55. This rapid change in the time series may suggest a non-stationary statistic for LHF. As both NOC and the models do not cover this period, we cannot use them to support or contrast this hypothesis. However, we test the stationary time series by splitting the 52-year long OAflux data into 13-year sub-periods and re-computing the EOF analysis in each period (Fig. 11). The comparison of the second modes of all of these periods reveals a substantial difference in the EOF2 pattern of the last sub-period (1998-2010), which does no longer shows the characteristic dipole pattern and in which the explained variance drops to 7%. We also note that by excluding this period from the OAflux EOF decomposition, we find an explained variance for the EOF2 of 26%, which is close to what is explained by the ENSm-EOF2 (27%). Far from being conclusive, this observed change in the EOF2 structure during the

1998 to 2010 period may suggest a recent change in the climate controls of this region. The high number of years with anomalies resembling the dipole structure (e.g., spatial correlations as high as 0.80) is an indication that this statistical mode is an expression of a real physical mechanism. In the next section, we explore the forcing dynamics that lead to the DM.
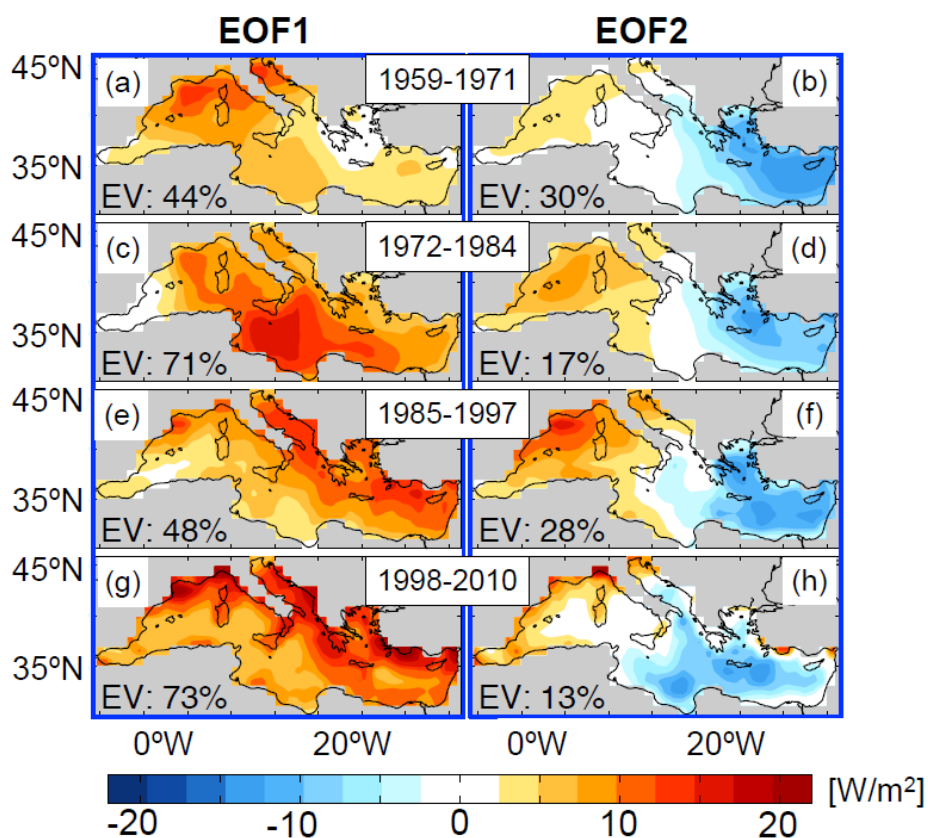

Fig. 11 EOF1 and EOF2 of winter LHFa for OAflux dataset computed over different periods:(a,b) 1959-1971; (c,d) 1972-1984; (e,f) 1985-1997; (g,h) 1998-2010. Units are in [W/m2]

3.5.2   What mechanism controls the dipole mode?

From the previous analysis, we conclude that the DM is a recurrent physical structure in the Mediterranean Sea and controls an important fraction of the spatial and temporal variability of the LHF anomalies. Josey et al. (2011) used a regression analysis to relate this dipole structure to the EA/WR pattern and

hypothesized that "the EA/WR pattern produces a northerly flow of cold dry air over the eastern basin and a southerly flow of relatively warm moist air over the western basin, leading to significant heat flux anomalies that are opposite in sign." Following this hypothesis, we perform a budget analysis to reconstruct the contribution of winds, humidity, and sea surface temperature on the LHF field using a bulk formula. The bulk formula consists of physical parameterizations that generally relate SST and atmospheric boundary layer variables with air-sea exchange fluxes of heat, momentum, and mass (e.g., Josey et al. 1999; Vickers and Mahrt 2006). In particular, we estimate the LHF field from wind speed ($|\vec{u}|$), 2m air specific humidity (Qa), and SST. We examine this relationship to quantify the contribution of each to the generation of the DM. We isolate each variable contribution by computing the "partial" composites of LHF anomalies for years (the winter season) when the DM is most active. We obtain these partial composites by calculating the LHF field using the composite for one variable and the climatologies of the other two. With this approach, the reconstructed LHF field will retain the contributions to the DM resulting from a particular variable, allowing its quantification by subtracting the partial LHF composite from the total LHF composite. For the composite, we select years in which the absolute value of the PC2 was above a threshold value set to 1.3, and then we subtract the average field of the positive years from the average field of the negative years. For this analysis, we use the RCMs, the ENSm, and the OAflux observational dataset, which does not provide $|\vec{u}|$; as a result, we obtain this variable from the NCEP dataset (reanalysis).

Before presenting the parameter-specific contributions to the DM, we verify that our bulk formula can effectively reconstruct the LHF field. In Fig. 12, the first column shows the winter LHFa composite while the second column shows the same field but reconstructed using the bulk formula with the composites of $|\vec{u}|$, Qa, and SST. Despite some minor differences, these two columns are similar and therefore, we conclude that the reconstruction is successful. It is worth mentioning that the DM composite pattern of the models can differ. For instance,

OURANOS shows a weak dipole while ETZH shows a strong dipole. We present the specific contributions of $|\vec{u}|$ and Qa to the DM mode in the third and in the fourth columns, respectively, of Fig. 12. This figure does not show the SST contribution to the LHFa composite, as this is significantly smaller than $|\vec{u}|$ and Qa contributions. While $|\vec{u}|$ and Qa are the dominant contributors to the east-west anomaly of opposite signs, their contributions differ. In both the observation and the ENSm, the LHF reconstruction composite obtained using Qa anomalies, produces strong negative LHF anomalies in a range of -15 to -20 W/m2 in the eastern basin and weak positive anomalies in a range of 5 to 10 W/m2 in the western basin. This spatial pattern closely resembles the corresponding DM presented in the second column of Fig. 12 and the EOF2 patterns of Fig. 7. The LHF reconstruction composite obtained using the $|\vec{u}|$ composite produces negative anomalies in a range of -3 to -7 W/m2 in the eastern basin and positive anomalies of 5 to 10 W/m2 in the western basin. This pattern accounts for the amplitude of the positive anomalies in the western basin. This analysis helps us identify specific humidity as an important contributor to the DM. In the next section, we investigate the mechanism controlling the Qa in the OAflux observational dataset.
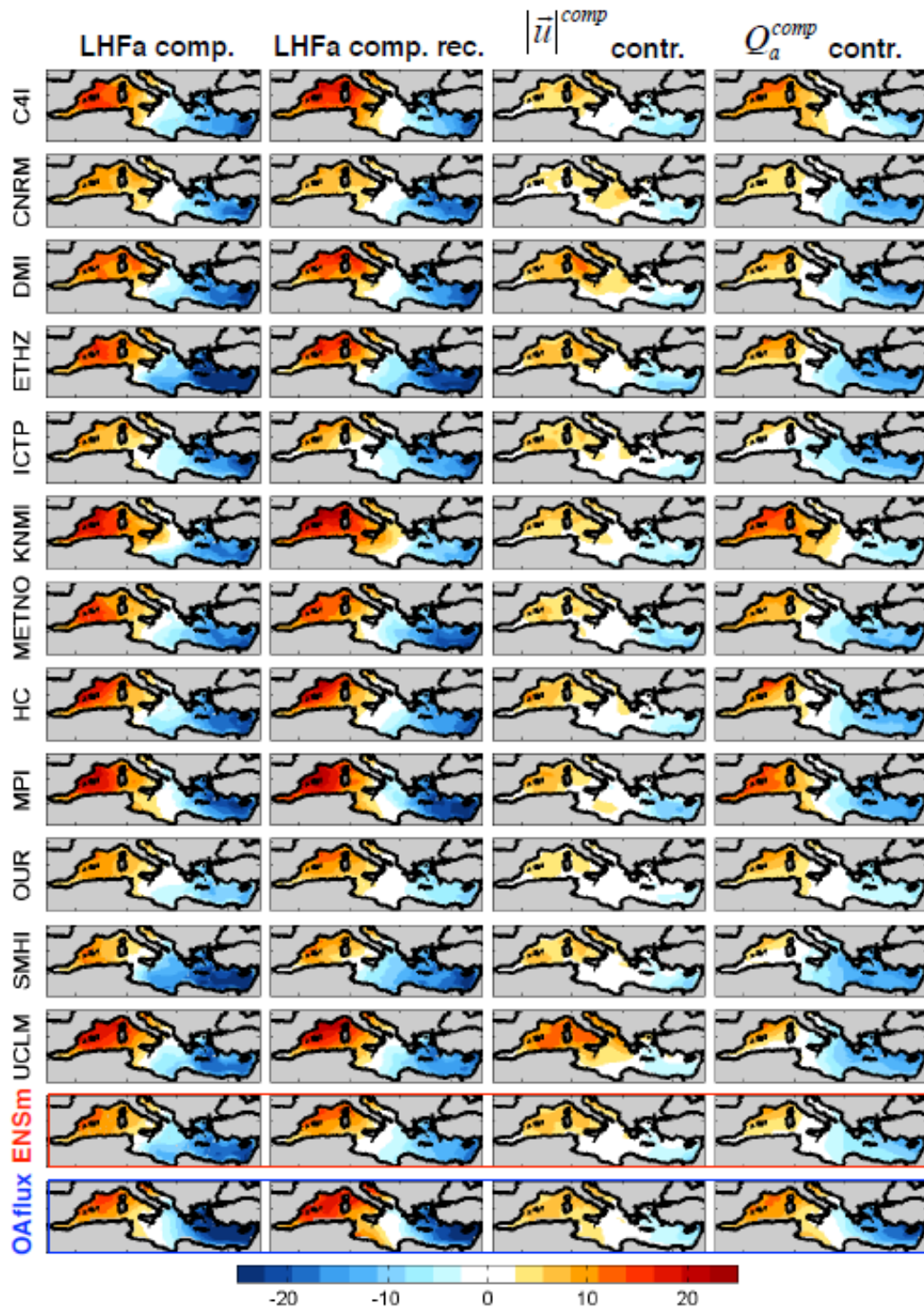
Fig.12 LHFa composites. Bulk formula reconstruction of the LHF anomalies using combination of climatological and composite fields of SST, wind speed (|u|), and 2m air specific humidity (Qa). For the composite, we selected years where the absolute value of the PC2 were above a threshold value set to 1.3 units. Then we subtracted the average field of the positive years to the average field of the negative years. The first column

shows the LHFa composite computed directly from the dataset (no bulk formula is used) while the second column shows the reconstruction using all composite fields. In the third and fourth column, only one composite filed is used for each reconstruction, respectively, |u|, and Qa. For the OAflux reconstruction we used |u| from NCEP reanalysis. Units are [W/m2].

3.5.2.1   What mechanism controls the Qa?

The LHF reconstruction exercise reveals that both winds and relative humidity play an important role in the formation of the DM. However, the role of winds is likely not limited to direct effects on the LHF. If we examine a composite of wind direction anomalies during DM, we find southerly winds over the western basin and northerly winds over the eastern basin (Fig. 13a). As we have hypothesized, this dipole in the wind direction has an indirect effect on the LHF through the horizontal advection dynamics of the Qa (e.g., transporting dryer northern air over the eastern basin and wetter southern air over the western basin during the positive phase of the DM). The rate of change of Qa associated with changes in horizontal advection is

$$\left.\frac{\partial Q_a}{\partial t}\right|_{ADV} = -\vec{u}_H \cdot \nabla_H Q_a - \frac{Q_a}{\tau} \tag{1}$$

where $\vec{u}_H$ and $\nabla_H Q_a$ denote the horizontal wind vector and the horizontal gradient of Q_a, respectively, and the second term on the right represents the dissipation of the specific humidity with timescale τ. If we split both wind field and specific humidity into both a mean component, or climatological component, and a fluctuation around the mean state, or an anomaly with respect to the climatology, we derive

$$Q_a = Q_a^{clm} + Q_a^{ano} \tag{2a}$$

$$\vec{u}_H = \vec{u}_H^{clm} + \vec{u}_H^{ano} \tag{2b}$$

Combining (1), (2a), and (2b), and neglecting the second-order term, $\vec{u}_H^{ano} \cdot \nabla_H Q_a^{ano}$, we obtain

$$\left.\frac{\partial Q_a^{ano}}{\partial t}\right|_{ADV} = -\vec{u}_H^{clm} \cdot \nabla_H Q_a^{ano} - \vec{u}_H^{ano} \cdot \nabla_H Q_a^{clm} - \frac{Q_a^{ano}}{\tau}$$

(3)

This equation can be interpreted as follows. The rate of change of the Qa anomaly resulting from advection processes is the sum of two contributions: the mean advection of the Qa anomaly and an anomalous advection of the mean specific humidity.

Given that $\partial t \ll \tau$, the dominant balance in Eq. 3, obtained by setting the right-hand side to zero, results in an explicit solution for the specific humidity:

$$Q_a^{ano} \approx [-\vec{u}_H^{clm} \cdot \nabla_H Q_a^{ano} - \vec{u}_H^{ano} \cdot \nabla_H Q_a^{clm}] \cdot \tau$$

(4)

To evaluate the contribution of each advective component to the Qa tendency associated with the DM, we define the anomalous terms of Eq. 4 using the composites of values during years in which the DM was strong. Furthermore, to optimize the fit of Eq. 4 when reconstructing the DM-driven Q_a^{ano} (Fig. 13a,b), the dissipation timescale is set to τ = 0.5d, which lies within the range of the dissipation timescales ($\tau_{min} = 6\ hours, \tau_{max} = 3\ days, \tau_{mean} = 1\ day$) estimated from the auto-decorrelation function of six-hourly specific humidity data over the Mediterranean. A comparison of the advection contributions (Fig. 13c,d) reveals that anomalous advection dominates the spatial structure and size of the Q_a^{ano} (Fig. 13a). Large values of the anomalous advection term $\vec{u}_H^{ano} \cdot \nabla_H Q_a^{clm}$ are due to the component of anomalous wind circulation oriented normal to the mean gradient of Q_a^{clm}. This finding is consistent with our initial hypothesis: that changes in winds play an even more important indirect role in the LHF dipole by influencing the advection dynamics of the Qa. Although this analysis does not constitute a full budget of the Qa, it does suggest that wind-induced anomalous advection is a major contributor to the dipole in Qa.
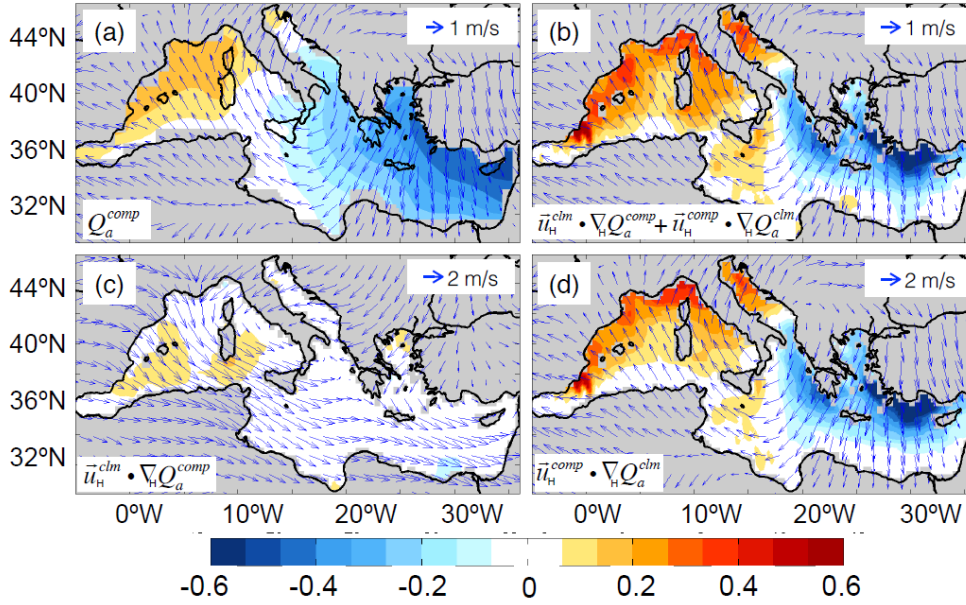
Fig.13 (a) Specific humidity anomaly composite for years of strong-phase DM. (b) Specific humidity anomaly computed using Eq. 4 with τ = 12 hours. (c) and (d) show the two terms of the right hand side of Eq. 4 representing the mean advection of the specific humidity anomaly and of the anomalous advection of the mean specific humidity, respectively. In this analysis, we used 2m air specific humidity from OAflux, and 10m wind components from NCEP reanalysis. Units are in [g kg2].

3.6 Summary and Discussion

In this work, we used two observational datasets, OAflux and NOC, and an ensemble of 12 RCMs from the EU-FP6 ENSEMBLES to investigate the dynamics of winter heat flux variability in the Mediterranean Basin from interannual to decadal time scales during 1958 to 2011. We described the first two leading modes as they appear in both observational and model data, and then we studied how they are connected with the most relevant atmospheric modes of variability for the Mediterranean region. The first few EOFs of NHF and LHF were strongly correlated (R=~0.99) and the LHF dominated NHF spatial and temporal variability (Fig. 1 and 2). Thus, our analysis focused on identifying the dynamics controlling the two dominant modes of LHF variability, which explains about ~80% of the total variance (e.g., Papadopoulos et al. 2012b; Ruiz et al. 2008; Zveryaev and Hannachi 2011) (Figs. 4 and 7).

The first mode of LHF has been characterized by a monopole and reflects coherent variations over the entire Mediterranean Basin. Depending on the datasets, this mode explains about 40% to 60% of the total variance. Its temporal variability, which tracks the domain average fluctuations of LHF (up to R=0.99, see Fig. 5), is strongly correlated with the atmospheric variability of the EA (R=0.5) (Zveryaev and Hannachi 2011). However, we found that the PC1 of LHF exhibited, after 1990, a clear trend not visible in the EA index. The nature of this LHF trend has been attributed to SST-driven changes in the surface humidity gradient linked to global warming (Mariotti 2010; Skliris et al. 2011). Moreover, using six-year low- and high-pass filtered time series on the detrended data, we found (Fig. 6) that the dynamical link between the first mode and the EA slightly decreased at high frequencies while it increased at low frequencies.

In contrast to the first mode, the second mode (i.e., DM) of LHF does not show any trend and has been characterized by a well-defined dipole structure, which represents opposite variations of LHF in the eastern and western Mediterranean Sea basins. Depending on the datasets analyzed this mode explains from 16% to 26% of the total variance. The analysis of the LHF PC2 revealed a significant correlation with the EA/WR index, which to the best of our knowledge is a new finding. While previous studies have characterized this DM statistically, we explored the spatial relevance and forcing dynamics of the mode. Given that the dipole could emerge statistically as an orthogonal pattern to the first EOF, we assessed the relevance of this mode examining how often the DM explains the spatial structure of the observed interannual anomalies of LHF. Our analysis revealed that despite the DM accounts only for about one fifth of the total variance, the spatial pattern of LHF winter anomaly is often determined by the phase of the second mode, which recurrently shows spatial correlations with observations above R=0.80 (Fig. 10).

To understand the mechanism responsible for the generation of the DM, we performed a budget analysis of the LHF winter anomalies using bulk formulas. We found that the main driver of the dipole structure is associated with changes in

the regional atmospheric circulation of EA/WR mode. Changes in the winds impact the LHF primarily through the specific humidity and wind speed (Fig. 12). The changes in specific humidity are controlled by the EA/WR wind-induced anomalous advection of cold (dry) air masses from the northeast and warm (moist) air masses from the southwest (Fig. 13). Although this work focuses on statistically derived modes of LHFa, there are direct connections between these modes and fundamental processes, such as the deep water formation in the main convection regions occurring, occurring in the basin. To establish a relationship between the results of our EOF analysis and the deep water formation, we examined the time series of the winter latent heat flux in the convection regions defined as in Josey at al. (2011). There are three specific regions in the Mediterranean Sea where dense water formations occur: the Gulf of Lions (GOL), the Aegean Sea (EAG), and the southern Adriatic Sea (ADR). Fig. 14a shows the time series of the box-averaged LHFa for both observations and models. Except for the GOL region, and similar to most of the analyses performed in this work, OAflux and ENSm are highly correlated while NOC shows some major differences. Most of the models (grey curves of Fig. 14a) are close to the ENSm in all the regions analyzed and the inter-model spread is significant only for few models and only during few specific winters. Overall, the simulations are consistent with OAflux observations.

To assess the importance of the first two basin modes of LHFa in the air-sea heat exchange over the convection regions, we computed the correlation between the box-averaged time series and the first two PCs (Fig. 14b). In addition, we estimated the total variance explained by these two modes by computing the correlation between these box-averaged anomalies and the best fitting model obtained by linearly combining the PCs (LIN, LIN= α PC1 + β PC2, where α and β are two fitting parameters determined by solving the least square problem). For both observations and models, the two leading modes show large loading in the GOL region (Fig. 4 and 7); therefore, it is not surprising that both PCs, and thus the LIN models, are significantly correlated with the LHFa times series in that region. The correlation for OAflux and ENSm is about 0.70 for both PCs, and it increases to 0.96 for the LIN model of OAflux and 0.99 for that of ENSm. Excluding

the NOC dataset, in the Aegean Sea region we found significant correlations for PCs of OAflux, ENSm, and most of the models. However, in this region, the PC1 is more strongly correlated than PC2 (e.g., for OAflux, R=0.86 for PC1 and R=-0.34 for PC2), which shows negative correlations that are consistent with the dipole nature of the second mode. The situation is different for the ADR region, where, except for the NOC dataset, PC1 shows the highest correlation among the all the convection regions considered, and PC2 is never significantly correlated. The last result is not surprising if one considers that in the ADR region the EOF2 loading is almost null (Fig. 7). In conclusion, the LHFa time series in the convection regions are tightly connected to the first two leading modes of LHFa, which when combined (i.e., LIN model) explain most of the LHF variability in the convection regions.
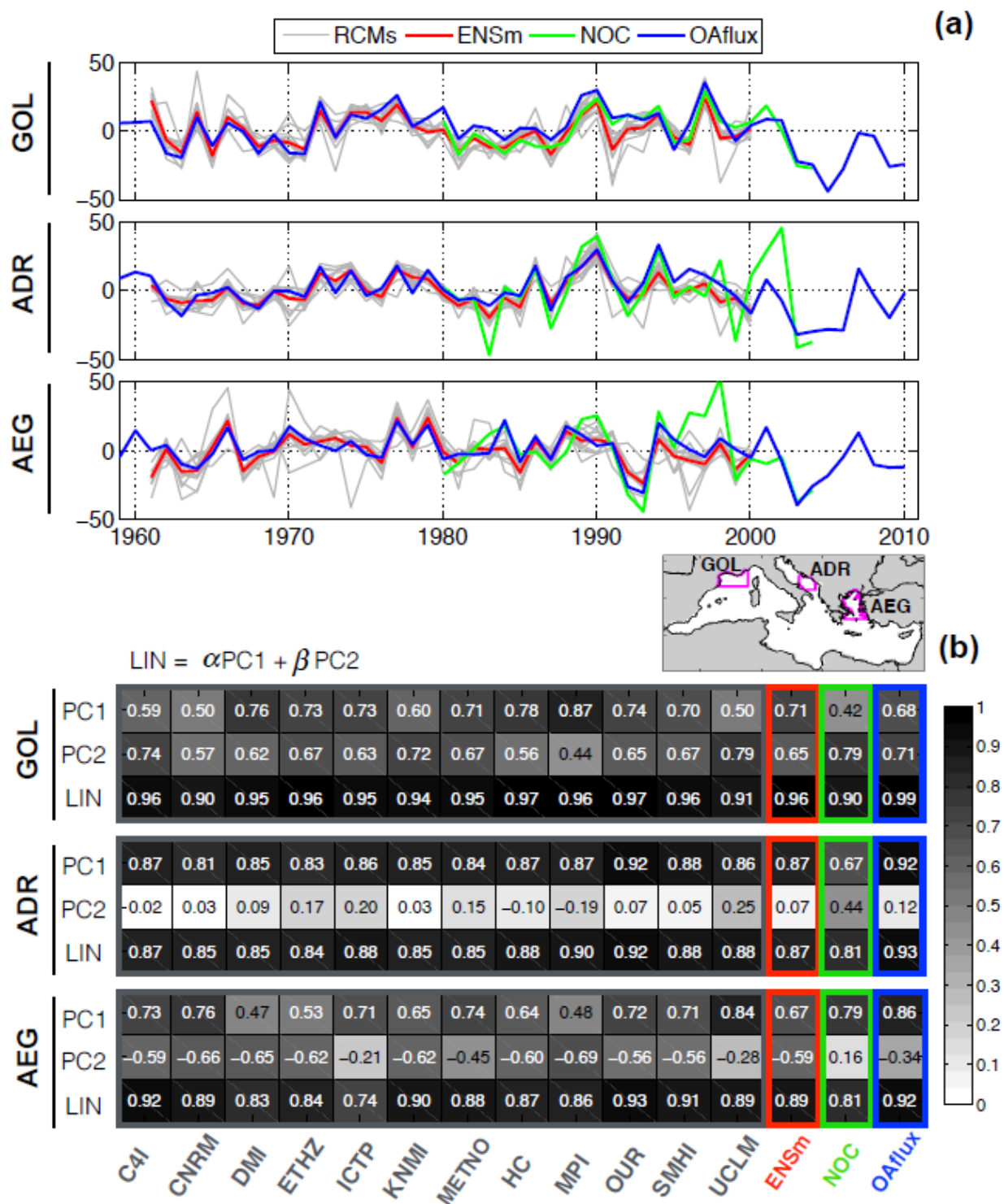
Fig.14 Variability over the convection regions. (a) Time series of winter LHF anomalies for observations, models, and ENSm, in the three main dense water formation regions: Gulf of Lion (GOL), southern Adriatic Sea (ADR), and Aegean Sea (AEG). (b) Correlation between the first two leading PCs and the time series presented in (a). The "LIN" raw shows the correlation between the box-averaged winter LHF anomalies and the best

linear model obtained by linearly combining the first two PCs. The magenta outlined regions in the map between figures (a) and (b) show the areas chosen for the calculation of the box-averaged time series shown in (a). In the subfigure (a) units are in [W/m2].

We note that the DM structure has weakened during the last decades (1996-2010) and its pattern appears less frequently in the LHF anomaly maps (Fig. 10, OAflux). Further analyses using EOFs reveal that the statistics of the DM are no longer stationary after the 1990s, and the DM no longer emerges as the second mode. Given the important role that the DM plays in determining the pattern of LHF anomalies, which in turn is an important factor controlling the deep water formation (e.g., Josey 2003), understanding significance and dynamics of these decadal changes in the DM may enhance our predictability of the Mediterranean climate. Furthermore, previous studies report how this region is one of the climate change hot-spots highlighted by the IPCC simulations (de Sherbinin 2014; Giorgi 2006). Further analyses, for example of MedCORDEX and CMIP5 climate models, are required to explore if these recent decadal changes in the DM are linked to climate change or natural internal variability.

3.7   References

Alexander MA, Blade I, Newman M, Lanzante JR, Lau NC, Scott JD (2002) The atmospheric bridge: The influence of ENSO teleconnections on air-sea interaction over the global oceans J Climate 15:2205-2231 doi:Doi 10.1175/1520-0442(2002)015<2205:Tabtio>2.0.Co;2

Andersson A, Bakan S, Fennig K, Grassl H, Klepp C-P, Schulz J (2007) Hamburg Ocean Atmosphere Parameters and Fluxes from Satellite Data - HOAPS-3 - monthly mean World Data Center for Climate doi:DOI:10.1594/WDCC/HOAPS3_MONTHLY

Artale V, Calmanti S, Malanotte-Rizzoli P, Pisacane G, Rupolo V, Tsimplis M (2006) The Atlantic and the Mediterranean Sea as connected systems. Mediterranean Climate Variability, vol 4. Elsevier,

Bignami F, Marullo S, Santoleri R, Schiano ME (1995) Longwave Radiation Budget in the Mediterranean-Sea J Geophys Res-Oceans 100:2501-2514 doi:Doi 10.1029/94jc02496

Bueh C, Nakamura H (2007) Scandinavian pattern and its climatic impact Q J Roy Meteor Soc 133:2117-2131 doi:Doi 10.1002/Qj.173

Calmanti S, Artale V, Sutera A (2006) North Atlantic MOC variability and the Mediterranean outflow: a box-model study Tellus A 58:416-423 doi:Doi 10.1111/J.1600-0870.2006.00176.X

de Sherbinin A (2014) - Climate change hotspots mapping: what have we learned? - 123

Dommenget D, Latif M (2003) Comments on "A cautionary note on the interpretation of EOFs" - Reply J Climate 16:1094-1097 doi:Doi 10.1175/1520-0442(2003)016<1094:R>2.0.Co;2

Garrett C, Outerbridge R, Thompson K (1993) Interannual Variability in Mediterranean Heat and Buoyancy Fluxes J Climate 6:900-910 doi:Doi 10.1175/1520-0442(1993)006<0900:Ivimha>2.0.Co;2

Gilman C, Garrett C (1994) Heat-Flux Parameterizations for the Mediterranean-Sea - the Role of Atmospheric Aerosols and Constraints from the Water-Budget J Geophys Res-Oceans 99:5119-5134 doi:Doi 10.1029/93jc03069

Giorgi F (2006) Climate change hot-spots Geophysical Research Letters 33 doi:Artn L08707 Doi 10.1029/2006gl025734

Haines K, Wu PL (1995) A modelling study of the thermohaline circulation of the Mediterranean Sea: Water formation and dispersal Oceanol Acta 18:401-417

Herrmann MJ, Somot S (2008) Relevance of ERA40 dynamical downscaling for modeling deep convection in the Mediterranean Sea Geophysical Research Letters 35 doi:Artn L04607 Doi 10.1029/2007gl032442

Hurrell JW (1995) Decadal Trends in the North-Atlantic Oscillation - Regional Temperatures and Precipitation Science 269:676-679 doi:DOI 10.1126/science.269.5224.676

Josey SA (2003) Changes in the heat and freshwater forcing of the eastern Mediterranean and their influence on deep water formation Journal of Geophysical Research 108 doi:10.1029/2003jc001778

Josey SA, Kent EC, Taylor PK (1999) New insights into the ocean heat budget closure problem from analysis of the SOC air-sea flux climatology J Climate 12:2856-2880 doi:Doi 10.1175/1520-0442(1999)012<2856:Niitoh>2.0.Co;2

Josey SA, Somot S, Tsimplis M (2011) Impacts of atmospheric modes of variability on Mediterranean Sea surface heat exchange Journal of Geophysical Research 116 doi:10.1029/2010jc006685

Kalnay E et al. (1996) The NCEP/NCAR 40-year reanalysis project Bulletin of the American Meteorological Society 77:437-471

Krichak SO, Kishcha P, Alpert P (2002) Decadal trends of main Eurasian oscillations and the Eastern Mediterranean precipitation Theor Appl Climatol 72:209-220 doi:DOI 10.1007/s007040200021

Lascaratos A, Roether W, Nittis K, Klein B (1999) Recent changes in deep water formation and spreading in the eastern Mediterranean Sea: a review Prog Oceanogr 44:5-36 doi:Doi 10.1016/S0079-6611(99)00019-1

Madec G, Chartier M, Delecluse P, Crepon M (1991) A 3-Dimensional Numerical Study of Deep-Water Formation in the Northwestern Mediterranean-Sea J Phys Oceanogr 21:1349-1371

Mariotti A (2010) Recent Changes in the Mediterranean Water Cycle: A Pathway toward Long-Term Regional Hydroclimatic Change? J Climate 23:1513-1525 doi:Doi 10.1175/2009jcli3251.1

North GR, Bell TL, Cahalan RF, Moeng FJ (1982) Sampling Errors in the Estimation of Empirical Orthogonal Functions Mon Weather Rev 110:699-706 doi:Doi 10.1175/1520-0493(1982)110<0699:Seiteo>2.0.Co;2

OrtizBevia MJ, Alvarez-Garcia FJ, de Elvira AR, Liguori G, Carretero JH (2012) The Western Mediterranean summer variability and its feedbacks Clim Dynam 39:3103-3120 doi:DOI 10.1007/s00382-012-1409-x

Papadopoulos VP, Josey SA, Bartzokas A, Somot S, Ruiz S, Drakopoulou P (2012a) Large-Scale Atmospheric Circulation Favoring Deep- and Intermediate-Water Formation in the Mediterranean Sea J Climate 25:6079-6091 doi:Doi 10.1175/Jcli-D-11-00657.1

Papadopoulos VP, Kontoyiannis H, Ruiz S, Zarokanellos N (2012b) Influence of atmospheric circulation on turbulent air-sea heat fluxes over the Mediterranean Sea during winter J Geophys Res-Oceans 117 doi:Artn C03044

Doi 10.1029/2011jc007455

Rahmstorf S (1996) On the freshwater forcing and transport of the Atlantic thermohaline circulation Clim Dynam 12:799-811 doi:Doi 10.1007/S003820050144

Rahmstorf S (1998) Influence of Mediterranean Outflow on climate Eos, Transactions American Geophysical Union 79:281-282 doi:10.1029/98EO00208

Roether W, Klein B, Manca BB, Theocharis A, Kioroglou S (2007) Transient Eastern Mediterranean deep waters in response to the massive dense-water output of the Aegean Sea in the 1990s Prog Oceanogr 74:540-571 doi:DOI 10.1016/j.pocean.2007.001

Roether W et al. (1996) Recent changes in eastern Mediterranean deep waters Science 271:333-335

Ruiz S, Gomis D, Sotillo MG, Josey SA (2008) Characterization of surface heat fluxes in the Mediterranean Sea from a 44-year high-resolution atmospheric data set Global and Planetary Change 63:258-274 doi:10.1016/j.gloplacha.2007.12.002

Sanchez-Gomez E, Somot S, Josey SA, Dubois C, Elguindi N, Déqué M (2011) Evaluation of Mediterranean Sea water and heat budgets simulated by an ensemble of high resolution regional climate models Clim Dynam 37:2067-2086 doi:10.1007/s00382-011-1012-6

Schroeder K, Ribotti A, Borghini M, Sorgente R, Perilli A, Gasparini GP (2008) An extensive western Mediterranean deep water renewal between 2004 and 2006 Geophysical Research Letters 35 doi:Artn L18605

Doi 10.1029/2008gl035146

Simmons AJ, Wallace JM, Branstator GW (1983) Barotropic Wave-Propagation and Instability, and Atmospheric Teleconnection Patterns J Atmos Sci 40:1363-1392 doi:Doi 10.1175/1520-0469(1983)040<1363:Bwpaia>2.0.Co;2

Skliris N, Sofianos S, Gkanasos A, Mantziafou A, Vervatis V, Axaopoulos P, Lascaratos A (2011) Decadal scale variability of sea surface temperature in the Mediterranean Sea in relation to atmospheric variability Ocean Dynamics 62:13-30 doi:10.1007/s10236-011-0493-5

Theocharis A, Nittis K, Kontoyiannis K, Papageorgiou E, Balopoulos E (1999) Climatic changes in the Aegean Sea influence the Eastern Mediterranean thermohaline circulation (1986-1997) Geophysical Research Letters 26:1617-1620

Uppala SM et al. (2005) The ERA-40 re-analysis Q J Roy Meteor Soc 131:2961-3012

Vickers D, Mahrt L (2006) Evaluation of the air-sea bulk formula and sea-surface temperature variability from observations J Geophys Res-Oceans 111 doi:Artn C05002 Doi 10.1029/2005jc003323

Wallace JM, Gutzler DS (1981) Teleconnections in the Geopotential Height Field during the Northern Hemisphere Winter Mon Weather Rev 109:784-812 doi:Doi 10.1175/1520-0493(1981)109<0784:Titghf>2.0.Co;2

Zhang YC, Rossow WB, Lacis AA, Oinas V, Mishchenko MI (2004) Calculation of radiative fluxes from the surface to top of atmosphere based on ISCCP and other global data sets: Refinements of the radiative transfer model and the input data J Geophys Res-Atmos 109 doi:Doi 10.1029/2003jd004457

Zveryaev II, Hannachi AA (2011) Interannual variability of Mediterranean evaporation and its relation to regional climate Clim Dynam 38:495-512 doi:10.1007/s00382-011-1218-7

CHAPTER 4

Climate variability of the Iberian Peninsula

Nature is relentless and unchangeable, and it is indifferent as to whether its hidden reasons and actions are understandable to man or not.

Galileo Galilei

This chapter we studied the present climate variability of the Iberian Peninsula using a multi-model ensemble of 4 regional climate models and observations. We first focused on the mean fields and interannual variability and then investigated climate extremes of temperature and precipitation. The content of this chapter has been published in the following manuscripts:

Jimenez-Guerrero P, Montavez JP, Dominguez M, Romera R, Fita L, Fernandez J, Cabos WD, **Liguori G**, Gaertner MA (2013)
Mean Fields and Interannual Variability in RCM Simulations over Spain: The ESCENA Project.
Clim Res 57 (3): 201–20.

Dominguez M, Romera R, Sanchez E, Fita L, Fernandez J, Jimenez-Guerrero P, Montavez JP, Cabos WD, **Liguori G**, Gaertner MA (2013)
Present-climate precipitation and temperature extremes over Spain from a set of high resolution RCMs.
Clim Res 58: 149-164, doi: 10.3354/cr01186

Present-climate precipitation and temperature extremes over Spain from a set of high resolution RCMs

Marta Domínguez[1],*, Raquel Romera[1], Enrique Sánchez[2], Lluis Fita[3], Jesús Fernández[3], Pedro Jiménez-Guerrero[4], Juan Pedro Montávez[4], William David Cabos[5], Giovanni Liguori[5], Miguel Ángel Gaertner[2]

[1]Environmental Sciences Institute, Environmental Science Institute, 45071 Toledo, Spain
[2]Environmental Science Faculty, University of Castilla-La Mancha, 45071 Toledo, Spain
[3]Grupo de Meteorología, Dept. Applied Mathematics and Computer Science, University of Cantabria, 39005 Santander, Spain
[4]Department of Physics, Regional Campus of International Excellence 'Campus Mare Nostrum', University of Murcia, 30100 Murcia, Spain
[5]Department of Physics, Climate Physics Group, University of Alcalá de Henares, 28805 Madrid, Spain

ABSTRACT: In the frame of the Spanish project ESCENA, 5 regional climate model simulations were analyzed in terms of their representation of precipitation and temperature extremes over Spain. The climate complexity of the target domain poses a challenge for the models in terms of their ability to simulate precipitation and temperature extremes. There are important differences in comparison to previous similar studies (such as PRUDENCE and ENSEMBLES European projects): the domain of the present-climate simulations (1990 to 2007) is centered over the Iberian Peninsula (IP), and the simulations are nested in ERA-Interim reanalysis. Two of the models (WRF and MM5) were not part of the ENSEMBLES project. A new high-resolution (0.2° × 0.2°) database (Spain02) of daily temperature and precipitation observations over Spain was used to validate the results. The performance of the models depends on the climatic characteristics of the subregions. Results are better for the northern coastal area of Spain, but for other Atlantic basins there are some biases that cannot be linked to limitations in the representation of very heavy convective events. Several models underestimate the amount of rain for heavy-precipitation days. This aspect has not improved in general in comparison to ENSEMBLES results, despite the differences in setup. In other respects, all models are at a similar level as the best subgroup of ENSEMBLES models. The ESCENA simulations (covering more emissions scenarios and GCMs than ENSEMBLES project) can thus be considered a valuable complement of that European project for impact studies over Spain.

KEY WORDS: Climate extremes · Extreme precipitation · Extreme temperatures · Regional climate models · Iberian Peninsula · Heavy precipitation · Droughts · Heat waves

1. INTRODUCTION

The analysis of extreme events under the present climate is important in order to assess the reliability of climate change projections, because it is likely that the frequency and intensity of extreme events and the size of affected areas will increase in the future (Sánchez et al. 2011, Field et al. 2012). Beniston et al.

(2007) defines an extreme event as rare, intense and severe. Thus, extreme events are usually analyzed in terms of frequency distribution tails of climate variables, including high percentiles and record-breaking events, known to have caused severe impacts.

A global tendency towards an increased frequency of some extreme events during the 20th century has been found in several studies, but the results show

large spatial variability (Alexander et al. 2006, Vincent & Mekis 2006, López-Moreno & Beniston 2009, Hirschi et al. 2010). The socio-economic impact of extreme temperature is not only related to hot or cold individual days, but also to persistent events like cold and heat waves (Fischer & Schär 2010). More frequent and intense summer heat waves have been observed at global and European scales (Alexander et al. 2006, Della-Marta et al. 2007, Barriopedro et al. 2011).

To understand the mechanisms behind extreme events in present and future climate, global circulation models (GCMs) and regional climate models (RCMs) have been used. The increased frequency of observed extreme events has been studied at different spatial scales, from global (Frich et al. 2002), to continental (Beniston & Stephenson 2004, Schär et al. 2004) and down to regional scale (Huth et al. 2000). On this respect, the Intergovernmental Panel on Climate Change (IPCC 2001, 2007) recommended more adequate analyses and regional detail for model projections. At the same time, end-users, such as impact modellers, demand climate data at higher spatial resolution than given by GCMs (Castro et al. 2007). There is, thus, a need for high resolution climate projections. Additionally, model uncertainties are explored by means of multi-model ensembles of simulations. The generation of high-resolution regional climate information through an ensemble of RCM simulations has been the basis for several international projects (e.g. PRUDENCE, ENSEMBLES in Europe, NARCCAP in North America). Currently, such an approach is being extended to most continental regions of the world in the frame of CORDEX project (COordinated Regional climate Downscaling EXperiment; Giorgi et al. 2009). Among other advantages, the estimation of the spatial and temporal distribution of extreme precipitation episodes has been improved using climate models with high resolution (Beniston 2006, Frei et al. 2006, Beniston et al. 2007) compared to those using lower resolutions.

In the Mediterranean region, extreme events have strong impacts on ecosystems, socio-economic activities and agriculture (Vicente-Serrano et al. 2004, Lana et al. 2006, Vicente-Serrano 2006a). Results from RCMs including the Iberian Peninsula (IP) in their domains (Sánchez et al. 2004, 2011, López-Moreno & Beniston 2009, Herrera et al. 2010) highlight the importance of high spatio-temporal resolution for the study of extreme events over this area. The irregularity of precipitation and the strong seasonal variations in the IP make this region particularly interesting for the study of precipitation and temperature extremes,

which caused considerable damage over the last century (García-Herrera et al. 2005, Vicente-Serrano 2006b). Instead of considering the IP as a single region as in previous studies performed in the frame of PRUDENCE and ENSEMBLES European Projects (e.g. Boberg et al. 2009, 2010, Fischer & Schär 2010, Kjellström et al. 2010), in the present study the analyzed domain has been divided in 6 subregions to take into account the high spatial variability of the IP climate. A correct simulation of present climate is needed to detect changes in key variables that could modify the availability of water resources (Martin-Vide 2004, López-Moreno & Beniston 2009).

In previous modelling studies over Europe, RCM simulations were compared with the gridded observational climate database E-OBS (Haylock et al. 2008). E-OBS has been very useful in many analyses of temperature extremes (Fischer et al. 2007, Hirschi et al. 2010). However, due to the high spatial variability of the climate in the IP, the amount of stations underlying E-OBS is insufficient for this region. High resolution climate data (Brunetti et al. 2001, González-Hidalgo et al. 2003) and gridded data based on much denser station networks than E-OBS are needed for RCM evaluation studies (Kysely & Plavcova 2010). Here we use the $0.2° \times 0.2°$ gridded daily precipitation and temperature dataset Spain02 (see section 2.3), developed for Peninsular Spain (PS) and the Balearic Islands (BA) (Herrera et al. 2012). Spain02 was tested (Herrera et al. 2012) against point observations and compared to E-OBS database. This new database (Spain02) proved to represent better the intensity and spatial variability of several standard extreme climate indices defined by Sillmann & Roeckner (2008).

The present study analyzes the results for present climate from 5 RCM simulations, focusing on their ability to represent extreme events. The RCM simulations have been performed within the Spanish project ESCENA, and complement and extend ENSEMBLES results (using the same horizontal resolution of 25 km) through the use of improved and/or additional RCMs, new GCM/RCM matrix combinations, and a larger set of emission scenarios (A1B, A2 and B1). Results of ESCENA project are publicly available for impact or regional climate studies (http://proyectoescena.uclm.es). An important difference with respect to PRUDENCE and ENSEMBLES is the simulation domain. It is centered over the IP and covers larger parts of the Atlantic Ocean, including the Canary Islands, which were not included in these European projects. Additionally, evaluation model runs are forced by the ERA-Interim reanalysis instead of the ERA-40 reanalysis used in ENSEMBLES. We focused this study on PS

and the BA, where the high-resolution Spain02 database is available.

2. METHODS AND DATA

2.1. Regional climate models

The RCM ensemble includes 5 different models (PROMES, 2 versions of WRF model, MM5 and REMO). These models have been developed at different institutions. A summary of the physics parameterizations for each of them is shown in Table 1. These models are described in more detail in Jiménez-Guerrero et al. (2013).

The RCM PROMES (Castro et al. 1993, Sánchez et al. 2004) was developed at the Complutense University of Madrid and the University of Castilla-La Mancha (Spain). Several changes have been introduced in PROMES with respect to previous simulations. The most significant changes are the coupling to OR-CHIDEE land surface model (Krinner et al. 2005) and the change of radiation parameterization, as explained in Domínguez et al. (2010). The Weather Research and Forecasting (WRF) model is a state-of-the-art limited area model developed in collaboration between the National Center for Atmospheric Research (NCAR) and a number of research institutions in the US. In this study we used the Advanced Research WRF core (version 3.1.1; Skamarock et al.

2008), which is the research version of the model. WRF model simulations were run by the Santander Meteorology Group of the University of Cantabria, Spain. The model includes modifications introduced by this group to get averaged and extreme values of surface variables (Fita et al. 2010) and was run through the WRF4G execution workflow (Fernández-Quiruelas et al. 2010). Two different configurations were used in the simulations (labeled as WRF-A and WRF-B in Table 1). They only differ in the Planetary Boundary Layer (PBL) scheme. WRF-A uses a local scheme, whereas WRF-B uses a non-local scheme. MM5-UM is the climate version of the fifth-generation Pennsylvania State University–NCAR mesoscale model (Dudhia 1993, Grell et al. 1994, Gómez-Navarro et al. 2010). The physical configuration (Table 1) has been chosen in order to minimise the computational cost, since none of the tested configurations provides the best performance for all kinds of synoptic events and regions of the IP (Fernández et al. 2007). REMO is a hydrostatic, 3-dimensional regional climate atmospheric model, developed at the Max-Planck-Institute for Meteorology in Hamburg. It is based on the Europa Model, a former numerical weather prediction model of the German Weather Service and it is described in Jacob (2001) and Jacob et al. (2001). REMO uses the physical package of the global circulation model ECHAM4 (Roeckner et al. 1996). All models are configured with a relaxation boundary of 8 to 10 grid points.

Table 1. Physics parameterizations used by the models in the simulations analyzed in the study. PBL: planetary boundary layer, LSM: Land Surface Model, CAM: Community Atmosphere Model

Model	Microphysics	Cumulus	Radiation	PBL	Land surface
PROMES	Includes ice processes (Hong et al. 2004)	Kain & Fritsch (1993)	ECMWF (2004) with fractional cloud cover (Chaboureau & Bechtold 2002, 2005)	Cuxart et al. (2000)	ORCHIDEE LSM (Krinner et al. 2005)
WRF-A	Single-moment 5-class microphysics (Hong & Lim 2006)	Grell & Devenyi (2002)	CAM 3.0 (Collins et al. 2006)	Local Mellor-Yamada-Janjic (Janjić 1990, 1994)	NOAH LSM (Chen & Dudhia 2001a,b)
WRF-B	Single-moment 5-class microphysics (Hong & Lim 2006)	Grell & Devenyi (2002)	CAM 3.0 (Collins et al. 2006)	Non-local Yonsei University (Hong et al. 2006)	NOAH LSM (Chen & Dudhia 2001a,b)
MM5	Simple ice (Dudhia 1989)	Grell (1993)	Rapid radiative transfer model (RRTM) (Mlawer et al. 1997)	Medium-range forecast (MRF) (Hong & Pan 1996)	NOAH LSM (Chen & Dudhia 2001a,b)
REMO	Stratiform clouds (Sundqvist 1978), (Roeckner et al. 1996)	Mass flux convection scheme after Tiedtke (1989) with modifications after Nordeng (1994)	Morcrette et al. (1986) with modifications after Giorgetta & Wild (1996)	Higher-order closure scheme (Brinkop & Roeckner 1995)	Types of vegetation (FAO). Bucket scheme for hydrology. Five layers for thermal processes

2.2. Simulation set up

The RCM simulations cover part of Europe, with a domain centered on the IP (Fig. 1 showing the land mask and orography for each model) and 25 × 25 km of horizontal resolution in Lambert Conformal projection (PROMES, both versions of WRF and MM5) or in a rotated latitude–longitude coordinate system (REMO). The topography has been interpolated from GTOPO30 data (Verdin & Greenlee 1996). The horizontal coordinates are arranged in Arakawa-B (MM5) or Arakawa-C (PROMES, REMO and both versions of WRF) grids. PROMES model used 37 sigma levels in the vertical, WRF 33, MM5 30 and REMO 31 levels (up to 10 hPa for all models). The simulations cover the period from 1990 to 2007, with 1 yr of spin-up.

The ERA Interim reanalysis derived from the latest version of the operational ECMWF system has several differences to ERA-40 (Uppala et al. 2005), such as improvements in model physics, new humidity analysis, variational bias correction of satellite radiance data, among others (Dee & Uppala 2009). In this study all models used boundary conditions from ERA-Interim with a spatial resolution of 0.7° × 0.7°, updated every 6 h.

2.3. Spain02 observation database

The Spain02 precipitation and temperature database is a daily gridded dataset developed by Herrera et al. (2012) using surface station data from a set of
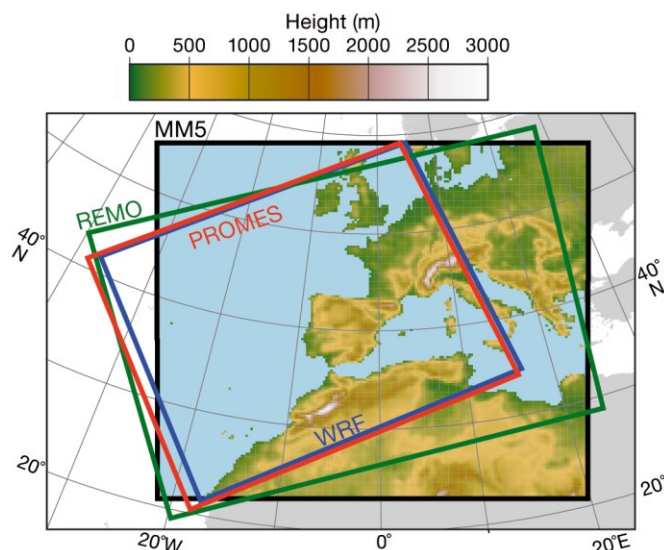

Fig. 1. Simulation domain of the 5 models used in the study: MM5, PROMES, REMO, WRF-A and -B

2756 quality-controlled stations over PS and the BA. There are currently insufficient surface observations to include the Canary Islands in the database. Here we present the most important features of this observational data. This data set spans from 1950 to 2008, with daily frequency and 0.2° × 0.2° resolution. The fields were interpolated in a 2-step process. First, the monthly means were interpolated using thin-plate splines. Second, daily departures from the monthly means were interpolated using a kriging methodology. In the case of precipitation, occurrence and amounts are interpolated through indicator and ordinary kriging, respectively. The interpolation procedure for precipitation is similar to that of the E-OBS European database (Haylock et al. 2008), except for the absence of the elevation-dependent splines applied to E-OBS database, which was not used in Spain02 (the topography is well represented by the large amount of stations).

For temperature, the Spain02 database applied a more stringent filter to the station data in order to provide a product better suited for trend analyses. Unlike the precipitation product, where the maximum number of available stations at a given day were used, the temperature data set was built from a reduced set of stations with the longest records. In particular, only those stations with a record longer than 40 yr and <1 % of missing data were included in the interpolation. This led to a set of 186 stations. These stations were gridded using the same methodology as E-OBS (including the use of elevation as covariable, given the smaller amount of stations). The differences to E-OBS are the better quality and larger amount of stations. The large number of stations used in this product compared with E-OBS database, provides a better representation of the precipitation (Herrera et al. 2012) and temperature variability over Spain. Details of the interpolation procedure can be found in Herrera (2011) and Herrera et al. (2012).

2.4. Statistical analysis

The analyzed variables present a high spatial variability in a relatively small area, especially precipitation (Herrera et al. 2010). In the study of the climate features of a given region, information provided by the frequency distribution is complementary to simpler statistical analyses from which an integrated representation of climatic conditions over a region is provided (Giorgi et al. 2004a,b, Christensen & Christensen 2007, Déqué et al. 2007, Jacob et al. 2007).

Additionally, the use of subregions provides more useful results for some impact studies. Thus, our precipitation analysis was performed using the upper tail of the precipitation distribution for the subregions, and by examining the values of some standard extreme climate indices.

The probability density function (PDF) for precipitation was approximated by a histogram of the relative frequencies of daily precipitation amounts (days with precipitation ≥1 mm) binned into 1 mm d^{-1} bins. A clearer visualization of the highest precipitation values is provided using a logarithmic scale. The PDFs are normalized by dividing by the total amount of precipitation data (1 value per day and grid point) in order to take into account the different size of the subregions. Comparison of the simulated results with observed values was performed using the PDFs calculated directly at the original grids for each subregion. Due to the similar resolution of both sources (0.2° × 0.2° for Spain02 and 25 × 25 km for RCMs), the differences in subregion limits and extension are rather small among the different grids. This avoids the smoothing of extreme values which may arise from regridding.

In order to take into account the different precipitation regimes, the PDFs and the related analyses were carried out for different subregions obtained by grouping the 11 basins described in Herrera et al. (2010) according to the similarity of their annual cycles. In Fig. 2 these subregions are shown for the Spain02 grid; for the RCMs, equivalent subregions in the original grid of each model have been used. The 6 subregions are North (NO), Center-South (CE-SU), Levant (LE), Ebro (EB), Cataluña (CA) and the BA.

For the purpose of quantifying the overlap of the upper tail of the precipitation PDF between every RCM and Spain02, we applied a skill score (Perkins et al. 2007), previously used by Boberg et al. (2009), Boberg et al. (2010) and Kjellström et al. (2010). We introduced a small variation in Perkins' score, computing only the upper tail of the PDF, defined as the truncated PDF obtained using events larger than the 95th percentile of the observed precipitation. This metric has been calculated on all grid points and results are given as spatial averages for each subregion. It takes values between 0 to 1, where 1 indicates maximum overlap.

Extreme temperatures are represented selecting different percentiles of daily maximum and minimum temperature depending on the season: the 10th percentile in winter (December to February) and the 90th percentile in summer (June to August). Moreover, in order to analyse extreme events in a comple-
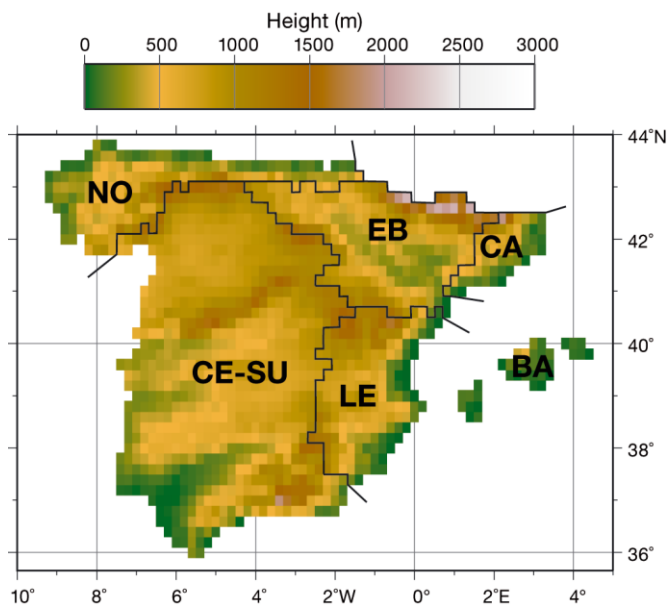

Fig. 2. Spain02 database orography and subregions: North (NO; 178 grid points), Center-South (CE-SU; 756), Levant (LE; 183), Ebro (EB; 234), Cataluña (CA; 57) and Balearic Islands (BA; 37)

mentary way, we used several indices (Klein Tank et al. 2009) applied over the IP by authors like de la Cruz Gallego et al. (2004), Sánchez et al. (2004), Gallego et al. (2005) and Herrera et al. (2010), among others. The selected indices are indicated in Table 2.

For precipitation, we selected medium-high intensity indices representing droughts or high intensity precipitation episodes. As frequency indices, we took the consecutive dry days (<1 mm) index (CDD) and the very heavy precipitation (>20 mm) days index (R20mm). As intensity index, we chose the fraction of precipitation due to events above the 95th percentile (R95PTOT). We calculated some other indices, but their spatial distribution was similar to the indices shown. All indices (see Table 2) are presented as yearly averages except R95PTOT.

For temperature, we used the yearly number of heat waves (HWn), the yearly maximum heat wave duration (HWd) and a set of temperature indices. A heat wave is defined as an event with maximum temperatures >35°C during at least 5 consecutive days. This threshold has been calculated by averaging over the whole domain the 95th percentile of Spain02 climatology (1961 to 1990). These indices are more sensitive to model biases, since they are defined by absolute values rather than relative ones. The complementary temperature indices include the tropical nights index (TR) (number of days with minimum temperature >20°C) and the combined tropical

Table 2. Precipitation and temperature extreme indices. Tx (Tn): maximum (minimum) temperature

Index	Description	Units
Precipitation		
CDD	Consecutive dry days index (yearly mean)	d yr^{-1}
R20MM	Very heavy precipitation days index (yearly mean)	d yr^{-1}
R95PTOT	Precipitation fraction due to 95 percentile	%
Temperature		
HWd	Maximum heat wave duration per year (yearly mean)	d yr^{-1}
HWn	Heat wave number index (yearly mean)	heat waves yr^{-1}
TR	Tropical nights index (Tn > 20°C)	d yr^{-1}
CHT	Combined HW and TR (Tn > 20°C and Tx > 35°C)	d yr^{-1}

nights and summer days index (CHT, number of days with minimum temperature >20°C and maximum temperature >35°C; Fischer & Schär 2010).

The spatial representation of extreme indices is analysed with the Pearson correlation for the whole PS and BA. Regarding ensemble values, the ensemble mean of the models indices was calculated for each statistical index. In contrast, the PDF ensemble was created using all daily precipitation data from all the models without averaging.

3. RESULTS

3.1. Precipitation

3.1.1. PDF tail analyses

Fig. 3 shows the simulated precipitation PDF for the different RCMs, the multi-model ensemble and the observed Spain02 data for the 6 subregions. The large spatial variability of precipitation over the IP is clearly seen from the observed precipitation PDFs. Differences are relatively high: CE-SU subregion shows comparatively low frequency of the most extreme values (>100 mm d^{-1}), whereas LE, CA and BA show a relatively high frequency of such values. This reflects the division between Atlantic and Mediterranean precipitation regimes.

The spread of the simulated PDFs is highly dependent on the considered subregion. The lowest spread of the simulations is seen in the NO subregion. At the same time, differences between simulated and observed values are the lowest there, basically due to the small temporal variability in the area. Atlantic frontal systems are very frequent here. The precipitation associated with these systems is in general well represented by RCMs (Herrera et al. 2010). By contrast, Mediterranean subregions have

a marked seasonal precipitation regime with high spatio-temporal variability. Extreme precipitation is quite often related to severe convective events which are more difficult to simulate by RCMs (e.g. Herrera et al. 2010). This result in a high spread of simulated precipitation for the CE-SU subregion. This area includes Atlantic basins, where precipitation is typically linked to Atlantic depressions; however, the seasonality of precipitation is much higher than for the NO subregion. Most models tend to underestimate precipitation for the CE-SU subregion, as found in previous studies (e.g. Herrera et al. 2010).

Fig. 3 also shows the 95th percentile of Spain02 data, used as the threshold for the modified Perkins score. Subregions like BA or CA have the highest 95th percentile values (~30 mm d^{-1}), while for the rest of the domain it most often does not exceed 25 mm d^{-1}. Table 3 shows the calculated skill scores values. The values at the NO and CE-SU subregions are rather high (≥0.90). The spread is smaller there than for the eastern part of PS. Maximum differences of about 25% are found at the BA. Subregions with higher spreads have lower scores. The RCMs present in general a good agreement with the observed PDF, with score values between 0.75 and 0.95, except for the BA that have the lowest score (<0.74 for all models). These lower values could be related to the small number of grid points representing the islands, and the consequent worse representation of orography in this subregion. The ensemble scores are consistently higher than the scores obtained for the individual models.

3.1.2. Extreme precipitation indices

Regarding dry spells, the CDD index (Fig. 4, left column) has a spatial distribution with a strong north–south gradient. Center and South PS show the
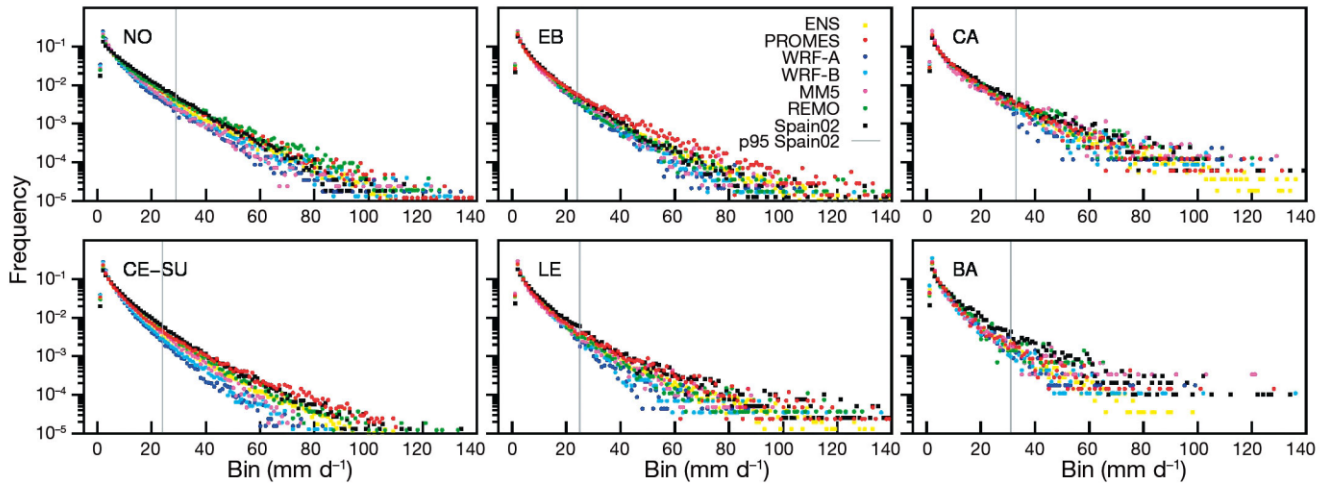
Fig. 3. Precipitation PDF of Spain02 data (black dots) and the 5 RCMs: PROMES (red), WRF-A (dark blue), WRF-B (light blue), MM5 (pink) and REMO (green), and the ensemble mean (ENS; yellow) over 6 Spanish subregions (North: NO, Center-South: CE-SU, Ebro: EB, Levant: LE, Cataluña: CA, Balearic Islands: BA) from January 1990 to December 2007. Gray lines: 95th percentile (p95) for each region

Table 3. Results for the modified Perkins' skill score (see Section 2.4) of extreme precipitation (higher than p95 of Spain02) for the 6 Spanish subregions (North: NO, Center-South: CE-SU, Levant: LE, Ebro: EB, Cataluña: CA, Balearic Islands: BA), the 5 RCMs (PROMES, WRF-A, WRF-B, MM5 and REMO) and the ensemble (ENS) mean

	NO	CE-SU	LE	EB	CA	BA
PROMES	0.93	0.93	0.88	0.88	0.83	0.73
WRF-A	0.93	0.90	0.82	0.92	0.75	0.67
WRF-B	0.93	0.93	0.84	0.93	0.83	0.74
MM5	0.92	0.92	0.87	0.94	0.80	0.61
REMO	0.90	0.96	0.89	0.91	0.82	0.55
ENS	0.94	0.97	0.91	0.94	0.86	0.79

highest observed values, with maximum values >100 d yr^{-1}. This reflects the summer dry period. Differences among RCMs are not high. Results show generally an underestimation of observed values over most of the domain, except some models (WRF-A, WRF-B and REMO) in parts of the Mediterranean subregions (LE, CA and BA). RCMs and observations differ considerably in some areas, particularly near the Mediterranean southern coast, where for example PROMES or MM5 simulate values of ~40% of the observed CDD. However, spatial correlations of ~0.90 for all models indicate a good concordance between observed and simulated spatial distributions of this index (see Fig. 7). The ensemble mean only gives a better value of the index in comparison with some models in certain subregions.

The observed spatial distribution for R20MM index and the corresponding model biases are shown in the middle column of Fig. 4. The highest values are found in the northern part of PS, in coherence with its precipitation regime. The next highest values are observed in mountainous areas of the CE-SU subregion, followed by CA subregion. The spatial distribution of this index shows no clear relationship to the distribution of CDD index, as high numbers of days >20 mm occur both for low and high CDD areas. This illustrates well the large differences of rain regimes in this small domain. The smallest differences with respect to observations are obtained by PROMES, whereas the other RCMs underestimate this index, especially both versions of WRF model (spatial correlation values vary from 0.72 [WRF-A] to 0.79 [WRF-B]).

The R95PTOT index (Fig. 4, right column) is related to the heaviest precipitation events. Observed values obtained from Spain02 data show a clear maximum for the Mediterranean coastal areas. The RCMs are able to reproduce the observed climatic contrast between areas with high and low values of the heaviest rain events. However, they slightly overestimate this index over most of the domain. PROMES and MM5 show the largest positive bias extending over the widest areas. WRF-A values are the closest of all models to the observed data over most of the domain. The R95PTOT spatial correlations (see Fig. 7) are the lowest among all precipitation indices. These low R95PTOT correlation values could indicate the difficulty of simulating the precise spatial location of heavy convective events using RCMs.
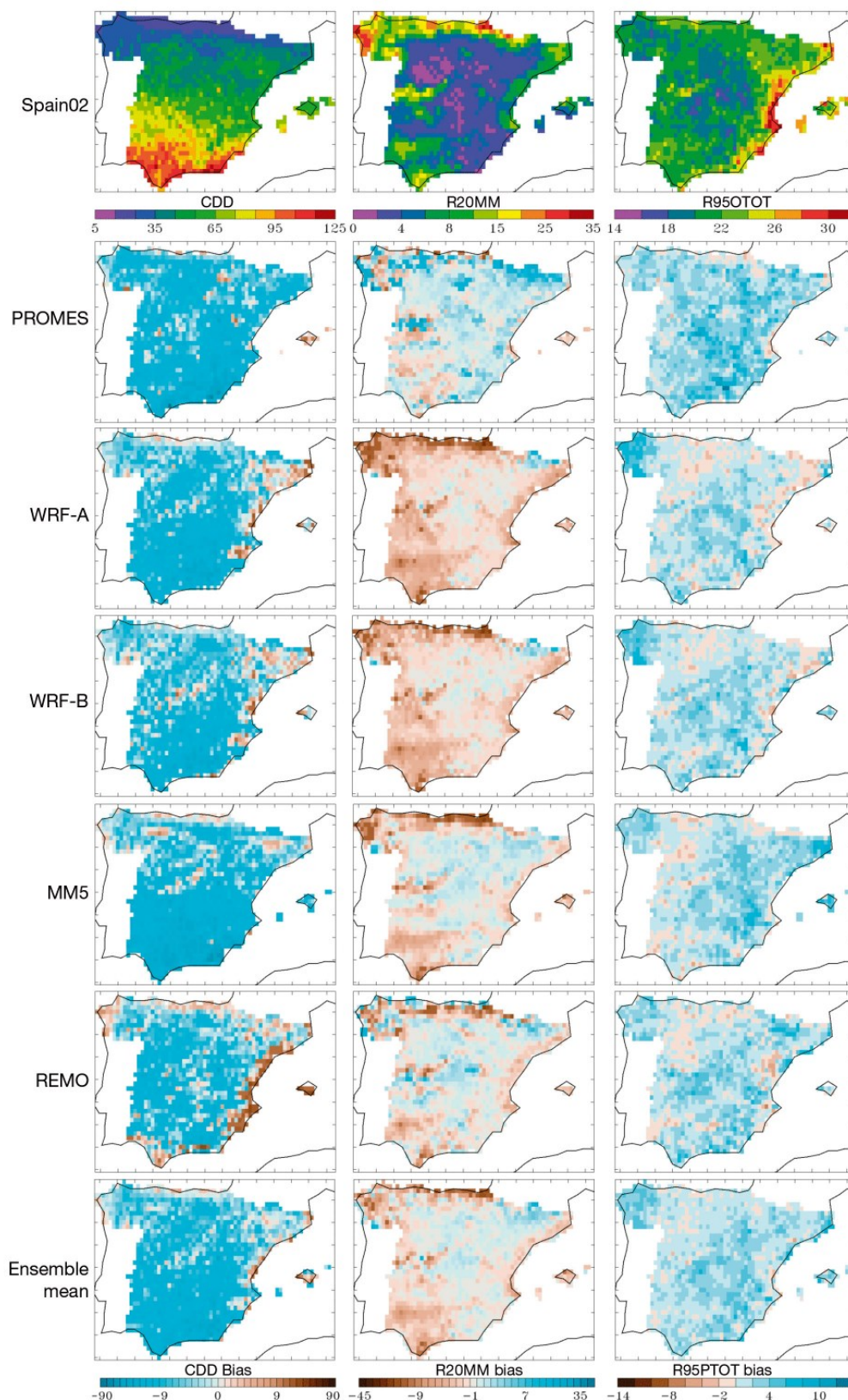
Fig. 4. Spatial distribution of precipitation extreme indices (CDD: consecutive dry days index, R20MM: very heavy precipitation days index, and R95PTOT: precipitation fraction due to 95th percentile) of Spain02 data (1st row) and the RCM biases for PROMES, WRF-A, WRF-B, MM5, REMO and the ensemble mean (rows 2–7, respectively) from January 1990 to December 2007

3.2. Maximum and minimum temperature

3.2.1. Seasonal percentiles

Fig. 5 presents the seasonal percentiles for maximum (Tx) and minimum (Tn) temperature. The first and second columns show the 10th percentile respectively of maximum (Tx10) and minimum (Tn10) temperatures in winter. Spain02 shows the lowest values of Tx10 in the northern part of PS (reaching −3°C in the Pyrenees) while the lowest values (down to −10°C) for Tn10 are found in the central-eastern highlands around the Iberian Mountain Range. This reflects the continental characteristics of the interior climate (Castro et al. 2007). The 90th percentile for maximum (Tx90) and minimum (Tn90) temperatures in summer are represented in the third and fourth columns of Fig. 5. The highest values of Tx90 (~40°C) appear in the CE-SU subregion of the IP, related to the typical summer thermal lows over this area (Hoinka & de Castro 2003). The thermal inertia of the oceans leads to smaller differences between Tx90 and Tn90 in coastal areas (with values between 4 and 14°C in NO, LE and CA subregions, not shown) and to higher differences in continental areas (with values between 14 and 24°C in CE-SU and EB subregions).

In general, a similar spatial distribution was obtained for all models, with a low spread among them, except for REMO Tn percentiles. The spatial distribution of the Spain02 percentiles was generally well reproduced by the models. The highest correlation was found for Tx (see Fig. 7). Correlation values obtained for percentiles of Tx are 0.83 to 0.95, and 0.79 to 0.86 for Tn percentiles. REMO has the lowest values for cold nights (0.79).

Most of the RCMs underestimate the Tx10 values, with moderate differences in some areas. REMO is the model with values closer to Spain02. Both versions of WRF and MM5 also underestimate the Tx90, while PROMES matches Spain02 percentiles in the western part of PS and overestimates them, particularly on the Mediterranean coast and the BA. Regarding minimum temperature percentiles, the values obtained by REMO are higher than the simulated by the rest of models, and also higher than the observations in most of the domain, as discussed below. These biases of REMO reach up to 10°C in areas where these percentiles reach their minimum values.

3.2.2. Extreme temperature indices

Fig. 6 presents the indices that have been used to describe temperature extreme events like heat waves (defined in Table 2). Spain02 shows that the highest heat wave frequency (HWn; first column) is located in the CE-SU subregion (up to 5 heat waves yr^{-1}), with a maximum duration (HWd; second column) that varies between 6 and 16 d in PS. It should be noted that these indices are sensitive to model biases as they are related to a fixed observational threshold.

The spread of HWn values is large among the RCMs. There is some tendency of the models to underestimate this index compared with observations, with the exception of PROMES and REMO, which overestimate the number of heat waves particularly in southern and eastern coastal areas. The models which underestimate the number of heat waves also tend to underestimate their duration. In contrast, PROMES and REMO simulate longer than observed heat waves, especially over the southwestern part of PS. The spatial distribution of these indices presents correlation values between 0.43 (HWd for WRF-A) and 0.88 (HWn for MM5) (Fig. 7); HWd is the index with the lowest spatial correlation values for all models.

Fig. 6 also shows other indices related to factors that have a social and economical impact on the studied area (AEMET 2007, Fischer & Schär 2010): TR (third column) and CHT (last column), defined in Table 2.

Spain02 present the highest TR value in the eastern coasts and the BA, with >100 d yr^{-1}. Values around 20 or 30 d yr^{-1} are observed in most of the southern half of PS and the Ebro valley, while in the remaining areas TR has a value of <2 d yr^{-1}. The thresholds used to compute CHT are the same as those used for TR and HW, but the spatial distribution of the CHT index is more similar to HWn than to the TR index, with highest values in CE-SU subregion (up to 40 d yr^{-1}). This fact highlights the need for studying the TR index separately in extreme temperature analysis. For instance, in the case of the BA, the value of TR is >100 d yr^{-1}, while CHT is <15 d yr^{-1}.

Differences of TR values among RCMs are related to the differences obtained for Tn90 index (see last column in Fig. 5), with higher values for the BA and the southern part of PS. In general, all the models underestimate TR in the central area of PS except REMO, which overestimates this index in most of the domain. CHT is also clearly overestimated by REMO in many parts of PS, reaching values up to 3 times higher than the observed ones. If we consider the biases of maximum and minimum temperature percentiles (Fig. 5), this latter bias is probably more related to the minimum temperature biases. Higher
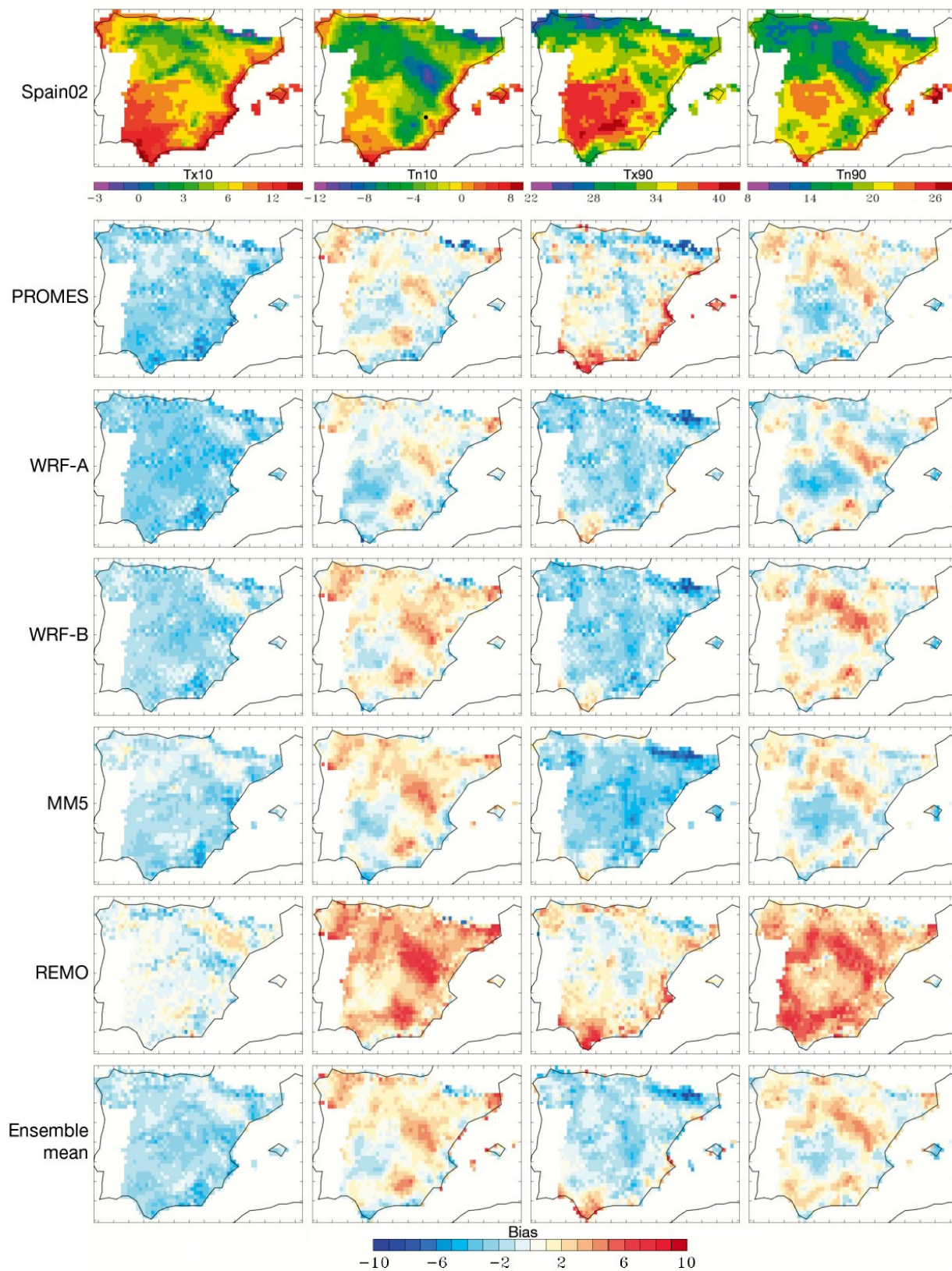
Fig. 5. Spatial distribution for temperature seasonal percentiles: Tx10 (Tn10) = 10th percentile for maximum (minimum) temperatures for winter; Tx90 (Tn90) = 90th percentile for maximum (minimum) temperature for summer. Top row: Spain02 data. Rows 2–7: RCM biases for PROMES, WRF-A, WRF-B, MM5, REMO and the ensemble mean
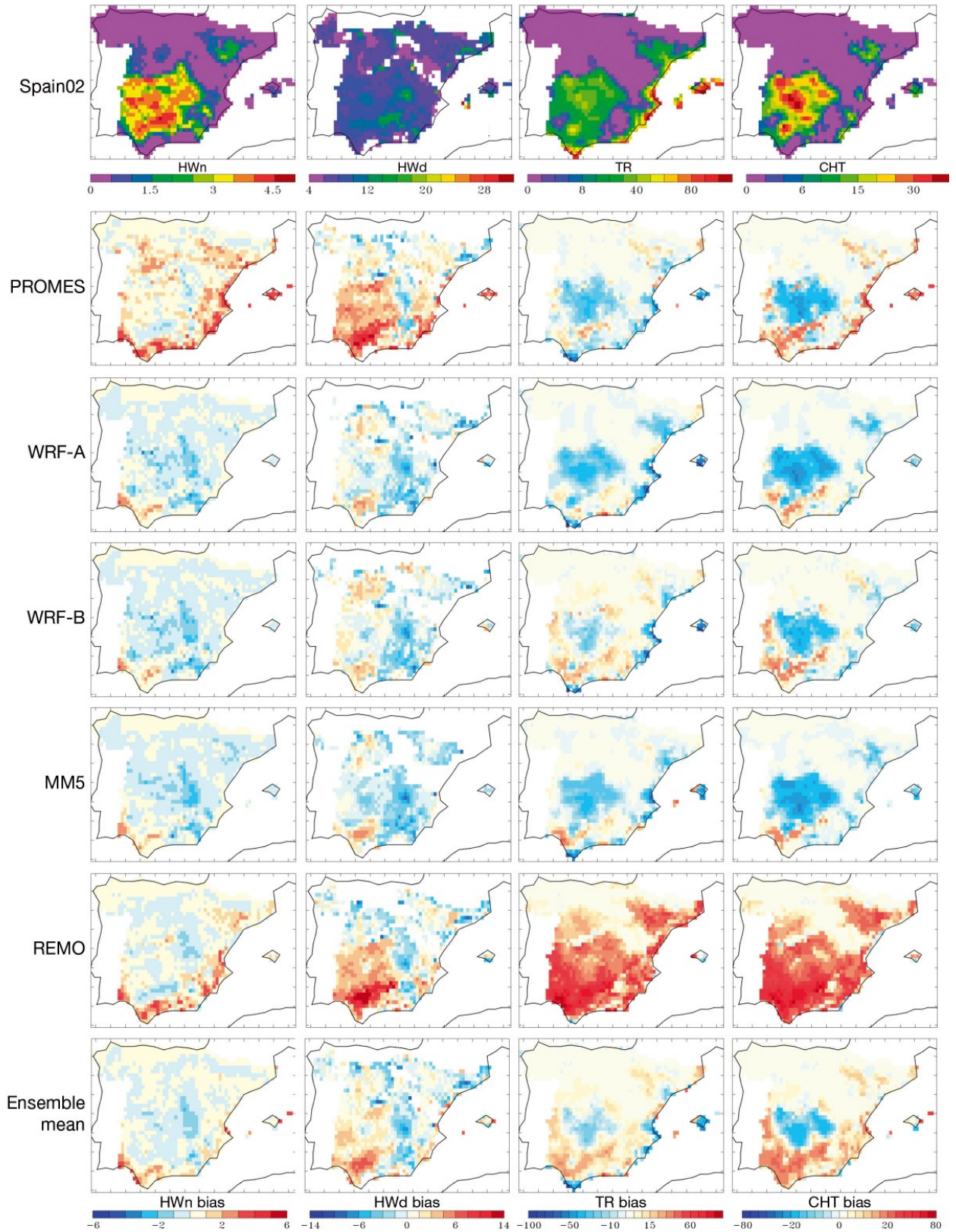
Fig. 6. Spatial distribution for yearly heat wave indices: HWn (heat wave frequency), HWd (heat wave duration), tropical nights (TR), combined tropical, and summer days (CHT). Top row: Spain02, Rows 2–7: RCM biases for PROMES, WRF-A, WRF-B, MM5, REMO and the ensemble mean
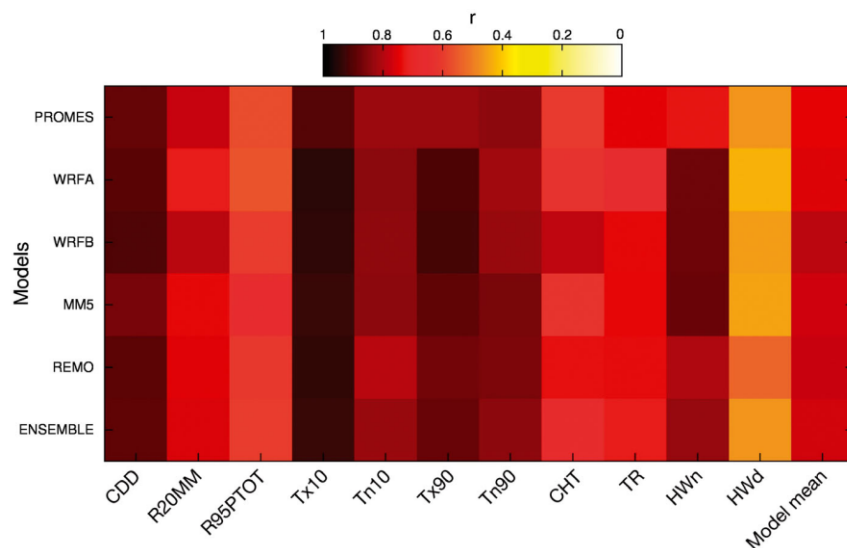
Fig. 7. Spatial correlations between simulated and observed precipitation and temperature indices of the 5 RCMs (PROMES, WRF-A, WRF-B, MM5 and REMO) and the ensemble mean, and the mean correlation of all indices for each model (last column). Index definitions in Table 2 and Fig. 5

There is a very large range of precipitation regimes in this small analyzed region. Three areas stand out for at least one of the extreme indices: the northern coast, the southwestern area and the Mediterranean coast. The northern coast is an area with low CDD and high R20MM values. Precipitation occurs throughout the year, and the interannual variability (shown in the companion paper, Jiménez-Guerrero et al. 2013) is rather low. For this regime, the spread of the model results is the lowest, as indicated by the Perkins skill score (Table 3). CDD and R95PTOT are rather well reproduced by all models, but they clearly differ in the R20MM index, for which several models show an important negative bias.

By contrast, the spread of the results for the southwestern area is higher, and there is a clear tendency of most models to underestimate precipitation. This occurs despite the fact that the PDF shows comparatively low frequency for very high precipitation values, and therefore model errors cannot be linked mainly to problems in simulating very heavy convective precipitation events. This is an area where model biases in a previous study with ENSEMBLES project results (Herrera et al. 2010) were also large. A possible reason for those biases in ENSEMBLES simulations could have been the proximity of lateral boundaries, or limitations of moisture values of ERA40 reanalysis. ERA-Interim, among other improvements, has introduced a new humidity analysis. But the present setup, with western lateral boundaries far away from this region and nesting in ERA-Interim, does not improve previous results. We can obtain more information about biases in this area from the companion paper (Jiménez-Guerrero et al. 2013). As shown there, the interannual variability is high and is not well captured by most models. But at the same time, results shown in this companion paper indicate that all models show high temporal correlations. This suggests that the timing of precipitation events is well captured (a result that could be linked to the fact that major precipitation events are frequently due to large scale Atlantic depressions), but the precipitation amounts are not. The fact that there is one model (PROMES) showing better results over this area indicates that the negative bias could be associated with some aspect of the model formulation.

than observed values are also simulated by PROMES in the southern and eastern coasts. This positive bias for PROMES is also noticeable in the BA, which is in agreement with Tx90 percentile (Fig. 5) and HWn and HWd indices (Fig. 6). All models except REMO underestimate CHT for the area with the highest observed values of this index. Spatial correlations for both indices vary between 0.60 and 0.79. The ensemble mean of the CHT index does not present an important improvement compared to the results of the individual models.

4. DISCUSSION AND CONCLUSIONS

We have analyzed the ability of 4 RCMs (WRF, MM5, PROMES and REMO) to reproduce climate extremes in an evaluation simulation over PS and the BA, for the period 1990–2007. This work is part of a Spanish project (ESCENA) for generating a set of regional climate change scenarios over this region. In comparison to previous climate validation studies over this domain, there are important differences: the domain is centered over the IP, unlike the domain used in ENSEMBLES project in which the lateral boundaries were very near to this region, and the models are nested in the ERA-Interim reanalysis. The multi-model ensemble also includes WRF (WRF-A and -B, with different PBL schemes) and MM5, which were not included in ENSEMBLES.

For the Mediterranean coast, the number of days with >20 mm of precipitation is smaller than for the southwestern part, but R95PTOT is much larger, and the PDF tails show a large frequency of very high precipitation. A similar negative bias in R20MM can be seen for all models except PROMES, but R95PTOT is rather well captured by all models. In contrast to the southwestern area, the temporal correlation (Jiménez-Guerrero et al. 2013) is much lower for all the models here. This indicates that the errors for the Mediterranean coast are also linked to deficiencies in the simulation of the temporal distribution of precipitation. An interesting result, specific to the Mediterranean subregions, is that the ensemble mean is worse than the individual models in representing the frequency of very high precipitation events. The ensemble mean underestimates this frequency. A possible reason is that strong convective events are spatially localized, and the specific locations are simulated differently by the models. Thus, the average would tend to smooth out these very high precipitation amounts.

Modelled values of maximum temperature percentiles are generally lower than observed, with the exception of REMO. By contrast, this model shows a considerable overestimation of minimum temperature percentiles and of TR and CHT indices, indicating a problem with minimum temperatures. The REMO version used here already includes the improvements discussed in Kjellström et al. (2010) for winter minimum temperatures. The present biases in REMO results must have different causes, which are still unknown. The spatial distribution of temperature percentiles is particularly well simulated by all models, as illustrated by the high spatial correlation values.

ESCENA also explored a very limited part of the uncertainty accounted for by the physical parameterizations using the WRF model in 2 configurations. The differences between the local and non-local PBL closure schemes used are most noticeable in the minimum temperature indices, since the local closure configuration (WRF-A) shows a weaker low level mixing during nighttime (García-Díez et al. 2013), which leads to cooler minimum temperatures (and associated percentiles). WRF-B used a non-local closure scheme, very similar to that used by MM5, leading to very similar biases in the winter cold extremes (Fig. 5, Tn10).

The present multi-model ensemble can be compared to the one of ENSEMBLES project (Herrera et al. 2010). The spatial correlations of the precipitation indices of models involved in both projects (PROMES

and REMO) are similar in both cases. In the case of ENSEMBLES models, for some indices there was a clear division between models with high and low correlation values. In particular, results for R20MM index can be compared directly. The comparison indicates that all models of the present ensemble are at a similar level to the best subgroup of ENSEMBLES models, and clearly above the worse models of that project. Therefore, the ESCENA simulations (covering more emissions scenarios and GCMs) can be considered a valuable complement to the ENSEMBLES results for impact studies over Spain.

LITERATURE CITED

AEMET (Agencia Estatal de Meteorología) (2007) Resumen de extremos climatológicos en España (2007). AEMET (in Spanish)

Alexander L, Zhang X, Peterson T, Caesar J and others (2006) Global observed changes in daily climate extremes of temperature and precipitation. J Geophys Res 111:D05109, doi:10.1029/2005JD0062 90

Barriopedro D, Fischer E, Luterbacher J, Trigo R, García-Herrera R (2011) The hot summer of 2010: redrawing the temperature record map of Europe. Science 332:220–224

Beniston M (2006) August 2005 intense rainfall event in Switzerland: not necessarily an analog for strong convective events in a greenhouse climate. Geophys Res Lett 33:L05701, doi:10.1029/2005GL025573

Beniston M, Stephenson DB (2004) Extreme climatic events and their evolution under changing climatic conditions. Global Planet Change 44:1–9

Beniston M, Stephenson DB, Christensen OB, Ferro CAT and others (2007) Future extreme events in European climate: an exploration of regional climate model projections. Clim Change 81:71–95

Boberg F, Berg P, Thejll P, Gutowski WJ, Christensen JH (2009) Improved confidence in climate change projections of precipitation evaluated using daily statistics from the PRUDENCE ensemble. Clim Dyn 32:1097–1106

Boberg F, Berg P, Thejll P, Gutowski WJ, Christensen JH (2010) Improved confidence in climate change projections of precipitation further evaluated using daily statistics from ENSEMBLES models. Clim Dyn 35:1509–1520

Brinkop S, Roeckner E (1995) Sensitivity of a general circulation model to parameterizations of cloud–turbulence interactions in the atmospheric boundary layer. Tellus A 47:197–220

Brunetti M, Colacino M, Maugeri M, Nanni T (2001) Trends in the daily intensity of precipitation in Italy from 1951 to 1996. Int J Climatol 21:299–316

Castro M, Fernández C, Gaertner MA (1993) Description of

a mesoscale atmospheric numerical model. In: Diaz JI, Lions Jl (eds) Mathematics, climate and environment. Mason, Paris, p 230–253

Castro M, Gallardo C, Jylhä K, Tuomenvirta H (2007) The use of a climate-type classification for assessing climate change effects in Europe from an ensemble of nine regional climate models. Clim Change 81(S1):329–341

Chaboureau JP, Bechtold P (2002) A simple cloud parameterization derived from cloud resolving model data: diagnostic and prognostic applications. J Atmos Sci 59: 2362–2372

Chaboureau JP, Bechtold P (2005) Statistical representation of clouds in a regional model and the impact on the diurnal cycle of convection during Tropical Convection, Cirrus and Nitrogen Oxides (TROCCINOX). J Geophys Res 110:D17103, doi:10.1029/2004JD005645

Chen F, Dudhia J (2001a) Coupling an advanced land surface-hydrology model with the Penn State-NCAR MM5 modeling system. I. Model implementation and sensitivity. Mon Weather Rev 129:569–585

Chen F, Dudhia J (2001b) Coupling an advanced land surface-hydrology model with the Penn State-NCAR MM5 modeling system. II. Preliminary model validation. Mon Weather Rev 129:587–604

Christensen JH, Christensen OB (2007) A summary of the PRUDENCE model projection of changes in European climate by the end of this century. Clim Change 81:1–30

Collins WD, Rasch PJ, Boville BA, Hack JJ, McCaa JR, Williamson DL, Briegleb BP (2006) The formulation and atmospheric simulation of the Community Atmosphere Model version 3 (CAM3). J Clim 19:2144–2161

Cuxart J, Bougeault P, Redelsperger JL (2000) A turbulence scheme allowing for mesoscale and large-eddy simulations. QJR Meteorol Soc 126:1–30

de la Cruz Gallego M, García JAG, Vaquero JM (2004) Distribución espacial de índices de frecuencia de precipitación diaria en la Peninsula Ibérica. Física de la Tierra 16: 161–174

Dee DP, Uppala S (2009) Variational bias correction of satellite radiance data in the ERA-Interim reanalysis. QJR Meteorol Soc 135:1830–1841

Della-Marta P, Haylock M, Luterbacher J, Wanner H (2007) Doubled length of western European summer heat waves since 1880. J Geophys Res 112:D15103, doi:10. 1029/2007JD008510

Déqué M, Rowell DP, Lthi D, Giorgi F and others (2007) An intercomparison of regional climate simulations for Europe: assessing uncertainties in model projections. Clim Change 81(S1):53–70

Domínguez M, Gaertner M, De Rosnay P, Losada T (2010) A regional climate model simulation over West Africa: parameterization tests and analysis of land-surface fields. Clim Dyn 35:249–265

Dudhia J (1989) Numerical study of convection observed during the winter monsoon experiment using a mesoscale two-dimensional model. J Atmos Sci 46:3077–3107

Dudhia J (1993) A nonhydrostatic version of the Penn State-NCAR mesoscale model: validation tests and simulation of an Atlantic cyclone and cold front. Mon Weather Rev 121:1493–1513

ECMWF (European Centre for Medium-Range Weather Forecasts) (2004) IFS documentation CY28r1. ECMWF, Reading, p 7–32, www.ecmwf.int/research/ifsdocs/CY28r1/ pdf_files/Physics.pdf

Fernández J, Montávez JP, Sáenz J, González-Rouco JF,

Zorita E (2007) Sensitivity of the MM5 mesoscale model to physical parameterizations for regional climate studies: annual cycle. J Geophys Res 112(D4):D04101, doi: 10.1029/2005JD006649

Fernández-Quiruelas V, Fita L, Fernández J no AC (2010) WRF workflow on the Grid with WRF4G. Proc 11th WRF Users' Workshop, 21–25 June, Boulder, CO. www.meteo. unican.es/files/pdfs/WRFusers_wrf4g.pdf

Field C, Barros V, Stocker T, Qin D and others (eds) (2012) Managing the risks of extreme events and disasters to advance climate change adaptation. A Special Report of Working Groups I and II of the Intergovernmental Panel on Climate Change. Cambridge University Press, Cambridge

Fischer EM, Schär C (2010) Consistent geographical patterns of changes in high-impact European heatwaves. Nat Geosci 3:398–403

Fischer EM, Seneviratne SI, Lüthi D, Schär C (2007) Contribution of land–atmosphere coupling to European summer heat waves. Geophys Res Lett 34:L06707, doi:10. 1029/2006GL029068

Fita L, Fernández J, García-Díez M (2010) CLWRF: WRF modifications for regional climate simulation under future scenarios. Proc 11th WRF Users' Workshop, 21–25 June, Boulder, CO

Frei C, Schöll R, Fukutome S, Schmidli J, Vidale PL (2006) Future change of precipitation extremes in Europe: intercomparison of scenarios from regional climate models. J Geophys Res 111:D06105, doi:10.1029/2005JD005965

Frich P, Alexander LV, Della-Marta P, Gleason B, Haylock M, Klein Tank AM, Peterson T (2002) Observed coherent changes in climatic extremes during the second half of the twentieth century. Clim Res 19:193–212

Gallego MC, García JA, Vaquero JM (2005) The NAO signal in daily rainfall series over the Iberian Peninsula. Clim Res 29:103

García-Díez M, Fernández J, Fita L, Yagüe C (2013) Seasonal dependence of WRF model biases and sensitivity to PBL schemes over Europe. QJR Meteorol Soc 139:501–514

García-Herrera R, Díaz J, Trigo R, Hernández E and others (2005) Extreme summer temperatures in Iberia: health impacts and associated synoptic conditions. Ann Geophys 23:239–251

Giorgetta M, Wild M (1996) The water vapour continuum and its representation in ECHAM4. MPI Rep 162

Giorgi F, Bi X, Pal JS (2004a) Mean, interannual variability and trends in a regional climate change experiment over Europe. I. Present-day climate (1960–1990). Clim Dyn 22:733–756

Giorgi F, Bi X, Pal JS (2004b) Mean, interannual variability and trends in a regional climate change experiment over Europe. II. Climate change scenario (2071–2100). Clim Dyn 23:839–858

Giorgi F, Jones C, Asrar G (2009) Addressing climate information needs at the regional level: the CORDEX framework. WMO Bulletin 58:3

Gómez-Navarro JJ, Montávez JP, Jiménez-Guerrero P, Jerez S, García-Valero JA, González-Rouco JF (2010) Warming patterns in a regional climate projections over the Iberian Peninsula. Met Zeit 19:275–285

González-Hidalgo JC, De Luis M, Raventós J, Sánchez JR (2003) Daily rainfall trend in the Valencia region of Spain. Theor Appl Climatol 75:117–130, www.ua.es/ personal/martin.deluis/Gonzalez-Hidalgo%20et%20al., %202003%20(TAC).PDF

Grell GA (1993) Prognostic evaluation of assumptions used by cumulus parameterizations. Mon Weather Rev 121: 764–787

Grell GA, Devenyi D (2002) A generalized approach to parameterizing convection combining ensemble and data assimilation techniques. Geophys Res Lett 29:L1693, doi: 10.1029/2002GL015311

Grell GA, Dudhia J, Stauffer DR (1994) A description of the fifth-generation Penn State/NCAR mesoscale model (MM5). Tech Note TN-398+ IA. NCAR:1–125

Haylock MR, Hofstra N, Klein-Tank AMG, Klok EJ, Jones PD, New M (2008) A European daily high-resolution gridded data set of surface temperature and precipitation for 1950–2006. J Geophys Res 113:D20119, doi:10.1029/ 2008JD010201

Herrera S (2011) Desarrollo, validación y aplicaciones de Spain02: una rejilla de alta resolución de observaciones interpoladas para precipitación y temperatura en España. PhD thesis, Universidad de Cantabria, available at www.meteo.unican.es/tesis/herrera

Herrera S, Fita L, Fernández J, Gutiérrez JM (2010) Evaluation of the mean and extreme precipitation regimes from the ENSEMBLES regional climate multimodel simulations over Spain. J Geophys Res 115:D21117, doi:10. 1029/2010JD013936

Herrera S, Gutiérrez JM, Ancell R, Pons MR, Frías MD, Fernández J (2012) Development and analysis of a 50-year high-resolution daily gridded precipitation dataset over Spain (Spain02). Int J Climatol 32:74–85

Hirschi M, Seneviratne SI, Alexandrov V, Boberg F and others (2010) Observational evidence for soil-moisture impact on hot extremes in southeastern Europe. Nat Geosci 4:17–21

Hoinka KP, de Castro M (2003) The Iberian peninsula thermal low. QJR Meteorol Soc 129:1491–1511

Hong SY, Lim JOJ (2006) The WRF Single-Moment 6-Class Microphysics Scheme (WSM6). J Korean Meteorol Soc 42:129–151

Hong SY, Pan HL (1996) Nonlocal boundary layer vertical diffusion in a medium-range forecast model. Mon Weather Rev 124:2322–2339

Hong S, Dudhia J, Chen S (2004) A revised approach to ice microphysical processes for the bulk parameterization of cloud and precipitation. Mon Weather Rev 132:103–120

Hong SY, Noh Y, Dudhia J (2006) A new vertical diffusion package with an explicit treatment of entrainment processes. Mon Weather Rev 134:2318–2341

Huth R, Kyselý J, Pokorná L (2000) A GCM simulation of heat waves, dry spells, and their relationships to circulation. Clim Change 46:29–60

IPCC (2001) Climate Change 2001: the scientific basis. Contribution of Working Group I to the Third Assessment Report of the Intergovernmental Panel on Climate Change. Houghton JT, Ding Y, Griggs DJ, Noguer M and others (eds) Cambridge University Press, Cambridge

IPCC (2007) Climate Change 2007: the physical science basis. Contribution of Working Group I to the Fourth Assessment Report of the Intergovernmental Panel on Climate Change. Solomon S, Quin D, Manning M, Chen Z and others (eds) Cambridge University Press, Cambridge

Jacob D (2001) A note to the simulation of the annual and inter-annual variability of the water budget over the Baltic Sea drainage basin. Meteorol Atmos Phys 77:61–73

Jacob D, Van den Hurk B, Andrae U, Elgered G and others (2001) A comprehensive model inter-comparison study investigating the water budget during the BALTEX-PIDCAP period. Meteorol Atmos Phys 77:19–43

Jacob D, Barring L, Christensen OB, Christensen JH and others (2007) An inter-comparison of regional climate models for Europe: model performance in present-day climate. Clim Change 81(S1):31–52

Janjić ZI (1990) The Step-Mountain Coordinate: physical package. Mon Weather Rev 118:1429–1443

Janjić ZI (1994) The Step-Mountain Eta coordinate model: further developments of the convection. Mon Weather Rev 122:927–945

Jiménez-Guerrero P, Montávez JP, Domínguez M, Romera R and others (2013) Mean fields and interannual variability in RCM simulations over Spain: ESCENA project. Clim Res 57:201–220

Kain JS, Fritsch JM (1993) Convective parameterization for mesoscale models: the Kain–Fritsch scheme. The representation of cumulus convection in numerical models. Am Meteorol Soc 46:165–170

Kjellström E, Boberg F, Castro M, Christensen JH, Nikulin G, Sánchez E (2010) Daily and monthly temperature and precipitation statistics as performance indicators for regional climate models. Clim Res 44:135–150

Klein Tank AMG, Zwiers FW, Zhang X (2009) Guidelines on analysis of extremes in a changing climate in support of informed decisions for adaptation. Climate Data and Monitoring, WCDMP 72:WMO–TD No. 1500, WMO, Geneva, www.wmo.int/pages/prog/wcp/wcdmp/wcdmp _series/documents/WCDMP_72_TD_1500_en_1.pdf

Krinner G, Viovy N, de Noblet-Ducoudré N, Ogée J and others (2005) A dynamic global vegetation model for studies of the coupled atmosphere–biosphere system. Global Biogeochem Cycles 19:GB1015, doi:10.1029/2003GB002199

Kysely J, Plavcova E (2010) A critical remark on the applicability of E-OBS European gridded temperature dataset for validating control climate simulations. J Geophys Res 115:D23118, doi:10.1029/2010JD014123

Lana X, Martínez MD, Burgueño A, Serra C, Martín-Vide J, Gómez L (2006) Distributions of long dry spells in the Iberian Peninsula, years 1951–1990. Int J Climatol 26: 1999–2021

López-Moreno JI, Beniston M (2009) Daily precipitation intensity projected for the 21st century: seasonal changes over the Pyrenees. Theor Appl Climatol 95:375–384

Martin-Vide J (2004) Spatial distribution of a daily precipitation concentration index in peninsular Spain. Int J Climatol 24:959–971

Mlawer EJ, Taubman SJ, Brown PD, Iacono MJ, Clough SA (1997) Radiative transfer for inhomogeneous atmospheres: RRTM, a validated correlated-k model for the longwave. J Geophys Res 102(D14):16663–16682

Morcrette JJ, Smith L, Fourquart Y (1986) Pressure and temperature dependance of the absorption in longwave radiation parameterizations. Beitr Phys Atmos 59:455–469

Nordeng TE (1994) Extended versions of the convective parametrization scheme at ECMWF and their impact on the mean and transient activity of the model in the tropics. Tech Rep ECMWF, Tech Memo No. 206, Reading

Perkins SE, Pitman AJ, Holbrook NJ, McAneney J (2007) Evaluation of the AR4 climate models' simulated daily maximum temperature, minimum temperature, and precipitation over Australia using probability density functions. J Clim 20:4356–4376

Roeckner E, Arpe K, Bengtsson L, Christoph M and others (1996) The atmospheric general circulation model

ECHAM-4: model description and simulation of present-day climate. MPI Meteorol Rep 218, Hamburg

Sánchez E, Gallardo C, Gaertner MÁ, Arribas A, de Castro M (2004) Future climate extreme events in the Mediterranean simulated by a regional climate model: a first approach. Global Planet Change 44:163–180

Sánchez E, Domínguez M, Romera R, López de la Franca N, Gaertner MA, Gallardo C, Castro M (2011) Regional modeling of dry spells over the Iberian Peninsula for present climate and climate change conditions. Clim Change 107:625–634

Schär C, Vidale PL, Lüthi D, Frei C, Häberli C, Liniger MA, Appenzeller C (2004) The role of increasing temperature variability in European summer heatwaves. Nature 427: 332–336

Sillmann J, Roeckner E (2008) Indices for extreme events in projections of anthropogenic climate change. Clim Change 86:83–104

Skamarock WC, Klemp JB, Dudhia J, Gill DO and others (2008) A description of the advanced research WRF version 3. NCAR TN 475, www.mmm.ucar.edu/wrf/users/docs/arw_v3.pdf

Sundqvist H (1978) A parameterization scheme for non-convective condensation including prediction of cloud water content. QJR Meteorol Soc 104:677–690

Tiedtke M (1989) A comprehensive mass flux scheme for cumulus parameterization in large scale models. Mon Weather Rev 117:1779–1800

Uppala SM, Kallberg PW, Simmons AJ, Andrae U and others (2005) The ERA-40 re-analysis. QJR Meteorol Soc 131: 2961–3012

Verdin KL, Greenlee SK (1996) Development of continental scale digital elevation models and extraction of hydrographic features. Proc 3rd Int Conf/Workshop on Integrating GIS and Environmental Modeling, Santa Fe, NM, January 21–26, 1996. National Center for Geographic Information and Analysis, Santa Barbara, CA

Vicente-Serrano SM (2006a) Differences in spatial patterns of drought on different time scales: an analysis of the Iberian Peninsula. Water Resour Manage 20:37–60

Vicente-Serrano SM (2006b) Spatial and temporal analysis of droughts in the Iberian Peninsula (1910–2000). Hydrol Sci J 51:83–97

Vicente-Serrano SM, Lasanta T, Romo A (2004) Analysis of spatial and temporal evolution of vegetation cover in the Spanish central Pyrenees: role of human management. Environ Manag 34:802–818

Vincent LA, Mekis E (2006) Changes in daily and extreme temperature and precipitation indices for Canada over the Twentieth Century. Atmos-Ocean 44:177–193

Mean fields and interannual variability in RCM simulations over Spain: the ESCENA project

P. Jiménez-Guerrero[1],*, J. P. Montávez[1], M. Domínguez[2], R. Romera[2] , L. Fita[3],
J. Fernández[4], W. D. Cabos[4], G. Liguori[4], M. A. Gaertner[5]

[1]Department of Physics, Regional Campus of International Excellence 'Campus Mare Nostrum', University of Murcia,
30100 Murcia, Spain

[2]Environmental Science Institute, Universidad de Castilla la Mancha, 45071 Toledo, Spain

[3]Grupo de Meteorología, Dept. Applied Mathematics and Computer Science, Universidad de Cantabria, 39005 Santander, Spain

[4]Department of Physics, Climate Physics Group, Universidad de Alcalá de Henares, 28805 Madrid, Spain

[5]Environmental Science Faculty, Universidad de Castilla la Mancha, 45071 Toledo, Spain

ABSTRACT: The ESCENA (2008 to 2012) project is a Spanish initiative, which applies the dynamical downscaling technique to generate climate change scenarios based on an ensemble of Regional Climate Models (RCMs) consisting of PROMES, WRF, MM5 or REMO over Peninsular Spain and the Balearic and Canary Islands using a high resolution of 25 km. We describe the mean fields and interannual variability for temperature and precipitation in an ensemble of simulations forced by the high resolution ERA-Interim reanalysis (1990 to 2007) and compare them to the Spain02 observed data set. Maximum surface air temperature shows seasonal cold biases up to −2.5K in all models and it is clearly underestimated during the coldest seasons, but less so during summertime (JJA). Generally, there is a better agreement between observed and simulated minimum surface air temperature, which is slightly overestimated (up to +2K) especially during wintertime (DJF). Regarding precipitation, all models except PROMES tend to show low dry biases during all seasons, especially for autumn on the Mediterranean coast of the Iberian Peninsula. With respect to the interannual variability, the PROMES simulations overestimate the standard deviation of maximum surface air temperature, while the remaining models tend to slightly underestimate it, and most models tend to underestimate the standard deviation of precipitation. The results highlight the ability of these RCMs to reproduce the mean fields and the interannual variability in a very complex terrain such as the Iberian Peninsula, showing a great diversity of climatic behavior. The evaluation of the ensemble results indicates a great improvement in the temporal correlation and the representation of the spatial patterns of temperature and precipitation for all seasons with respect to the individual models.

KEY WORDS: Regional climate models · Spain · Interannual variability · Present climate · Spain02 gridded dataset

1. INTRODUCTION

The climate over regions characterized by complex topographical and land-ocean features exhibits fine scale structure that can be captured only by Regional Climate Models (RCMs) (Gao et al. 2006). Therefore, high-resolution climate information provided by RCMs is required for the assessment of the regional impacts of climate variability and change. This work focuses on the Iberian Peninsula (IP), as an example of a topographically complex region, and characterizes the ability of a new set of RCM simulations in reproducing the observed climate at a regional scale.

The IP presents a large climate heterogeneity because of its position with respect to the North Atlantic circulation and its complex orography. The region exhibits a wide range of precipitation and temperature regimes. This heterogeneity necessitates the use of RCMs to simulate the regional climate details under present, past or future climate change conditions. Thus, the IP is an ideal test area for studying the accuracy of RCMs (see e.g. Jacob et al. 2007, Gómez-Navarro et al. 2010). There is also a great deal of RCM sensitivity experiments over the area. For instance, Fernández et al. (2007) showed the sensitivity of the climatology (mean temperature and precipitation) to the changes in the model physics. More recent studies have shown the influence of land-surface model choice on the reproduction of observed climate (Jerez et al. 2010). Most of the previous studies considered a single RCM. The relative performance of RCMs over the region has been compared only recently (e.g. Herrera et al. 2010).

The climate simulated by an RCM suffers from uncertainties arising from a variety of sources such as internal variability, different model formulations, and imperfections in the boundary conditions. Such uncertainties can be explored by running an ensemble of simulations, varying the source of the uncertainty. For example, the uncertainty associated with imperfections in the model formulation can be addressed by running a multi-model ensemble. Climate signals common to all models are usually given more confidence. This reasoning relies on the independence of the errors of the different models, even though this is not fully justified due to the common building blocks of the diverse models (Fernández et al. 2009, Knutti et al. 2010).

A recent series of EU-funded projects exploited this multi-model ensemble approach to provide an estimation of the uncertainties of regional climate change over Europe. The latest projects in this series were PRUDENCE (Christensen & Christensen 2007) and ENSEMBLES (Van der Linden & Mitchell 2009). In PRUDENCE (2001 to 2004), 2 SRES emission scenarios (A2 and B2) were analyzed for the last 3 decades of this century (2071 to 2100) with an ensemble of 11 RCMs at a spatial resolution of 50 km. Most of the simulations were forced with the same General Circulation Model (GCM) (HadCM3). The main objective of the subsequent ENSEMBLES project (2004 to 2009) was to generate an objective probabilistic estimate of uncertainty in future climate scenarios. Several combinations of 13 RCMs and 7 GCMs were applied to the SRES emissions scenarios A1B and A2, with a finer horizontal resolution (25 km). All RCMs

simulated a common period extending over the first decades of the century, up to 2050. Additionally, ENSEMBLES included RCM evaluation simulations nested into 'perfect' boundary conditions taken from the ERA-40 Reanalysis (Uppala et al. 2005).

Unfortunately, the Spanish territory is not well covered in these pan-European multi-model experiments. For this reason, the Spanish government funded a strategic action to generate high-resolution downscaled scenarios over Spain, complementing those produced within ENSEMBLES. The ESCENA project is in charge of generating downscaled scenarios using nested RCMs, including perfect-boundary evaluation simulations, which are analyzed in this study. The simulations produced within ESCENA and, in particular, those described in this work, are publicly available at http://proyectoescena.uclm.es.

Compared to ENSEMBLES, ESCENA uses improved (PROMES) or additional RCMs (MM5, WRF), new GCM/RCM combinations, and a larger set of emission scenarios (A1B, A2 and B1), with the target domain centered over the IP and covering parts of the Atlantic Ocean, including the Canary Islands. One of the RCMs (WRF) has been run with 2 different configurations of the boundary layer scheme. Additionally, the evaluation runs in ESCENA are forced by the higher resolution ERA-Interim reanalysis, instead of the ERA-40 reanalysis used in ENSEMBLES.

Several previous studies analyzed the performance of an ensemble of RCM simulations forced by perfect boundaries and focused on the IP or included the IP in their analyses. The main source for those analyses has been the ENSEMBLES RCM database. In particular, Herrera et al. (2010) validated the mean and extreme precipitation regimes simulated by the ENSEMBLES RCMs over the IP. They used the Spain02 gridded observational data set (Herrera et al. 2012), which is also used in our study. Our work extends that of Herrera et al. (2010) by including the analysis of maximum and minimum temperature and considering the ability of reproducing the interannual variability. We also performed a seasonal analysis, given that the climate in the IP exhibits a marked intra-anual variability.

A number of references provide a measure of current state-of-the-art RCM seasonal biases. For instance, Christensen et al. (2010) explored different metrics in order to weight the RCM simulations from ENSEMBLES. They showed seasonal temperature and precipitation climatologies all over Europe, but did not find compelling evidence of an improved description of mean climate states using performance-based weights in comparison to the use of equal

weights. Coppola et al. (2010) indicate a wide variability in the performance across models included in an ensemble of ENSEMBLES-project simulations for the European region, mostly deriving from the magnitude/sign of precipitation-based functional metrics. The authors indicate that weighting leads to an overall improvement of the performance of the ensemble especially over topographically complex regions. Lastly, Kjellström et al. (2011) use an ensemble of 16 regional climate model simulations to indicate that the spread of the results and the biases in the 1961–1990 period are strongly related to the representation of the large-scale circulation in the GCMs.

Thus, the objectives of the present study were to (1) characterize the ability of a multi-model ensemble of RCMs to reproduce the observed regional climate over peninsular Spain and the Balearic Islands; (2) quantify the performance of the RCMs, focusing on the mean seasonal climate. not only on the climatology, but particularly on the interannual variability, which usually receives little attention (Giorgi et al. 2004); (3) compare the performance of the ensemble mean with that of the individual models; and (4) compare the model-to-model variability with the intra-model variability induced by the use of a local and a non-local planetary boundary layer (PBL) scheme. The present work focuses on the mean climate and interannual variability, while a companion paper by Domínguez et al. (2013) characterizes the ability of this new set of model simulations in reproducing the extreme climatic situations over the region.

2. METHODOLOGY AND DATA

2.1. RCM description

This study involved 4 different RCMs: PROMES, WRF, MM5 and REMO. The WRF model was run with 2 different physical parameterization configurations in order to compare the model-to-model variability with the variability induced by changing the physical scheme within the same RCM. All simulations cover a present-day 18 yr period (1990 to 2007) and were driven by ECMWF/ERA-Interim reanalysis (Section 2.2). The simulations cover most of Europe, with domains centered in the IP (Fig. 1). Some model domains (PROMES, WRF and REMO) were rotated in order to include the area of the Canary Islands (for the ESCENA project) with a domain smaller than the unrotated one used by MM5. The different domain sizes and locations may bring additional uncertainty

to the model results. All models were run with a horizontal resolution of ~25 km and set the top vertical layer at 10 hPa using a different number of vertical levels (see Table 1). A lateral boundary relaxation zone of 5 to 10 additional grid points was used by the different models. A brief description of each model configuration is provided in the following sections and is summarized in Table 1.

2.1.1. PROMES

The regional climate model PROMES (Castro et al. 1993) has been developed by MOMAC (Modelización para el Medio Ambiente y el Clima) research group at the Complutense University of Madrid (UCM) and the University of Castilla-La Mancha (UCLM). PROMES has been applied over many different simulation domains: IP (Gaertner et al. 2001, Arribas et al. 2003), Europe (Gaertner et al. 2007, Sánchez et al. 2009), West Africa (Domínguez et al. 2010, Gaertner et al. 2010) and South America (Boulanger et al. 2010). The PROMES version used in this work includes several improvements to the physical parameterizations which have been introduced during the last years. The resolved-scale cloud formation and its associated precipitation processes are modeled according to Hong et al. (2004). This scheme includes ice microphysics processes. The sub-grid scale convective clouds and their precipitation are simulated with the Kain-Fritsch parameterization (Kain & Fritsch 1993). The shortwave
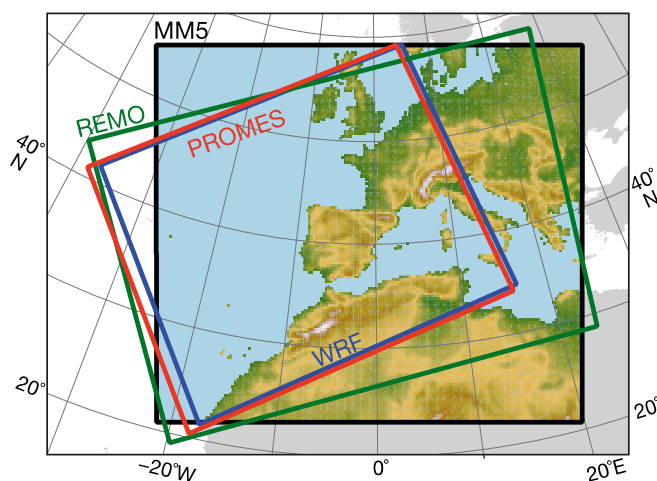

Fig. 1. Simulation domains used in the models used in the ESCENA project. Color shades: topography of domain. Relaxation zone, where the regional climate model output is relaxed towards the reanalysis, is excluded

Table 1. Configurations used in each of the models run in this study. Columns: model name, geographical projection (Geo. proj), number of vertical levels (Vert. level), horizontal resolution (Horiz. resol.), and physical parameterizations for convective clouds and precipitation (Cumulus), resolved cloud microphysics, radiation, planetary boundary layer (PBL) and land surface models (LSM). See Section 2.1 for details; Fig. 1 shows domain covered by each model

| Model | Geo. proj. | Vert. level | Horiz. resol. | Physics parameterizations | | | | |
				Microphysics	Cumulus	Radiation	PBL	LSM
PROMES	Lambert	37	25 km	Includes ice processes (Hong et al. 2004)	Kain & Fritsch (1993)	ECMWF (2004) with fractional cloud cover (Chaboureau & Bechtold 2002, 2005)	Cuxart et al. (2000)	ORCHIDEE LSM (Krinner et al. 2005)
WRF-A	Lambert	33	25 km	WSM5	GD	CAM	MYJ	Noah
WRF-B	Lambert	33	25 km	WSM5	GD	CAM	YSU	Noah
MM5	Lambert	30	25 km	Simple ice	Grell	RRTM	MRF	Noah
REMO	Rotated lat-lon	31	0.22°	Roeckner et al. (1996)	Tiedtke (1989) with modifications after Nordeng (1994)	Morcrette et al. (1986) with modifications after Giorgetta & Wild (1995)	Higher-order closure scheme (Brinkop & Roeckner 1995)	Bucket scheme for hydrology; 5 layers for thermal processes

and longwave radiation parameterizations described in ECMWF (2004) are used, and the clouds-radiation interaction is simulated with a fractional cloud cover parameterization (Chaboureau & Bechtold 2002, 2005). The turbulent vertical exchange in the PBL is modeled following Cuxart et al. (2000). PROMES has been coupled to the land surface model ORCHIDEE (Organizing Carbon and Hydrology in Dynamic Eco-systEms, Krinner et al. 2005) with the aim of improving the land surface-atmosphere coupling. A contour band of 10 points is used to relax the model variables following Davies (1976). The method for the vertical interpolation of the large scale variables to model levels is described in Gaertner & Castro (1996).

2.1.2. WRF

The Weather Research and Forecasting (WRF) model is a state-of-the-art limited area model developed in a collaboration between the National Center for Atmospheric Research (NCAR; Boulder, CO, USA) and a number of research institutions in the United States. In this study we used the Advanced Research WRF (ARW) core (version 3.1.1), which is the research version of the model and incorporates the latest advances in the physics schemes. The ARW solver (Klemp et al. 2007, Skamarock et al. 2008) integrates the non-hydrostatic fully compressible Euler equations in flux form, using a conservative scheme over a staggered (Arakawa-C) horizontal grid and a vertical mass coordinate. The WRF model simulations

were run by the Santander Meteorology Group (SMG) of the University of Cantabria (Fita et al. 2010) through the WRF4G execution workflow (Fernández-Quiruelas et al. 2010), and represent the first WRF simulations available over the IP, together with the work of Argüeso et al. (2012). The main physical schemes used were the Grell & Devenyi (2002; GD) cumulus ensemble scheme, the WRF single-moment 5-class microphysics (WSM5; Hong & Lin 2006) and the Community Atmospheric Model (CAM) 3.0 radiation scheme (Collins et al. 2006). The simulations used 2 different configurations (labeled WRF-A and WRF-B in Table 1), which only differ in the PBL scheme. WRF-A uses a local scheme (Mellor-Yamada-Janjic; MYJ), whereas WRF-B uses a non-local scheme (Yonsei University; YSU). The non-local scheme treats vertical mixing of the entire PBL, meanwhile in the local scheme, vertical mixing is computed successively between contiguous vertical layers. As with the MM5 model, the Noah LSM was used to solve the soil processes on 4 layers to a depth of 2 m (Chen & Dudhia 2001a,b).

2.1.3. MM5

MM5 consists of a climatic version developed at the University of Murcia (Gómez-Navarro et al. 2011, Jerez et al. 2012a, 2013) of the Fifth-Generation Pennsylvania State University-NCAR Mesoscale Model (Dudhia 1993, Grell et al. 1994). MM5 has been extensively used in a number of regional cli-

mate simulations under different configurations (e.g. Boo et al. 2006, Nunez et al. 2009, Gómez-Navarro et al. 2010, among others). The physical configuration has been chosen in order to minimize the computational cost, since none of the tested configurations provides the best performance for all kinds of synoptic events and regions (Fernández et al. 2007, Jerez et al. 2012a). The physical options used were Grell cumulus parameterization (Grell 1993), Simple Ice for microphysics (Dudhia 1989), rapid radiative transfer model (RRTM) radiation scheme (Mlawer et al. 1997) and medium-range forecast scheme (MRF) for planetary boundary layer (Hong & Pan 1996). The Noah Land-Surface model (Chen & Dudhia 2001a,b) has been used in summer over the southern part of the IP, as it simulates the climate more accurately, especially in dry areas (Jerez et al. 2012b).

2.1.4. REMO

REMO is a hydrostatic, three-dimensional regional climate atmospheric model developed at the Max-Planck-Institute for Meteorology in Hamburg. It is based on the Europa Model, a former numerical weather prediction model of the German Weather Service and is described in Jacob et al. (2001). REMO uses the physical package of the global circulation model ECHAM4 (Roeckner et al. 1996). In the vertical, variations of the prognostic variables are represented by a hybrid vertical coordinate system (Simmons & Burridge 1981). The relaxation scheme according to Davies (1976) is applied.

2.2. Driving data

All the simulations were forced at the boundaries by the latest reanalysis product from the ECMWF: ERA-Interim (Dee et al. 2011). ERA-Interim has several differences with respect to ERA-40 (Uppala et al. 2005), such as variational bias correction of satellite radiance data, improvements in model physics and new humidity analysis, among others. The ERA-Interim atmospheric model and reanalysis system uses cycle 31r2 of ECMWF's Integrated Forecast System (IFS), which was introduced operationally in September 2006, configured for the following spatial resolution: (1) 60 levels in the vertical, with the top level at 0.1 hPa; (2) T255 spherical-harmonic representation for the basic dynamical fields; (3) a reduced Gaussian grid with approximately uniform 79 km spacing for surface and other grid-point fields. In the

study, all models have used boundary and initial conditions from ERA-Interim every 6 h with a spatial resolution of $0.7° × 0.7°$.

With respect to the forcings along the ERA-Interim period, all models use a sea surface temperature interpolated from ERA-Interim data and updated every 6 h. Aerosols in PROMES follow the GADS climatology (d'Almeida et al. 1991, Koepke et al. 1997), while the rest of the models do not include aerosols in their forcing for regional climate simulations. For greenhouse gases, REMO uses trends in the amounts of specified radiatively active gases (CO_2, CH_4, N_2O, CFC-11, CFC-12) according to the ones used to generate the ERA reanalysis (Houghton et al. 1996). PROMES, WRF and MM5 use constant values of greenhouse gases.

2.3. Observational database

We used the Spain02 precipitation and temperature database (Herrera et al. 2012). Spain02 is a daily gridded dataset developed using surface station data from a set of 2756 quality-controlled stations over peninsular Spain and the Balearic islands. This data set covers the period 1950–2008, with a daily frequency and $0.2° × 0.2°$ resolution. A 2-step interpolation procedure was used: firstly, the monthly means were interpolated using thin-plate splines, and secondly, daily departures from the monthly means were interpolated using a kriging methodology. In the case of precipitation, occurrence and amounts are interpolated through indicator and ordinary kriging, respectively. The interpolation procedure for precipitation is similar to that of the E-OBS European database (Haylock et al. 2008), except for the absence of the elevation-dependent splines applied to the E-OBS database, which was not used in Spain02 since the topography is well represented by the large amount of stations. For temperature, the Spain02 database applied a more stringent filter to the station data in order to provide a product better suited for trend analyses (Herrera et al. 2012). Unlike the precipitation product, where the maximum number of available stations at a given day were used, the temperature data set was built from a reduced set of only those stations with a record longer than 40 yr and <1 % of missing data, leaving 186 stations. These stations were gridded using the same methodology as E-OBS, the only difference being the better quality and higher number of stations over spain.

The large number of stations used in this product compared with the ECA database provides a better

representation of precipitation (Herrera et al. 2010) and temperature variability (Herrera et al. 2012) over Spain.

2.4. Validation methodology

The Spain02 regular latitude-longitude grid has been used as the reference for validation. Thus, all RCM data have been bilinearly interpolated onto the Spain02 grid. Since the resolution of the RCMs is similar to that of Spain02 and we are interested in the mean climate, the interpolation procedure is not expected to significantly alter any of our results.

All the statistical measures are calculated at individual grid points. Only land grid points over peninsular Spain and the Balearic islands are considered in the analysis. Since this work focuses on mean climate, we only worked with monthly averaged data. Thus, we will use the notation V_{iym}^k for a variable from model k at grid point i, in year $y = 1990, \ldots, 2007$ and month $m = 1, \ldots, 12$. If we use bracket notation for an average over a given index (e.g. $\langle \cdot \rangle_{ym}$ for an average over all years and months, i.e. a time average), we can express the bias (b) at a given grid point as:

$$b_i^k = \langle V_{iym}^k - O_{iym} \rangle_{ym} \tag{1}$$

where O_{iym} is the value observed. The model bias is the simplest measure of model performance.

The ensemble mean, $\langle V_{iym}^k \rangle_k$, is usually considered as an additional simulation that compensates the errors of the different ensemble members. Even though this is a very simplistic view of the ensemble (which should be considered from a probabilistic point of view), it can be useful to reinforce the common signal of the different models in our analysis of the mean climate. Notice, however, that the ensemble mean is not a physical realization of any of the models, but just a statistical average of different non-linear trajectories (Knutti et al. 2010).

For seasonal analyses, the seasons were defined as winter (DJF), spring (MAM), summer (JJA) and autumn (SON). Seasonal biases can be defined by averaging over months in a specific season, e.g. $b_{i,\mathrm{DJF}}^k = \langle V_{iym}^k - O_{iym} \rangle_{y,m=\mathrm{DJF}}$.

The seasonal cycle was calculated as follows:

$$V_{im}^k = \langle V_{iym}^k \rangle_y \tag{2}$$

Then, the interannual variability was assessed on the series without considering their annual cycle ($\hat{V}_{iym}^k$). The averaged monthly annual cycle was removed from each corresponding monthly value:

$$\hat{V}_{iym}^k = V_{iym}^k - V_{im}^k \tag{3}$$

The ability to represent the interannual variability can be decomposed into (1) the ability to represent its size, which can be represented by the standard deviation (SD) of the deseasonalized series as:

$$\mathrm{SD}[V]_i^k = \sqrt{\langle (\hat{V}_{iym}^k)^2 \rangle_{ym}} \tag{4}$$

and (2) can be compared to that of the observations $\mathrm{SD}[O]_i$, and (3) the ability to represent the year-to-year variations, which can be represented by the linear correlation coefficient with the observations:

$$\rho_i^k = \frac{\langle \hat{V}_{iym}^k \hat{O}_{iym} \rangle_{ym}}{\sqrt{\langle (\hat{V}_{iym}^k)^2 \rangle_{ym} \langle (\hat{O}_{iym})^2 \rangle_{ym}}} \tag{5}$$

The latter ability can only be expected on RCM simulations nested into 'perfect' boundary conditions such as those considered in this study.

Finally, pattern agreement between simulated and observed seasonal climatologies was quantified by means of the spatial correlation and the ratio between simulated and observed SDs, $V_i^k = \langle V_{iym}^k \rangle_{ym}$, as:

$$r^k = \frac{\langle (V_i^k - \langle V_i^k \rangle_i)(O_i - \langle O_i \rangle_i) \rangle_i}{\sqrt{\langle (V_i^k - \langle V_i^k \rangle_i)^2 \rangle_i \langle (O_i - \langle O_i \rangle_i)^2 \rangle_i}} \tag{6}$$

$$s^k = \sqrt{\frac{\langle (V_i^k - \langle V_i^k \rangle_i)^2 \rangle_i}{\langle (O_i - \langle O_i \rangle_i)^2 \rangle_i}} \tag{7}$$

This information can be summarized in a Taylor (2001) diagram, which is a polar plot, with radial coordinate s^k and angular coordinate related to r^k.

3. RESULTS

3.1. Bias

Seasonal model biases in representing the climatology of maximum and minimum temperature and precipitation are represented in Figs. 2 & 3 and summarized in Table 2a by their spatial averages, along with the average annual bias. The ensemble average is also displayed as if it were an additional simulation.

Annual maximum temperatures are cold-biased (Table 2a) in most models (ranging from −2.43K in MM5 to −1.74K in PROMES). REMO is the only exception and shows a warm bias (+0.64K). The models keep in all seasons the same bias sign as the annual values: REMO shows warm biases in all seasons and the other models show cold biases. The models show similar bias spatial patterns (Fig. 2). For

Table 2. Spatial average of (a) the mean bias and (b) interannual variability for maximum (T_{max}) and minimum (T_{min}) temperature and precipitation in the models included in ESCENA and the ensemble of simulations. Data in (b): SD for temperature, CV for precipitation. Seasons: winter (DJF), spring (MAM), summer (JJA), autumn (SON)

	T_{max} (K)					T_{min} (K)					Precipitation (mm d^{-1})				
	DJF	MAM	JJA	SON	Annual	DJF	MAM	JJA	SON	ANNUAL	DJF	MAM	JJA	SON	Annual
(a)															
PROMES	−2.08	−2.07	−0.62	−2.20	−1.70	0.51	0.06	0.27	0.53	0.34	0.30	0.65	0.52	0.38	0.44
WRF-A	−2.48	−2.33	−2.31	−2.49	−2.40	0.03	−0.42	−0.59	−0.45	−0.37	−0.48	−0.25	0.01	−0.80	−0.38
WRF-B	−1.80	−2.27	−2.44	−2.00	−2.13	1.25	0.67	0.60	0.65	0.79	−0.29	−0.17	−0.07	−0.71	−0.31
MM5	−1.72	−2.59	−2.99	−2.44	−2.43	0.79	−0.21	−0.15	0.09	0.13	−0.07	−0.13	0.00	−0.22	−0.10
REMO	0.30	0.26	1.01	0.98	0.64	2.34	2.10	3.21	2.87	2.63	−0.17	0.21	0.14	−0.24	−0.25
ENSEMBLE	−1.56	−1.80	−1.47	−1.63	−1.61	0.98	0.44	0.67	0.74	0.71	−0.14	0.06	0.12	−0.32	−0.08
(b)															
Spain02	1.64	1.86	1.86	1.80	1.81	1.83	1.26	1.20	1.59	1.50	0.92	0.74	1.07	0.74	0.87
PROMES	−0.07	0.33	0.32	0.22	0.21	−0.09	0.11	−0.04	0.07	0.00	0.04	0.16	0.28	0.04	0.29
WRF-A	0.07	−0.00	−0.02	0.04	0.02	−0.33	−0.04	0.06	−0.12	−0.13	−0.23	−0.18	−0.26	−0.28	−0.21
WRF-B	−0.11	−0.16	−0.12	−0.06	−0.12	−0.36	−0.18	0.01	−0.20	−0.20	−0.19	−0.14	−0.34	−0.23	−0.17
MM5	−0.27	−0.38	−0.20	−0.12	−0.24	−0.38	−0.16	−0.02	−0.01	−0.16	−0.06	−0.08	−0.15	−0.07	0.00
REMO	−0.08	−0.15	−0.17	−0.01	−0.10	−0.60	−0.21	0.08	−0.19	−0.25	−0.05	0.03	−0.07	−0.05	0.02
ENSEMBLE	−0.09	−0.07	−0.04	−0.01	−0.05	−0.35	−0.10	0.02	−0.09	−0.15	−0.09	−0.04	−0.10	−0.11	−0.01

instance, all models overestimate maximum temperature during summertime over the southern IP and some areas along the Mediterranean coast.

For minimum temperature (Table 2a), REMO is again strongly warm biased (+2.63K) compared with the other models, which range from −0.37 (WRF-A) to +0.79K (WRF-B). Two configurations of the same model provide a wide range of minimum temperatures. Regarding minimum temperature, the difference between different PBL parameterizations in a single model is larger than between completely different models in the ensemble (e.g. MM5 and PROMES), except in the case of REMO. Again, the spatial patterns (Fig. 2) of the different models are very similar. The topographical characteristics of minimum temperatures are well captured by the models, but they all show overestimations over mountainous areas and slight underestimations elsewhere. Note that these tend to partly compensate each other in the spatially averaged biases shown in Table 2a.

For precipitation, only those cells over land with observed precipitation >0.25 mm d^{-1} (monthly average) have been selected for comparisons. Annual biases (Table 2a) range from −0.38 (WRF-A) to +0.44 mm d^{-1} (PROMES). In this case, the spatial pattern of seasonal biases (Fig. 3) are presented as a relative difference (in %), since larger absolute biases tend to occur over areas with larger precipitation. The threshold chosen (0.25 mm d^{-1}) is especially noticeable for summertime in the south and southeastern Mediterranean coast. In autumn, most models show a large precipitation underestimation in southern and eastern peninsular Spain and the Balearic Islands, where torrential precipitation occurs. PROMES shows a different behaviour compared with the rest of the models, since it overestimates seasonal precipitation, especially during spring.

Table 2a and Figs. 2 & 3 include the biases of the ensemble mean, considered as an additional model simulation. As expected, the ensemble mean shows an intermediate behaviour, which in most cases leads to reduced biases. However, common biases, such as the cold-biased maximum temperature or the common pattern in minimum temperature, remain in the ensemble mean, although the most extreme biases are attenuated. For precipitation, the ensemble mean shows the smallest absolute bias compared to the individual simulations.

An especially remarkable result is the high spread of the simulated bias, despite the small amount of models used in this study. It is crucial to work with an
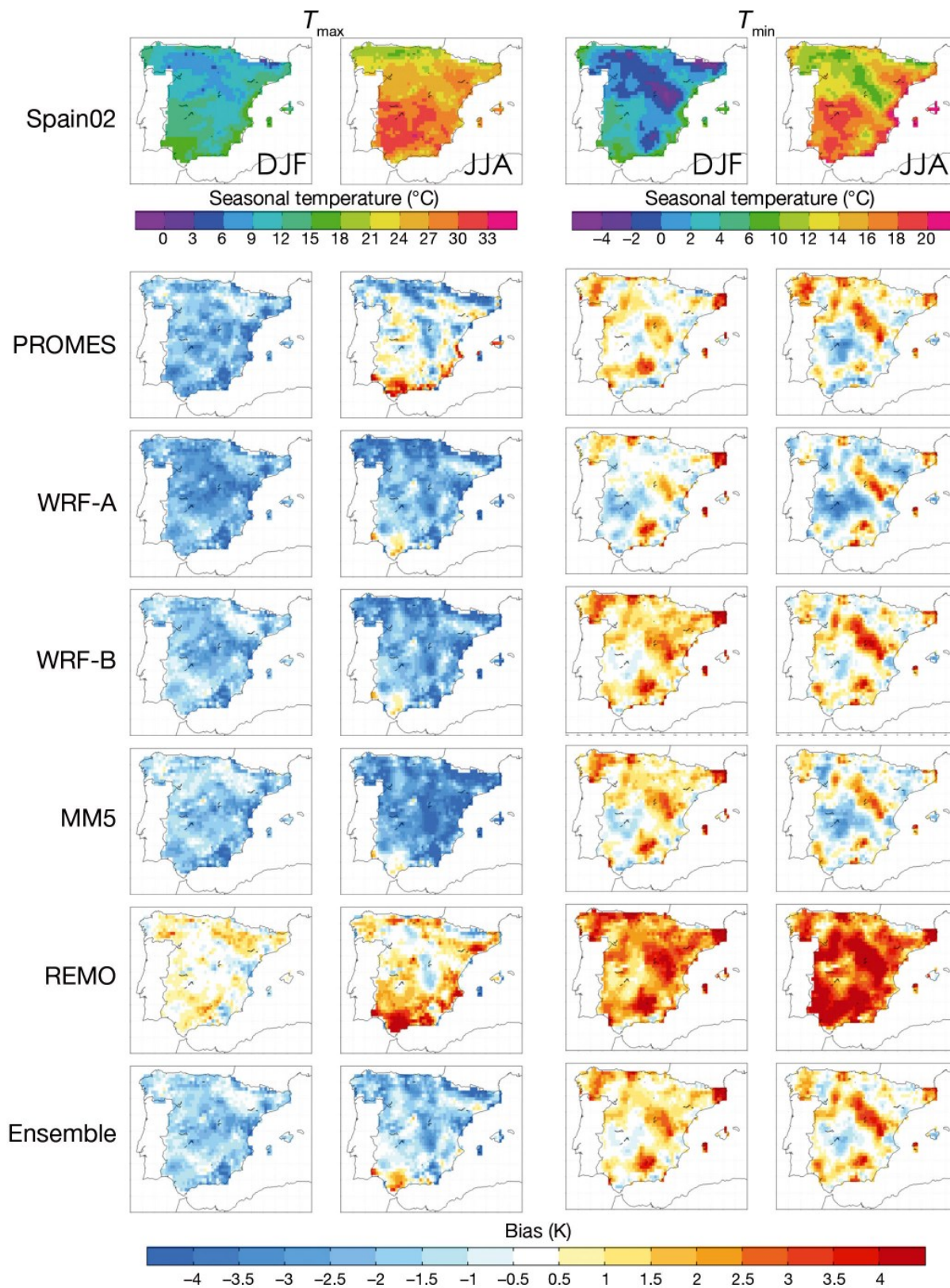
Fig. 2. Seasonal maximum (T_{max}) and minimum (T_{min}) temperature (°C; top row) for Spain02 and biases (K) for models. Columns: winter (DJF) and summer (JJA) values
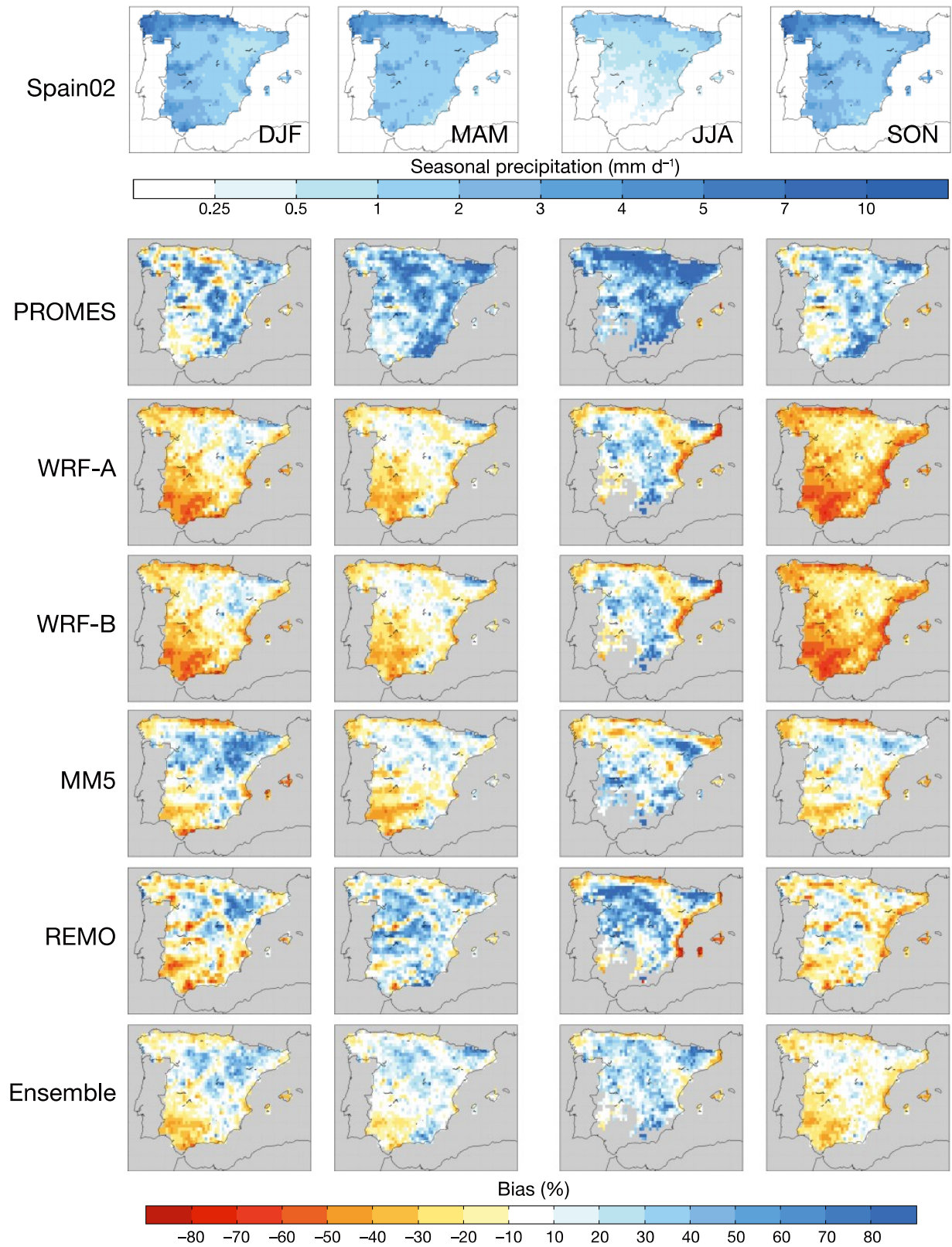
Fig. 3. Seasonal precipitation for Spain02 (mm d^{-1}, top row) and biases (%) for models. Columns (left to right): winter (DJF), spring (MAM), summer (JJA) and autumn (SON) values. Grey shading: areas where biases are not shown (ocean and precipitation <0.25 mm d^{-1})
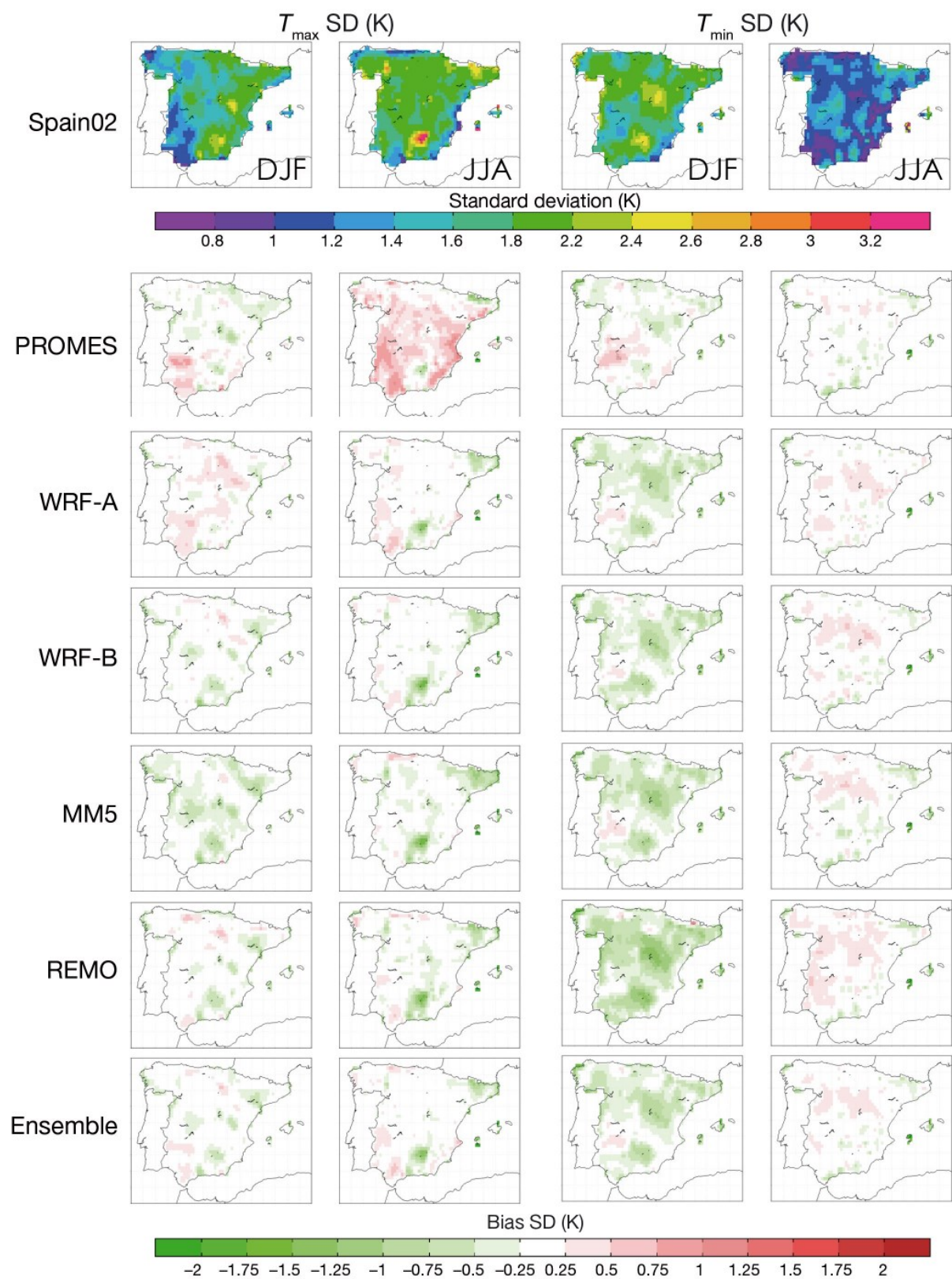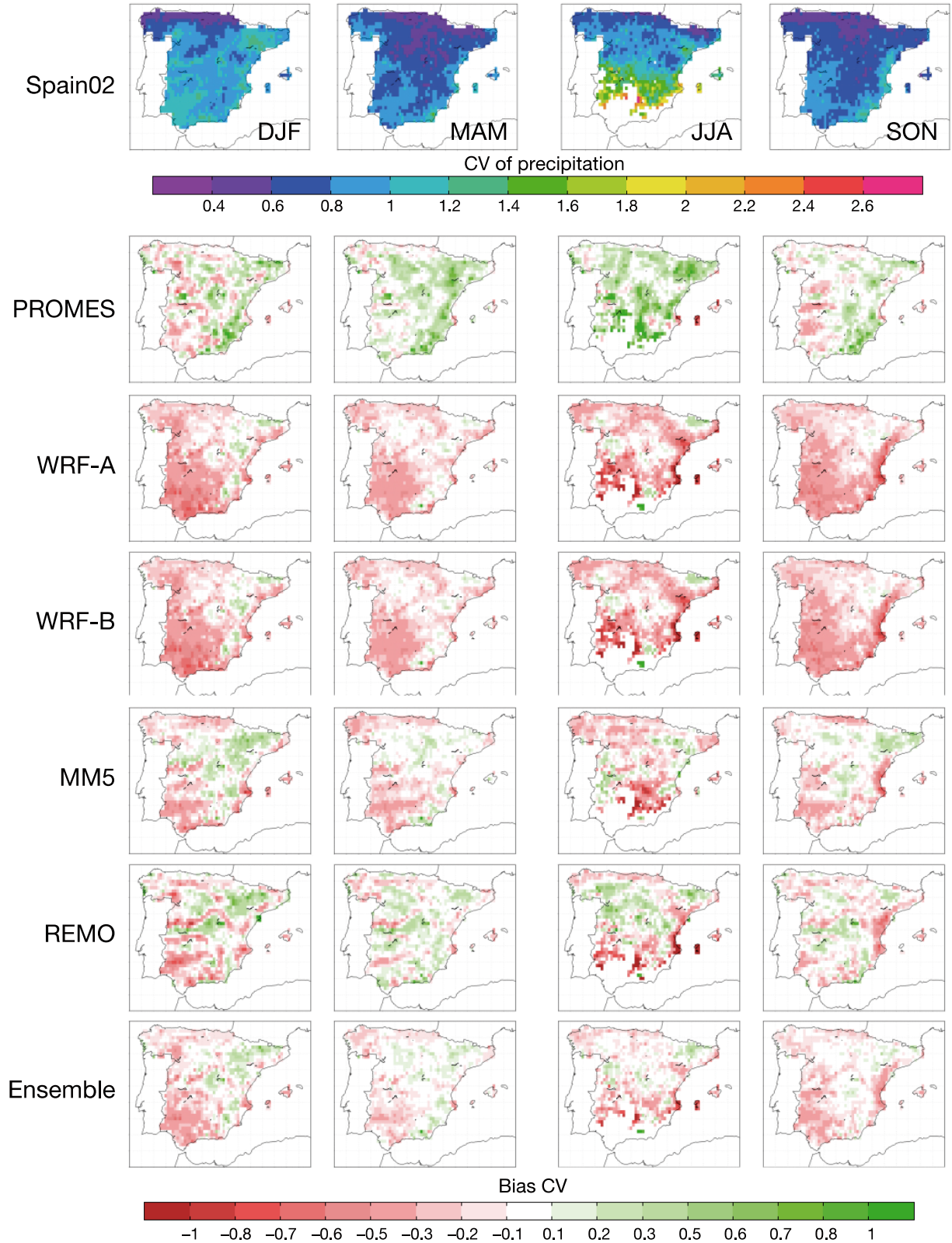
Fig. 4. Standard deviation (SD) of seasonal maximum (T_{max}) and minimum (T_{min}) temperature for Spain02 (K; top row) and SD biases (K) for models. Columns: winter (DJF) and summer (JJA) values

Fig. 5. Coefficient of variation (CV) of seasonal precipitation for Spain02 and CV biases for models. Columns: same order as in Fig. 3

ensemble of regional climate models instead of one individual model to get more robust future climate projections, for a better assessment of uncertainties due to the dynamical downscaling process. These climate projections have already been carried out in the ESCENA project. An important issue, which we do not address here but will be considered in future stages of the ESCENA project, is the relationship between past and future performance of models (as evaluated by Whetton et al. 2007 and Abe et al. 2009, among others). As stated by Annan & Hargreaves (2010), climate models have already been tuned to some extent to the recent climate data and therefore accurately reproduce present-day climate conditions. It would be interesting to further test the reliability of the ensemble in other ways, for example considering simulations of other epochs or other climatic observations that are less widely used during model construction and tuning.

3.2. Interannual variability

For precipitation, SD is normalized by the period average, therefore by obtaining a coefficient of variation (CV). This is done because the SD of precipitation is typically related to the mean (Giorgi et al. 2004), so that the CV is a more independent measure of interannual variability.

Table 2b shows the spatially averaged seasonal and annual interannual variability biases for maximum and minimum temperature and the spatially averaged CV biases for precipitation. The seasonal spatial distribution of the mentioned statistics are represented in Figs. 4 & 5, for maximum and minimum temperature and precipitation, respectively.

All models except for PROMES and WRF-A tend to slightly underestimate the interannual SD of maximum temperature (Fig. 4). Similar values and responses from models are observed for different seasons. In winter, the biases of maximum temperature SD vary between −0.27K in MM5 to +0.07K in WRF-A (Table 2b). The biases range from −0.38 (MM5) to +0.33K (PROMES) in spring, and −0.20 (MM5) to +0.32K (PROMES) during summer; meanwhile for autumn MM5 once more provides the largest underestimation of the SD (−0.12K) and PROMES the highest overestimation (+0.22K). The rest of the models show an intermediate behavior for representing the interannual SD, with the best skills during the autumn season.

For minimum temperature (Fig. 4), the results are similar to maximum temperature, but in this case it is

REMO which tends to provide the largest biases in the minimum temperature variability (Table 2b). The SD is generally underestimated by all models, especially during winter over the highest mountain chains of the IP. In this season, biases vary between −0.60 (REMO) and −0.09K (PROMES). All models predict spring variability better than for wintertime (−0.21K in REMO and 0.11K in PROMES during springtime). However, in summer all the models show values close to Spain02.

Regarding precipitation, the models (except PROMES) pervasively underestimate the interannual variability over the domain, especially in southwestern Spain in winter, and the Mediterranean coast and the Balearic Islands during summer and autumn (Fig. 5). The biases of the CV range from +0.04 (winter and autumn) to +0.28 (summer) in the case of PROMES, to underestimations in WRF-A (−0.28 in autumn to −0.18 in spring). MM5 and REMO present the smallest average biases, ranging from −0.15 to 0.03.

The multi-model ensemble mean outperforms most of the individual models in all seasons, showing the added value of using an ensemble of RCMs to improve the amount of interannual variability. However, common model deficiencies still remain (e.g. the low precipitation variability in autumn on the Mediterranean coast).

The temporal correlation (ρ) between simulated and observed deseasonalized series is shown in Fig. 6 for maximum and minimum temperature and precipitation. Maximum temperatures show the highest correlations (>0.85) over most of the domain, especially over the river valleys of northern Spain. The fact that the lowest correlations (~0.4) are found in northeastern Spain for all models may point to (1) problems with the quality of raw observed data used to create the Spain02 database or (2) to local climatic features that the models are unable to capture at the selected resolution. For minimum temperature, ρ is generally slightly lower than for maxima. The spatial structure of the correlation presents common minima in all models, and this points to a relation with topography, since the lowest correlation coefficients (ρ < 0.5) are located in the highest mountain chains in Spain, such as the Pyrenees, Sistema Ibérico or Sierra Nevada, from north to south of the domain. On the other hand, the highest correlations for minimum temperatures are observed over the Central Plateaus and the river valleys. The precipitation correlations show a strong east-west gradient reaching the lowest values (~0.30 to 0.50) towards the Ebro Valley and the southeastern IP (Fig. 6).
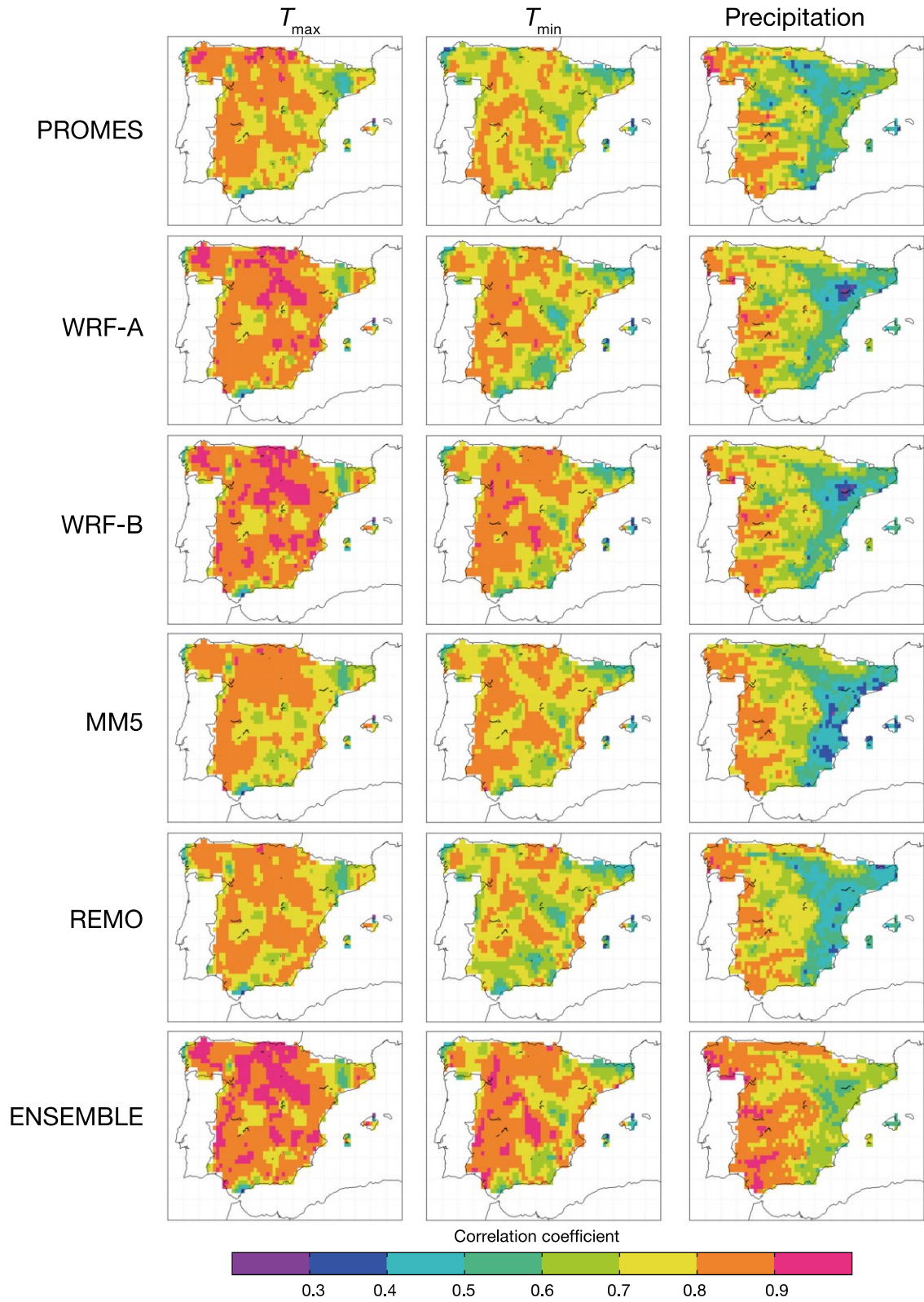
Fig. 6. Mean temporal correlation coefficients for simulated maximum (T_{max}) and minimum (T_{min}) temperature and precipitation vs. Spain02 observations. Correlations were calculated using individual months in each season yr^{-1} and for each point

In order to discriminate the seasonal behavior of this temporal correlation, Table 3 represents spatially averaged correlations for maximum and minimum temperature and precipitation. Maximum temperature shows the highest correlations and they present a low seasonal variability. Spring has slightly higher correlations than the rest of the seasons. In general, there is also a low model-to-model variability. Only WRF shows somewhat higher correlations (mostly >0.8). REMO, unlike the rest of the models, presents a value <0.70 in summer, indicating a lower capability to capture maximum temperature variability in summer. For minimum temperatures, correlations are, in general, lower than for maximum temperature and they exhibit a clearer seasonal variability, with higher correlations in winter and autumn. In this case, spring shows the lowest correlations, and several models show correlations <0.7 in different seasons. Only WRF-B is above this threshold throughout the year and performs best on average. For this variable, WRF-A is more similar to other models, such as MM5, than to WRF-B. Lastly, for precipitation the correlations are generally much lower than for temperature, and the seasonal dependence is very strong. As expected, higher correlation coefficients are attained during winter (0.77 to 0.80), when synoptic systems, well captured in the reanalysis data, drive precipitation. During summer, the synoptic activity is lower and precipitation is mostly driven by convective systems, less constrained by the boundary conditions; therefore, the lowest correlations are attained (0.42 to 0.55). An intermediate behaviour is shown in the transition seasons.

The most noticeable aspect regarding correlation (Fig. 6), is the large improvement achieved when considering the ensemble mean. Spatially (Fig. 6), there are areas where correlations are above any of the component members; most noticeably in precipitation over the eastern coast, where a common RCM defect is improved by the ensemble, softening the strong gradient present in each individual model. Also, after spatial averaging (Table 3), the ensemble mean performs at least as well as the best member, and in most cases shows better correlation than any of the members. This is true especially for precipitation.

3.3. Spatial variability

Here, we focus on the ability of the models to represent the observed spatial variability by using Taylor diagrams (Taylor 2001), which enable an easy comparison between the spatial and temporal pat-

Table 3. Time-correlation for modeled (a) maximum and (b) minimum temperature, and (c) precipitation vs. Spain02 observations for all seasons and diverse models included in ES-CENA. Seasons: winter (DJF), spring (MAM), summer (JJA), autumn (SON). Light to dark shading indicates low to high correlation coefficients, respectively

	DJF	MAM	JJA	SON	Annual
(a)					
PROMES	0.77	0.79	0.77	0.80	0.78
WRF-A	0.78	0.85	0.83	0.84	0.83
WRF-B	0.80	0.86	0.83	0.84	0.84
MM5	0.77	0.83	0.74	0.80	0.78
REMO	0.78	0.83	0.69	0.83	0.79
Ensemble	0.81	0.87	0.83	0.86	0.84
(b)					
PROMES	0.67	0.74	0.77	0.76	0.73
WRF-A	0.76	0.69	0.74	0.80	0.75
WRF-B	0.82	0.74	0.74	0.82	0.78
MM5	0.81	0.70	0.73	0.79	0.76
REMO	0.78	0.66	0.68	0.78	0.72
Ensemble	0.82	0.74	0.77	0.83	0.79
(c)					
PROMES	0.79	0.68	0.55	0.60	0.67
WRF-A	0.78	0.68	0.52	0.62	0.68
WRF-B	0.80	0.69	0.53	0.63	0.69
MM5	0.77	0.64	0.44	0.62	0.66
REMO	0.77	0.67	0.42	0.64	0.66
Ensemble	0.85	0.77	0.63	0.73	0.77

terns of 2 fields. In our diagrams (Fig. 7), the statistics displayed are the relative spatial SD (radial distance from the origin) and the correlation (cosine of the angular coordinate). Better models, in terms of centered root mean squared error (RMSE), are located closer to the black circle shown in Fig. 7, which corresponds to Spain02. Centered RMSE increases with distance from this point.

With respect to the mean field of maximum temperature (Fig. 7a), all models perform well, especially for winter, with very high spatial correlations and a normalized SD close to observations. However, PROMES and REMO represent excessive spatial variability during summertime. The spatial variability of the interannual SD (Fig. 7b), as well as its spatial mean (Table 2) is strongly overestimated by PROMES in spring and summer, providing higher values of spatial patterns of variability. There is a strong variation in the skill of the models as a function of the season of the year, with better correlation values during spring and autumn.

In the simulation of the mean minimum temperature (Fig. 7c), the models perform very similarly with each other, showing a high spatial correlation with the observations, but in most cases with a small underestimation of the spatial variability, except for

the cold season. The models do not capture the spatial structure of the variability during summer and wintertime (Fig. 7d). This variability is pervasively underpredicted for winter and summer, when spatial correlation does not exceed 0.45. Both for maximum and minimum temperature, the diverse models (and seasons) present a high spread in the representation of the spatial structure of the SD.

The mean precipitation pattern (Fig. 7e) is captured worse than those of temperature. This is expected, since the temperature patterns are strongly related to the orography. PROMES tends to provide a higher spatial variability than observations, especially for summertime (see red diamond outside the Taylor diagram in 7e), but with a high correlation (>0.88). In this case, REMO tends to better capture the field variability. For the SD pattern (Fig. 7f), a similar analysis can be performed, with PROMES tending to overestimate the SD of the spatial variability.

In this case, the added value of considering the ensemble mean is not clear for the maximum temperature (the ensemble mean outperforms most but not all models), albeit it generally improves the skill of most models. For minimum temperature and, overall, precipitation, the ensemble mean outperforms the individual models in all seasons, although it somewhat underestimates the variance of the SD patterns.

4. DISCUSSION AND CONCLUSIONS

In this work we have analyzed the RCM evaluation simulations of the ESCENA project over peninsular Spain and the Balearic Islands. This work evaluates, for the first time over a European region, the MM5 and WRF open-source, US-developed models along with European RCMs (PROMES and REMO). This study is also one of the earliest works using ERA-Interim as boundary conditions over Europe. As an initial evaluation of the ESCENA simulations, we used simple, widely used metrics to enable the comparison of the model performance with earlier studies. Also, we focused on the mean climate and interannual variability, therefore relying on monthly data.

As an indication of the quality of the simulations, we can compare the spatial correlation values for precipitation deduced from Fig. 7 with those obtained for RCMs in ENSEMBLES included in Herrera et al. (2010). That work classified the RCMs into 2 groups, according to a gap in the spatial correlation of precipitation. According to this classification, all individual RCMs in ESCENA would be in the group of the 'best' models. Also, the ensemble mean in

ESCENA is similar to the best ensemble in the aforementioned work. Therefore, the ability to reproduce precipitation within ESCENA is high, at least in this aspect, when compared to Herrera et al. (2010) and references therein. The temperature results can be qualitatively compared to the bias maps shown by Christensen et al. (2010), which show typical biases within ENSEMBLES of the order of 2K in this region, similar to those found in ESCENA. Temperature-outlier models in ENSEMBLES show biases much larger than those in ESCENA. Therefore, overall, the 5 regional climate simulations included in ESCENA show good quality in reproducing the climatology of the IP, even though these models are based on completely different approaches and physical parameterizations.

WRF was used in 2 different settings, which differ only in the representation of the PBL. WRF-A used a local closure scheme, which has been reported to develop shallower, colder, and moister PBLs than WRF-B, which used a non-local closure scheme (García-Díez et al. 2013). The weaker low-level mixing in WRF-A leads to colder nighttime (i.e. minimum) temperatures. Therefore, the largest differences between the WRF ensemble members appear in the minimum temperature. Remarkably, MM5 is the only other model in the ensemble using a non-local closure PBL scheme, but the results are closer to WRF-A. It seems that biases arising from other components (model dynamics, numerics or other parameterizations) are compensating the expected summer warm bias.

Regarding the inherent uncertainties of model validation methodologies, climate models here are assessed on their capacity to reproduce present climate conditions, which in turn are established by comparing the output of climate simulations with observational datasets including gridded products (here, Spain02 dataset). However, due to the nature of the procedures to obtain observations and the statistical techniques employed to extrapolate this information onto reference gridded databases, they contain important uncertainties which may compromise the evaluation process. A recent work by Gómez-Navarro et al. (2012) indicates that, even in areas covered by dense monitoring networks such as Spain, uncertainties in the observations are comparable to the uncertainties within state-of-the-art RCMs driven by reanalysis, such as those used in ESCENA. Therefore, some of the common deficiencies found, can probably be traced to problems in the observational database. For instance, the warm biased minimum temperatures over northeastern Spain are a
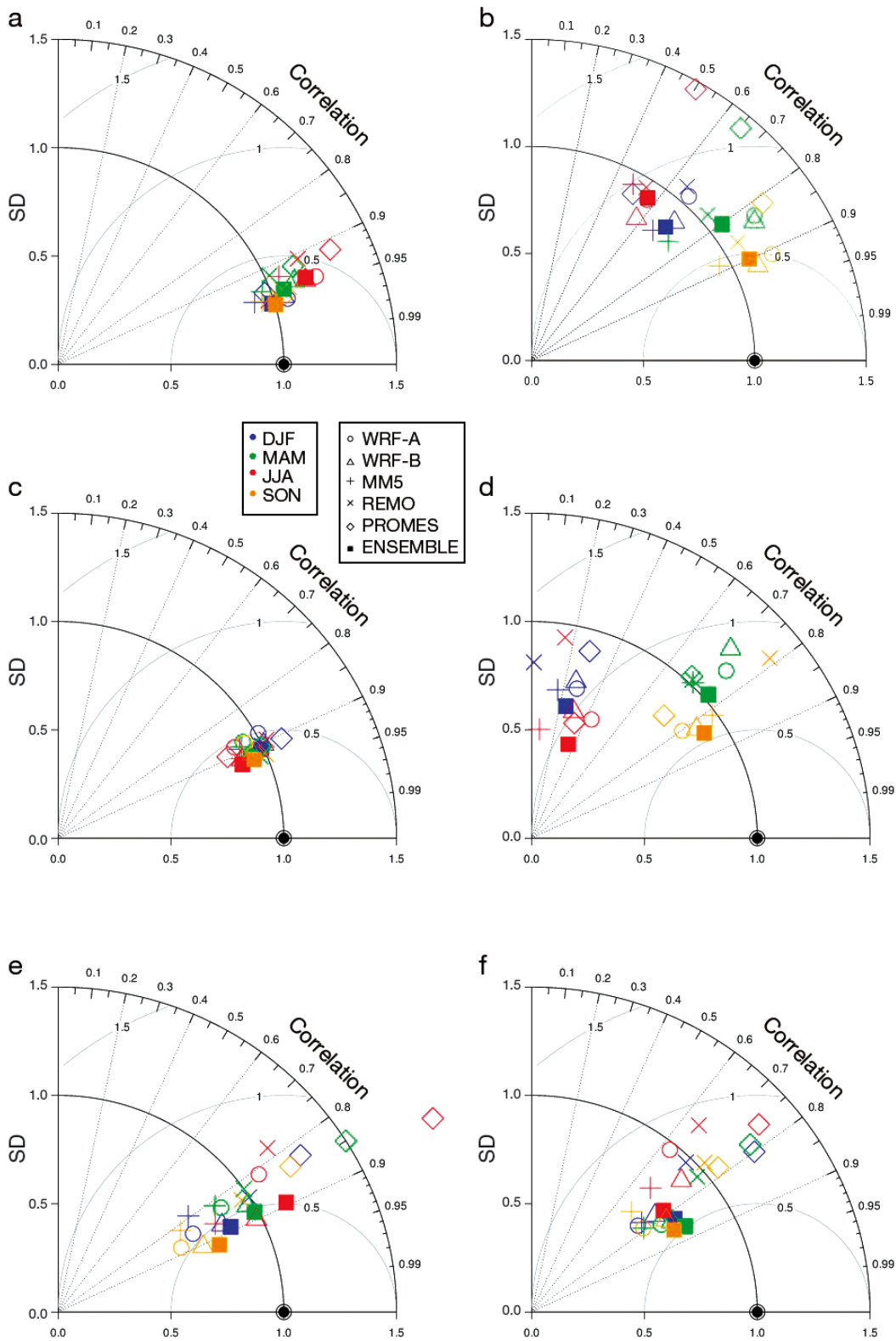
Fig. 7. Taylor diagrams for seasonal (a,b) maximum temperature, (c,d) minimum temperature, and (e,f) precipitation for all models included in the analysis. (a,c,e) Mean fields; (b,d,f) SD. Seasons: winter (DJF), spring (MAM), summer (JJA), autumn (SON)

candidate to a misrepresentation in the observational database, since (1) the problem is common to all models, (2) there are no complex topographic features over that area, and (3) the problem does not arise in any other variable.

No single model outperforms the rest of the models for all the variables analyzed. Depending on the variable and season, different models stand out. For example, REMO stands out for temperature (especially minimum temperature), PROMES shows a wet bias when the rest tend to be drier than observed, and WRF is also especially dry during autumn. Regarding the inclusion of US-developed models in the ensemble, we found no 'home court advantage' (Takle et al. 2007) for the European models. Unlike shown in other recent studies over north America (Mearns et al. 2012), the use of RCMs out of their 'home' domain did not lead to poorer performance.

The different performance of the RCMs in different seasons and variables encourages the use of the whole ensemble of simulations, taking the range of biases as an indicator of model uncertainty. The simplest way of considering the ensemble of RCMs is through the use of the ensemble mean as an additional simulation. The results show that the ensemble mean is usually less biased than the individual members or is close to the best member. Remarkably, the ensemble of simulations is able to correct the problems associated with the interannual variability for precipitation, showing substantially higher temporal correlation than the best individual model. These results are in accordance with previous works (Gleckler et al. 2008, Coppola et al. 2010, Kjellström et al. 2011). As stated by Annan & Hargreaves (2011), one hypothesis for the improvement of the ensemble mean when compared to the performance of the individual models is the paradigm of models being considered as independent samples from some distribution that is centered on the truth, as in this case the ensemble mean could be expected to converge to the truth as more models are added to the ensemble (Tebaldi & Knutti 2007). However, this hypothesis has been refuted by Knutti et al. (2010). Annan & Hargreaves (2010, 2011) defend the point that the statistically indistinguishable paradigm provides a reasonable basis for explanation of the properties of the CMIP3 ensemble. However, their results are only directly applicable to their specific comparisons and a convincing explanation for the outperformance of the ensemble mean is still an open question in climate science.

We can, therefore, conclude that the use of ensemble simulations in this kind of study substantially improves the representativity of the climatologies, and we also expect that studies of future climates, by using ensemble methodologies, will provide more robust climate projections and a valuable estimation of the associated uncertainty. As shown, these data can be complementary to other European projects such as ENSEMBLES over the Iberian Peninsula and surrounding areas. The data from this study are publicly available on the ESCENA project server (http://proyectoescena.uclm.es). The analyses shown are just an initial evaluation that needs to be extended in forthcoming studies by the climate and impact communities in the Iberian Peninsula, who are encouraged to use the whole RCM ensemble, thereby propagating the uncertainties found.

LITERATURE CITED

Abe M, Shiogama H, Hargreaves J, Annan J, Nozawa T, Emori S (2009) Correlation between inter-model similarities in spatial pattern for present and projected future mean climate. SOLA 5:133−136

Annan JD, Hargreaves JC (2010) Reliability of the CMIP3 ensemble. Geophys Res Lett 37:L02703, doi:10.1029/2009 GL041994

Annan JD, Hargreaves JC (2011) Understanding the CMIP3 multimodel ensemble. J Clim 24:4529−4538

Argüeso D, Hidalgo-Muñoz JJ, Gamiz-Fortis SR, Esteban-Parra MJ, Castro-Diez Y (2012) Evaluation of WRF mean and extreme precipitation over Spain: present climate (1970−1999). J Clim 25:4883−4897

Arribas A, Gallardo C, Gaertner MA, Castro M (2003) Sensitivity of Iberian Peninsula climate to land degradation. Clim Dyn 20:477−489

Boo KO, Kwon WT, Baek HJ (2006) Change of extreme events of temperature and precipitation over Korea using regional projection of future climate change. Geophys Res Lett 33:L01791, doi:10.1029/2005GL023378

Boulanger JP, Brasseur G, Carril AF, de Castro M and others (2010) A Europe-South America network for climate change assessment and impact studies. Clim Change 98: 307−329

Brinkop S, Roeckner E (1995) Sensitivity of a general circulation model to parameterizations of cloud-turbulence interactions in the atmospheric boundary layer. Tellus A 47(2):197−220

Castro M, Fernández C, Gaertner MA (1993) Description of a mesoscale atmospheric numerical model. In: Díaz JI,

Lions JL (eds) Mathematics, climate and environment. Rech Math Appl Ser 27, Masson, Paris, p 230–253

Chaboureau JP, Bechtold P (2002) A simple cloud parameterization derived from cloud resolving model data: diagnostic and prognostic applications. J Atmos Sci 59:2362–2372

Chaboureau JP, Bechtold P (2005) Statistical representation of clouds in a regional model and the impact on the diurnal cycle of convection during tropical convection, cirrus and nitrogen oxides (TROCCINOX). J Geophys Res 110: D17103, doi:10.1029/2004JD005645

Chen F, Dudhia J (2001a) Coupling an advanced land surface-hydrology model with the Penn State-NCAR MM5 modeling system. I. Model implementation and sensitivity. Mon Weather Rev 129:569–585

Chen F, Dudhia J (2001b) Coupling an advanced land surface-hydrology model with the Penn State-NCAR MM5 modeling system. II. Preliminary model validation. Mon Weather Rev 129:587–604

Christensen JH, Christensen OB (2007) A summary of the PRUDENCE model projections of changes in European climate by the end of this century. Clim Change 81:7–30

Christensen JH, Kjellström E, Giorgi F, Lenderink G, Rummukainen M (2010) Weight assignment in regional climate models. Clim Res 44:179–194

Collins WD, Rasch PJ, Boville DA, Hack JJ, McCaa JR, Williamson DK, Briegleb BP (2006) The formulation and atmospheric simulation of the Community Atmosphere Model. J Clim 19:2144–2161

Coppola E, Giorgi F, Rauscher SA, Piani C (2010) Model weighting based on mesoscale structures in precipitation and temperature in an ensemble of regional climate models. Clim Res 44:121–134

Cuxart J, Bougeault P, Redelsperger JL (2000) A turbulence scheme allowing for mesoscale and large-eddy simulations. Q J R Meteorol Soc 126:1–30

d'Almeida GA, Koepke P, Shettle EP (1991) Atmospheric aerosols: global climatology and radiative characteristics. A Deepak Publ, Hampton, VA

Davies HC (1976) A lateral boundary formulation for multi-level prediction models. Q J R Meteorol Soc 102:405–418

Dee DP, Uppsala SM, Simmons AJ, Berrisford P and others (2011) The ERA-Interim reanalysis: configuration and performance of the data assimilation system. Q J R Meteorol Soc 137:553–597

Domínguez M, Gaertner MA, de Rosnay P, Losada T (2010) A regional climate model simulation over West Africa: parameterization tests and analysis of land-surface fields. Clim Dyn 35:249–265

Domínguez M, Romera R, Sánchez E, Fita L and others (2013) Present climate precipitation and temperature extremes over Spain from a set of high resolution RCM. Clim Res (in press) doi:10.3354/cr01186

Dudhia J (1989) Numerical study of convection observed during the winter monsoon experiment using a mesoscale two-dimensional model. J Atmos Sci 46: 3077–3107

Dudhia J (1993) A nonhydrostatic version of the Penn State NCAR mesoscale model: validation tests and simulation of an Atlantic cyclone and cold front. Mon Weather Rev 121:1493–1513

ECMWF (2004) IFS Documentation CY28r1, Chapter 4: physical processes, Section 2: radiation. Available at www.ecmwf.int/research/ifsdocs/CY28r1/index.html

Fernández J, Montávez JP, Saenz J, Gonzalez-Rouco JF, Zorita E (2007) Sensitivity of the MM5 mesoscale model to physical parameterizations for regional climate studies: annual cycle. J Geophys Res 112(D4):D04101, doi:10.1029/2005JD006649

Fernández J, Primo C, Cofiño AS, Gutiérrez JM, Rodríguez MA (2009) MVL spatiotemporal analysis for model intercomparison in EPS: application to the DEMETER multimodel ensemble. Clim Dyn 33:233–243

Fernández-Quiruelas V, Fita L, Fernández J, Cofiño A (2010) WRF workflow on the Grid with WRF4G. Proc 11th WRF Users' Workshop, Boulder, CO

Fita L, Fernández J, García-Díez M (2010) CLWRF: WRF modifications for regional climate simulation under future scenarios. Proc 11th WRF Users' Workshop, Boulder, CO

Font-Tullot I (2000) Climatología de España y Portugal, 2nd edn. Universidad de Salamanca, Salamanca

Gaertner MA, Castro M (1996) A new method for vertical interpolation of the mass field. Mon Weather Rev 124: 1596–1603

Gaertner MA, Christensen OB, Prego JA, Polcher J, Gallardo C, Castro M (2001) The impact of deforestation on the hydrological cycle in the western Mediterranean: an ensemble study with two regional climate models. Clim Dyn 17:857–873

Gaertner MA, Jacob D, Gil V, Domínguez M, Padorno E, Sánchez E, Castro M (2007) Tropical cyclones over the Mediterranean Sea in climate change simulations. Geophys Res Lett 34:L14711, doi:10.1029/2007GL029977

Gaertner MA, Domínguez M, Garvert MA (2010) Modelling case-study of soil moisture-atmosphere coupling. Q J R Meteorol Soc 136:483–495

Gallardo C, Arribas A, Prego JA, Gaertner MA, de Castro M (2001) Multi-year simulations using a regional-climate model over the Iberian Peninsula: current climate and doubled CO_2 scenario. Q J R Meteorol Soc 127:1659–1682

Gao X, Pal JS, Giorgi F (2006) Projected changes in mean and extreme precipitation over the Mediterranean region from a high resolution double nested RCM simulation. Geophys Res Lett 33:L03706, doi:10.1029/2005GL024954

García-Díez M, Fernández J, Fita L, Yagüe C (2013) Seasonal dependence of WRF model biases and sensitivity to PBL schemes over Europe. Q J R Meteorol Soc 139:501–514

Giorgi F, Bi X, Pal JS (2004) Mean, interannual variability and trends in a regional climate change experiment over Europe. I. Present-day climate (1961–1990). Clim Dyn 22:733–756

Gleckler P, Taylor K, Doutriax C (2008) Performance metrics for climate models. J Geophys Res 113:D06104, doi:10.1029/2007JD008972

Gómez-Navarro JJ, Montávez JP, Jiménez-Guerrero P, Jerez S, García-Valero JA, González-Rouco JF (2010) Warming patterns in regional climate projections over the Iberian Peninsula. Met Zeit (Hambg) 19:275–285

Gómez-Navarro JJ, Montávez JP, Jerez S, Jiménez-Guerrero P, Lorente-Plazas R, González-Rouco JF, Zorita E (2011) A regional climate simulation over the Iberian Peninsula for the last millennium. Clim Past 7:451–472

Gómez-Navarro JJ, Montávez JP, Jerez S, Jiménez-Guerrero P, Zorita E (2012) What is the role of the observational dataset in the evaluation and scoring of climate models? Geophys Res Lett 39:L24701, doi:10.1029/2012GL054206

Grell GA (1993) Prognostic evaluation of assumptions used by cumulus parameterizations. Mon Weather Rev 121: 764–787

Grell GA, Dévényi D (2002) A generalized approach to parameterizing convection combining ensemble and data assimilation techniques. Geophys Res Lett 29(14), doi:10.1029/2002GL015311

Grell GA, Dudhia J, Stauffer DR (1994) A description of the fifth-generation PennState/NCAR mesoscale model (MM5). NCAR Tech Note NCAR/TN-398+STR, NCAR, Boulder, CO. Available at www.mmm.ucar.edu/mm5

Haylock MR, Hofstra N, Klein Tank AMG, Klok EJ, Jones PD, New M (2008) A European daily high-resolution gridded data set of surface temperature and precipitation for 1950–2006. J Geophys Res 113:D20119, doi:10.1029/2008JD010201

Herrera S, Fita L, Fernández J, Gutiérrez J (2010) Evaluation of the mean and extreme precipitation regimes from the ENSEMBLES regional climate multimodel simulations over Spain. J Geophys Res 115:D21117, doi:10.1029/2010JD013936

Herrera S, Gutiérrez JM, Ancell R, Pons MR, Frías MD, Fernández J (2012) Development and analysis of a 50-year high-resolution daily gridded precipitation dataset over Spain (Spain02). Int J Climatol 32:74–85

Hong SY, Lin JOJ (2006) The WRF Single-Moment 6-Class Microphysics Scheme (WSM6). J Korean Meteorol Soc 42:129–151

Hong SY, Pan HL (1996) Comparison of NCEP/NCAR Reanalysis with 1987 FIFE data. Mon Weather Rev 124:1480–1498

Hong SY, Dudhia J, Chen S (2004) A revised approach to ice microphysical processes for the bulk parameterization of cloud and precipitation. Mon Weather Rev 132:103–120

Houghton JT, Meira Filho LG, Callander BA, Harris N, Kattenberg A, Maskell K (eds) (1996) Climate change 1995. The science of climate change. Cambridge University Press, Cambridge

Jacob D, Van den Hurk BJJM, André U, Elgered G and others (2001) A comprehensive model inter-comparison study investigating the water budget during the BALTEX-PIDCAP period. Meteorol Atmos Phys 77:19–43

Jacob D, Bärring L, Christensen OB, Christensen JH and others (2007) An intercomparison of regional climate models for Europe: model performance in present-day climate. Clim Change 81:31–52

Jerez S, Montávez JP, Gomez-Navarro JJ, Jiménez-Guerrero P, Jiménez J, González-Rouco JF (2010) Temperature sensitivity to the land-surface model in MM5 climate simulations over the Iberian Peninsula. Met Zeit 19:363–374

Jerez S, Montávez JP, Jiménez-Guerrero P, Gómez-Navarro JJ, Lorente-Plazas R, Zorita E (2012a) A multiphysics ensemble of present-day climate regional simulations over the Iberian Peninsula. Clim Dyn 40:3023–3046

Jerez S, Montávez JP, Gómez-Navarro JJ, Jiménez PA, Jiménez-Guerrero P, Lorente R, González-Rouco JF (2012b) The role of the land-surface model for climate change projections over the Iberian Peninsula. J Geophys Res 117:D01109, doi:10.1029/2011JD016576

Jerez S, Montávez JP, Gómez-Navarro JJ, Lorente-Plazas R, García-Valero JA, Jiménez-Guerrero P (2013) A multiphysics ensemble of regional climate change projections over the Iberian Peninsula. Clim Dyn 41:1749–1768

Kain JS, Fritsch JM (1993) Convective parameterization for mesoscale models: the Kain-Fritsch scheme. The representation of cumulus convection in numerical models. Meteor Monogr 24:165–170

Kjellström E, Nikulim F, Hanson U, Strandberg G, Ullerstig A (2011) 21st century changes in the European climate: uncertainties derived from an ensemble of regional climate model simulations. Tellus 63A:24–40

Klemp JB, Skamarock WC, Dudhia J (2007) Conservative split-explicit time integration methods for the compressible non-hydrostatic equations. Mon Weather Rev 135:2897–2913

Knutti R, Furrer R, Tebaldi C, Cermak J, Meehl GA (2010) Challenges in combining projections from multiple climate models. J Clim 23:2739–2758

Koepke P, Hess M, Schult I, Shettle EP (1997) Global aerosol data set. Rep 243, Max Planck Inst Meteorol, Hamburg. Available at http://opac.userweb.mwn.de/radaer/gads.html

Krinner G, Viovy N, Noblet-Ducoudre N, Ogee J and others (2005) A dynamic global vegetation model for studies of the coupled atmosphere-biosphere system. Global Biogeochem Cycles 19:BG1015, doi:10.1029/2003GB002199

Mearns LO, Arritt R, Biner S, Bukovsky MS and others (2012) The North American Regional Climate Change Assessment Program: overview of phase I results. Bull Am Meteorol Soc 93:1337–1362

Mlawer EJ, Taubman SJ, Brown PD, Iacono MJ, Clough SA (1997) Radiative transfer for inhomogeneous atmospheres: RRTM, a validated correlated-k model for the longwave. J Geophys Res 102:16663–16682

Morcrette J, Smith L, Fourquart Y (1986) Pressure and temperature dependence of the absorption in longwave radiation parameterizations. Beitr Phys Atmos 59:455–469

Nordeng T (1994) Extended versions of the convective parametrization scheme at ECMWF and their impact on the mean and transient activity of the model in the tropics. Res Dep, Tech Memo 206, ECMWF, Reading

Nunez MN, Solman SA, Cabre MF (2009) Regional climate change experiments over southern South America. II. Climate change scenarios in the late twenty-first century. Clim Dyn 32:1081–1095

Roeckner E, Arpe K, Bengtsson L, Christoph M and others (1996) The atmospheric general circulation model ECHAM4: model description and simulation of present-day climate. Rep 218, Max Planck Inst Meteorol, Hamburg

Sánchez E, Romera R, Gaertner MA, Gallardo C, Castro M (2009) A weighting proposal for an ensemble of regional climate models over Europe driven by 1961–2000 ERA40 based on monthly precipitation probability density functions. Atmos Sci Lett 10:241–248

Simmons AJ, Burridge DM (1981) An energy and angular-momentum conserving vertical finite-difference scheme and hybrid vertical coordinates. Mon Weather Rev 109:758–766

Skamarock WC, Klemp JB, Dudhia J, Gill DO, Barker DM, Duda MG (2008) A description of the Advanced Research WRF version 3. NCAR Tech Note NCAR/TN20201c475+STR, available at www.mmm.ucar.edu/wrf/users/docs/arw_v3.pdf

Takle ES, Roads J, Rockel WJ, Gutowski WJ and others (2007) Transferability intercomparison. Bull Am Meteorol Soc 88:375–384

Taylor KE (2001) Summarizing multiple aspects of model performance in a single diagram. J Geophys Res 106:7183–7192

Tebaldi C, Knutti R (2007) The use of the multi-model ensemble in probabilistic climate projections. Philos Trans R Soc Lond A 365:2053–2075

Tiedtke M (1989) A comprehensive mass flux scheme for cumulus parameterization in large–scale models. Mon Weather Rev 117(8):1779–1800

Uppala SM, Kallberg PW, Simmons AJ, Andrae U and others (2005) The ERA-40 re-analysis. Q J R Meteorol Soc 131: 2961–3012

Van der Linden P, Mitchell JFB (2009) ENSEMBLES: climate change and its impacts: summary of research and results from the ENSEMBLES project. Met Office Hadley Centre Tech Rep, Exeter

Whetton P, Macadam I, Bathols J, O'Grady J (2007) Assessment of the use of current climate patterns to evaluate regional enhanced greenhouse response patterns of climate models. Geophys Res Lett 34:L14701, doi:10.1029/2007GL030025

CHAPTER 5

Conclusions

We have a closed circle of consistency here: the laws of physics produce complex systems, and these complex systems lead to consciousness, which then produces mathematics, which can then encode in a succinct and inspiring way the very underlying laws of physics that gave rise to it.

Roger Penrose - The Road to Reality

5.1   General conclusions

- The Mediterranean is expected to be one of the most prominent and vulnerable climate change "hot spots" of the 21st century, and the physical mechanisms underlying this finding are still not clear.

- Despite the limitation and the uncertainty characterizing the regional climate models, the multi-model ensemble has proven to be a valid approach to study the observed climate for both Mediterranean Basin and Iberian Peninsula climate.

- The quality of the observational datasets is crucial to evaluate correctly the simulated present climate and to assess model biases essential for climate projections evaluation.

- The comparison between model and observations based on *subregions* with coherent climate has proven to improve the model validation and highlight model specific biases

5.2   Conclusions by chapters

Med-CORDEX initiative for Mediterranean Climate studies

- To provide robust climate change information for use in Vulnerability/Impact/Adaptation assessment studies is important to consider the Mediterranean as a fully coupled environmental system.

- The Med-CORDEX initiative aims at coordinating the Mediterranean climate modeling community towards the development of fully coupled regional climate simulations, improving all relevant

components of the system, from atmosphere and ocean dynamics to land surface, hydrology and biogeochemical processes.

- The coordination activities and the scientific outcomes of Med-CORDEX can produce an important framework to foster the development of regional earth system models in several key regions worldwide.

A multi-model ensemble view of winter heat flux dynamics and the dipole mode in the Mediterranean Sea

- The variability of the air-sea heat fluxes is strongly captured by the variability in the latent heat flux, which has available estimations covering longer period with higher spatial resolution. In winter, the first few modes of variability between net and latent heat flux are essentially the same.
- The second mode of winter heat flux variability, which contribute to the anomaly maps of individual year more than the leading mode, is connected to the East Atlantic/Western Russia (EA/WR) atmospheric teleconnection pattern.
- A simple reconstruction of the heat flux variability over Mediterranean Sea deep-water formation regions reveals that the combination of the first two modes explains over 90% of the heat flux variance in these regions.

Climate variability of the Iberian Peninsula

- No single model outperforms the rest of the models for all the variables analyzed. Depending on the variable and season, different models stand out.

- The different performance of the RCMs in different seasons and variables encourages the use of the whole ensemble of simulations, taking the range of biases as an indicator of model uncertainty.

- The ensemble of simulations is able to correct the problems associated with the interannual variability for precipitation, showing substantially higher temporal correlation than the best individual model.

- The northern coast is an area with low the consecutive dry days (<1 mm) and high very heavy precipitation days' index values. By contrast, the spread of the results for the southwestern area is higher, and there is a clear tendency of most models to underestimate precipitation.

- All the models simulate correctly the spatial distribution of the temperature percentile. REMO, which is the only model which compare well with the observed percentile of maximum temperature, overestimate the indices related with the minimum temperature

Bibliography

The bibliography for the chapter two, three, and four is at the end of each chapter in the paragraph named *references*.

Cacho I, Valero Garces B, Gonzalez Samperiz P (2010) Revision de las reconstrucciones paleoclimaticas en la Peninsula Iberica desde el ultimo period glacial, In Clima en Espana: pasado, presente y futuro (Perez F. Fiz and Boscolo Roberta Editores) 9-24 pp

Deser, C., A. S. Phillips, M. A. Alexander, and B. V. Smoliak, 2014: Projecting North American Climate over the next 50 years: Uncertainty due to internal variability. J. Climate, 27, 2271-2296, doi: 10.1175/JCLI-D-13-00451.1.

de Sherbinin A (2014) - Climate change hotspots mapping: what have we learned? - 123

Flato G, Marotzke J, Abiodun B, Braconnot P, Chou SC, Collins W, Cox P, Driouech F, Emori S, Eyring V, Forest C, Glecker P, Guilyardi E, Jakob C, Kattsov V, Reason C, Rummukainen M (2013) Evaluation of Climate Models. In: Climate Change 2013: The Physical Science Basis. Contribution of Working Group I to the Fifth Assessment Report or the Intergovernmental Panel on Climate Change [Stocker, TF, Qin D, Plattner G-K, Tignor M, Allen SK, Boschung J, Nauels A, Xia Y, Bex V, Midgley PM(eds)] Cambridge University Press, Cambridge, United Kingdom and New York, NY, USA

Giorgi F (2006) Climate change hot-spots Geophysical Research Letters 33 doi:Artn L08707

Gutierrez JM, Pons MR (2006) Modelizacion numerica del cambio climatico: bases cientificas, incertidumbre y proyecciones para la Peninsula Iberica. Revista de

Cuaternario y Geomorfologia, 20 (3-4): 15-28.

Kerr,R.A. , "Forecasting Regional Climate Change Flunks Its First Test", Science,   vol.   339,   pp.   638-638, 2013. http://dx.doi.org/10.1126/science.339.6120.638

Klein Tank AMG, Wijngaard JB, Konnen GP, Bohm R, Demaree G, Gocheva A, Mileta M, Pashiardis S, Hejkrlik L, Kern-Hansen C, Heino R, Bessemoulin P, Muller-

Westermeier G, Tzanakou M, Szalai S, Palsdottir T, Fitzgerald D, Rubin S, Capaldo M, Maugeri M, Leitass A, Bukantis A, Aberfeld R, Van Engelen AFV, Forland E, Mietus M, Coelho F, Mares C, Razuvaev V, Nieplova E, Cegnar T, Lopez JA, Dahlstrom B, Moberg A, Kirchhofer W, Ceylan A, Pachaliuk O, Alexander LV, Petrovic P (2002) Daily dataset of 20th-century surface air temperature and precipitation series for the European climate assessment. Int J Climatol 22: 1441-1453

Lian Xie, Fredrick Semazzi, Adel Hanna, Richard Anyah, Huiwang Gao, and Yijun He, "Regional Climate Change: Downscaling, Prediction, and Impact Assessment," Advances in Meteorology, vol. 2015, Article ID 290281, 1 pages, 2015. doi:10.1155/2015/290281

Moberg A, Jones PD, Barriendos M, Bergstrom H, Camuffo D, Cocheo C, Davies TD, Demaree G, Martin-Vide J, Maugeri M, Rodriguez R, Verhoeve T (2000) Day-to-day temperature variability trends in 160-to-275-year-long European instrumental records. J Geophys Res 105(D18): 22.849-22.868

Raisanen J (2007) How realiable are climate models? Tellus 59: 2-29, doi: 10.1111/j.1600-0870.2006.00211.x

Staudt M, Esteban-Parra MJ, Castro-Diez Y (2005) Evolution and changes in Spanish monthly maximum and minimum temperatures with homogenized data, European Geosciences Union, General Assembly 2005, Geophysical Research

Thompson, D. W. J., E. A. Barnes, C. Deser, W. E. Foust, and A. Phillips, 2015: Quantifying the role of internal climate variability in future climate trends.Journal of Climate, 28, 6443-6456, doi:10.1175/JCLI-D-14-00830.1.

Xie, S.-P., C. Deser, G.A. Vecchi, M. Collins, T. L. Delworth, A. Hall, E. Hawkins, N. C. Johnson, C. Cassou, A. Giannini, and M. Watanabe, 2015: Towards predictive understanding of regional climate change. Nature Clim. Change, 5, 921-930, doi:10.1038/nclimate2689

Acknowledgments

Personal acknowledgments

Esta tesis ha sido posible gracias a muchas personas que directamente o indirectamente me han proporcionado su ayuda y apoyo.

En primer lugar, quiero dar las gracias a mi director de tesis que ha estado conmigo desde el comienzo y que me ha enseñado mucho de lo que voy a necesitar para defender esta tesis. Muchas gracias William Cabos.

Gracias a todos los miembros del Departamento de Física y sobre todo a los de grupo que pertenezco, el de Física del Clima. Gracias a María José, Antonio, William y Paco. A este último dedico un agradecimiento especial por haberme ayudado en un momento clave mi vida. Paco, gracias por ser una persona buena, sabia y brillante.

Muchas gracias también para todos los compañeros del departamento de física de la UAH que han compartido conmigo las alegrías y las penas que caracterizan el recorrido de una tesis doctoral. Gracias a Miguel, Jesús Aguado, Antonio, Héctor, Lupe y Guiomar por crear un ambiente de trabajo muy agradable y positivo. Gracias a German, por tus consejos, por las numerosas discusiones científicas y por las palizas que me has dado tanto en ping-pong como en padel. Gracias a Jesús Carretero, con el que he tenido interminables cuanto interesantes discusiones. Gracias a Judith, por muchas razones y por motivarme a acabar esta tesis cuanto antes.

Mis años de doctorado no hubieran sido tan bonitos si no se hubiese formado este increíble grupo de personas que en su tiempo llamamos Ecofisicos. Gracias a Cristina, Noelia, Eugenio, Borja, Sara, Silvia y a todos los que ya he nombrado.

Todas las tesis son un largo viaje, pero no todas se recuerdan como una Odisea. En mi Odisea Antoñito ha sido el mejor amigo de Ulises. Gracias por haberme ayudado año tras año y papeles tras papeles. Nunca me he sentido incomodo en pedirte otro favor y esto solo me pasa con grandes amigos. Gracias infinitas Rondeño.

Gracias a mis compañeros de piso durante mis años en Alcalá, los hermanos José Alberto y José Alejandro. Con vosotros, además del piso, he compartido muchas risas, muchas comidas y a veces también algunas penas... proprio como un hermano más.

Mis gracias van también a Christian y Alejandro, el primero por haber compartido muchos momentos inolvidables, y el segundo por haber hecho que me enamore de Alcalá.

Gracias a Alfredo Izquierdo que durante mi estancia en Alemania me ayudo a escribir la memoria con la que me concedieron la beca de doctorado. De mis estancias, hay más personas que quiero agradecer.

Thanks to Daniela Jacob for giving me the opportunity to spend precious time with her REMO group at Max-Planck Institute of Hamburg. Besides the great science, in Hamburg I found also great people, great company, and great friends. My amazing memories about Hamburg are usually associated with these people: Swantie, Suvarchal, Armelle, Eleftheria, and Thomas, my office mate and inseparable friend.

Dopo lo stage ad Amburgo venne il momento dello stage all'ENEA di Casaccia, dove andai per lavorare con Gianmaria Sannino, un grande scienziato e una grande persona. Arrivai all'ENEA come un dottorando straniero ma mi sentii subito a casa quando la prima sera ad Anguillara mi ritrovai a cenare nel covo del Maestro, Gianpaolo Caputo, una persona

eccezionale e con una filosofia di vita unica. Durante quella cena, e poi nei giorni seguenti, conobbi un gruppo di persone straordinarie che rese la mia permanenza a Roma un periodo indimenticabile della mia vita. Per quei giorni unici ringrazio Cristina, Claudia, Valentina, Erika, Calogero, Giancarlo, Daniele, Grazia, Giulianella, Chiara, Ivan, Fabio, Roberta, Esther ed infine Elena, che inserisco in questa lista anche se meriterebbe una intera pagina di ringraziamenti.

Ho tante ragioni per ringraziare a Pasquale e Gianfranco, ma in questa occasione lo faccio per l'indimenticabile ciclo di incontri europei durante i primi anni di dottorato.

Tra le tante persone che voglio ringraziare c'è ne una della quale conosco soltanto la sua professione e il luogo dove questi esercitava nel settembre 2001. Ringrazio lo psicologo che lavorava alla Caserma Militare di Corso Malta (Napoli) poiche', durante le visite mediche per l'allora obbligatorio servizio militare, mi convinse, dopo un brevissimo colloquio, a continuare gli studi.

Infine ringrazio le mie sorelle e i miei genitori, ultimi, ma di certo non per importanza, per essermi stati vicini in tutti questi anni e per non aver mai smesso di credere in me.